Systematic Investigation of Poly(ethylene oxide)-grafted Polymethacrylates as solvent-free Polymer Electrolytes

Zur Erlangung des akademischen Grades eines/einer

DOKTORS/DOKTORIN DER NATURWISSENSCHAFTEN

(Dr. rer. nat.)

von der KIT-Fakultät für Chemie und Biowissenschaften

des Karlsruher Instituts für Technologie (KIT)

genehmigte

DISSERTATION

von

M. Sc. Isabella Maria Weiß

1. Referent/Referentin: Prof. Dr. Patrick Theato
2. Referent/Referentin: Prof. Dr. Helmut Ehrenberg

Tag der mündlichen Prüfung: 12.12.2022

Against all odds.

Die vorgelegte Arbeit wurde im Zeitraum von Oktober 2018 bis Oktober 2022 am Institut für Technische Chemie und Polymerchemie am Karlsruher Institut für Technologie (KIT) unter Betreuung von Prof. Dr. Patrick Théato angefertigt.

Erklärung

Ich erkläre hiermit, dass ich die vorgelegte Arbeit im Rahmen der Bereuung durch Prof. Dr. Patrick Théato selbstständig verfasst und keine anderen als die angegebenen Quellen und Hilfsmittel verwendet habe. Wörtlich oder inhaltlich übernommene Stellen sind als solche kenntlich gemacht und die Satzung des Karlsruher Instituts für Technologie (KIT) zur Sicherung guter wissenschaftlicher Praxis wurde beachtet.

Des Weiteren erkläre ich, dass ich mich derzeit in keinem weiteren laufenden Promotionsverfahren befinde und auch keine vorausgegangenen Promotionsversuche unternommen habe.

_____

Ort, Datum Isabella Weiß

Abstract

Herein, we present a systematic investigation of the structure-property relationship of polymer electrolytes (PEs) based on brush polymers consisting of a methacrylate (MA) backbone and methoxy(poly(ethylene oxide)) (mPEO) side chains.

To do so, the influences of small changes in the chemical structure such as side chain length and backbone length onto the electrochemical performance of the resulting PEs were thoroughly investigated.

Based on the results shorter backbone lengths of 12 repeating units (ru) and four times longer side chains (in comparison to polymers with 100 ru in the backbone and 4.5 ethylene oxide (EO) ru) allow for an increase in ionic conductivity of two orders of magnitude to $1.57x10^{-3}$ mS cm^{-1} at 0°C for PEO-based electrolytes with a defined brush polymer structure.

It was also found that electrolytes with lower lithium salt concentrations of 1:15 and 1:20 as a ratio of lithium ion to EO ru delivers higher ionic conductivities. The relative increase in ionic conductivity due to lithium salt concentrations was found higher for polymers with shorter side chains.

The systematic investigations reveal insight into the complex trade-off between various parameters including favorable copolymerization patterns, as well as optimal lithium salt concentration.

Zusammenfassung

Hier wird eine systematische Untersuchung der Struktur-Eigenschafts-Beziehung von Polymerelektrolyten (PEs) auf Basis von Bürstenpolymeren vorgestellt, die aus einem Methacrylat (MA) Rückgrat und Methoxy(poly(ethylenoxid)) (mPEO) Seitenketten bestehen.

Dazu wurden die Einflüsse kleiner Änderungen in der chemischen Struktur wie Seitenkettenlänge und Rückgratlänge, sowie die Synthese von Copolymeren auf die elektrochemische Leistung der resultierenden PEs untersucht.

Basierend auf den Ergebnissen ermöglichen kürzere Hauptkettenlängen von 12 Wiederholungseinheiten (ru) und viermal längere Seitenketten (im Vergleich zu Polymeren mit 100 ru in der Hauptkette und 4,5 Ethylenoxid (EO) ru) eine Erhöhung der Ionenleitfähigkeit um zwei Ordnungen in der Größenordnung von $1{,}57 \times 10^{-3}$ mS cm^{-1} bei 0 °C für PEO-basierte Elektrolyte mit einer definierten Bürstenpolymerstruktur.

Weiter wurde festgestellt, dass Elektrolyte mit niedrigeren Lithiumsalzkonzentrationen von 1:15 und 1:20 an Verhältnis von Lithiumion zu EO-Wiederholeinheiten höhere Ionenleitfähigkeiten liefern. Der relative Anstieg der Ionenleitfähigkeit aufgrund von Lithiumsalzkonzentrationen ist für Polymere mit kürzeren Seitenketten höher.

Die systematischen Untersuchungen geben Einblick in den komplexen Kompromiss zwischen verschiedenen Parametern, einschließlich günstiger Verhältnisse von Monomeren zur Synthese von Copolymeren, sowie optimaler Lithiumsalzkonzentration.

Table of Contents

1. Introduction

With a growing sector of renewable energy technologies, there exists an enormous demand for energy storage systems. Yet, different applications require different needs of energy storage systems. One approach to solve the specific problem is the development of substantially efficient, new battery systems.[1] Polymers are hereby interesting materials that are investigated as (solid) polymer electrolytes (PEs) as cost effective, easily processable and lightweight materials. Herein, linear high molecular mass Poly(ethylene oxide) (PEO) is one of the most extensively investigated polymers.[2,3] At present, general challenges of PEO-based electrolytes lay in a comparably low conductivity at room temperature, due to high crystallization tendencies.[4–6]

To suppress the formation of crystalline domains various approaches are discussed in literature, such as the use of plasticizers[7,8], fillers[9–11], small molecule transporters[12] and PEO-based copolymers.[13–19] For the application in lithium-ion batteries (LIBs) the polymers are generally mixed with a lithium salt (like e.g., Lithium bis(trifluoromethylsulfonyl)imide (LiTFSI)) to form lithium-ion (Li^+) conducting PEs. The choice of lithium salt can cause tremendous difference in ionic conductivity[20]. While PEO is valued for its high ability to dissolve common Li-salts[21], this can also be a disadvantage. The conductivity is further reduced because of diffusion of linear PEO chains along with strongly coordinated Lithium ions at the O-moieties of ethylene oxide. The strong coordination environment can inhibit transfer of certain Li-ions independent from the coordinating molecule completely. Molecular dynamic simulations confirm that some cations remain coordinated to the same oxygen atoms or at least the same chain(s) throughout the whole simulation and do not participate in the charge transfer at all.[22,23]

The subject of this work is to investigate the ionic conductivity of PEO as side chains to a polymer backbone with a different chemical composition. As the main chain polymer, methacrylate is employed due to its relatively rigid backbone to separate the segmental motion of the PEO chain from the conductivity. As a result, the diffusion of PEO chains should be reduced because the movement of the copolymer as a whole entity is less likely. More specifically, with this approach the lithium transference number as well as the ionic conductivity is expected to benefit from the anticipated increase of inter-chain hopping of Li^+.

An additional advantage would be an enhanced mechanical stability with its origin in a higher glass transition of the backbone building block than the respective linear PEO. On the contrary reduction of crystallization will most notably reduce the mechanical stability. Additionally, the segmental motion and the need of mobile chains to enable Li-ion transfer across chains have the potential to counteract each other. While considering combinations of those parameters and thinking about the interplay between them, it becomes obvious that the structure-property-relationship needs to be understood on a deeper level.

The focus of this work lays on creating a matrix of polymers to compare the effects of changing one parameter directly with structurally related polymers which were synthesized, processed, and measured in the same manner. Only hereby statements can be made that observed values deviate due to the chemical structural change itself.

Firstly, low dispersity of the polymers and a high control over the polymerization is of great importance to exclude differences in the conductivity for instance from side products. To do so, reversible-addition-fragmentation chain-transfer (RAFT) polymerization was chosen and optimized for the targeted polymers.

Secondly, in literature values for ionic conductivities are often compared without full knowledge of the background of the polymer which might influence the properties. More precisely, it is a well-known phenomenon in polymer science that significant variations in the properties of the polymer can occur due to different synthesis and processing strategies. For example, crystallization can be significantly impacted by thermal treatment, the degree of crystallization then again has a great impact on ionic conductivity of PEO-based electrolytes and has been widely investigated in literature.[24] For this reason, all polymers in this work are handled as similar as possible.

Lastly, the electrolyte preparation, cell assembly and measurement setup play a major role in the comparability of obtained values. Especially the drying process and storage conditions must be considered when comparing ionic conductivities, since PEO is known to be highly hygroscopic and solvent residues result in a change of lithium-ion coordination/ lithium salt solvation. Both water and solvent addition to the electrolyte (un)intentionally alter the ionic conductivities.[12,25] Therefore, in this work the polymers were all prepared in the same solvents and extensively dried previous to electrochemical measurements.

It must be pointed out that strategies for synthesis and processing as well as thermal treatment, cell assembly and measurement technique need to coincide to the greatest possible extend. Nevertheless, in literature we find studies neglecting the fact that polymer properties highly depend on these mentioned parameters and ionic conductivities of electrolytes are compared despite unknown processing approaches.

Previous works have shown a low conductivity for very short (number of ethylene oxide repeating units of $x < 6$) as well as too long ($x > 24$) side chains at room temperature.[26] They show that in the first case this is due to low segmental motion and low salvation probability near the backbone. For the second case it is due to high tendencies of crystallization of the PEO chains and thus limited segmental motion, which reduces lithium-ion transport. Most studies focus on solid PEO (with $x > 19$ which equals a number average molecular weight $M_n > 900$ g mol^{-1} more often even higher than 1 000 000 g mol^{-1}) in this study we close the gap by looking at very short PEO chains as well as PEO exceeding the phase transition over a temperature range from 0 °C up to 80 °C.

To guarantee optimal comparability and give an extensive overview this work had to cover the whole range from homopolymers, polymer blends, as well as respective copolymers. In order to exploit the full potential and enhance the applicability, detailed insight of the counterplay of various influences on a structural level is required.

2. Theoretical Background

The golden book of IUPAC defines a macromolecule or polymer molecule as following:

"A molecule of high relative molecular mass, the structure of which essentially comprises the multiple repetition of units derived, actually or conceptually, from molecules of low relative molecular mass."[27]

The subjects of investigation are polymer molecules made up of a certain amount of relatively smaller repeating units called monomers.[27] With the knowledge that there are numerous monomers with different functional groups one can imagine that the possibilities of combinations are immense. Additionally, those monomers can be arranged in different molecular configurations / architectures.[28]

2.1.Polymer Architectures

The structurally simplest architecture is a linear polymer. From this structure branching can occur (compare b) and c) scheme1) randomly or in a more complex and defined way. Well known deviations from the linear polymer architecture are for example star, comb, brush, or ring polymers (compare scheme 1). Another possibility are crosslinked networks as well as linear or branched block copolymers. Polymers from different blocks can also occur for other

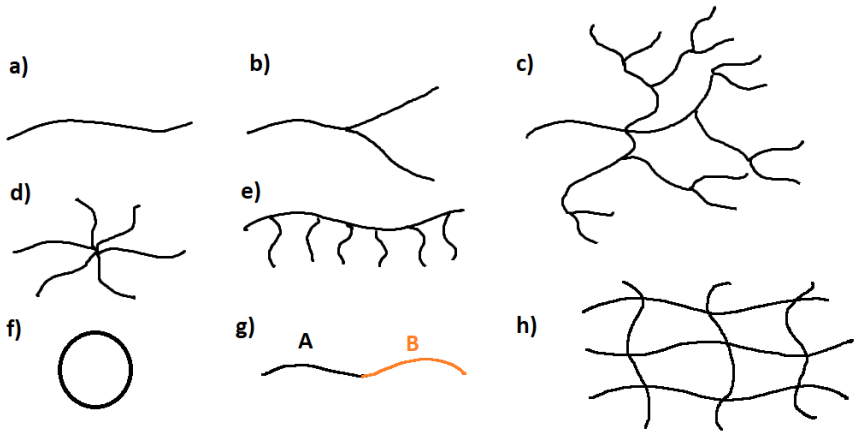

SCHEME 1: *Schematic depiction of different polymer architectures. a) Linear b) branched c) hyper branched d) star e) comb / brush f) ring g) AB-copolymer h) network.*

architectures, for example the side chains and backbone of brush polymers can consist of different types of monomers.

In this work the focus lays on graft polymers where side chains are grafted to a backbone (shown in scheme 1 e)). There are different definitions whether such a polymer can be called brush polymer or not. Firstly, there is a definition after which the side chains should be grafted densely onto the backbone and therefore are obliged to point away from it.[29] According to this definition the polymers examined in this work are no brush polymers but comb polymers. Those are mainly polymers with one side chain per branching point in the backbone unit and no (or only a sterically redundant) second side chain or functionality. The methacrylates in this work obviously have firstly the mPEO side chain and secondly a methyl group at each backbone repeating unit.

One other definition is, that the functionality of the branch point in the backbone is greater than three.[27] After this definition the polymers shown in this work are brush polymers, since the carbon atom at the branching point has chemical bonds to four different binding partners.

In the following I will refer to the synthesized polymers as brush or graft polymers.

To achieve such graft polymers, it can be distinguished between several approaches, namely `grafting onto´, `grafting from´ and `grafting through´ techniques[30] (see scheme 2).
The `grafting onto´ approach can be realized by attaching the polymer side chains onto the functional polymer via nucleophilic substitution or coupling reaction. However, the yield of polymers with high grafting densities is limited due to steric repulsion of the side chains.
For the `grafting from´ approach a macroinitiator bearing multiple initiator sides is the starting material. Monomers are subsequently added and build up the side chains bottom to top. With this approach the lengths of the side chains are not as uniform as aimed for in this work.
The third technique is the `grafting through´ approach in which a macromonomer is polymerized. This monomer already contains both the well-defined side chain as well as a polymerizable functionality, which builds up the backbone. Utilizing this method, the length of the side chain and the copolymerization pattern can easily be varied.

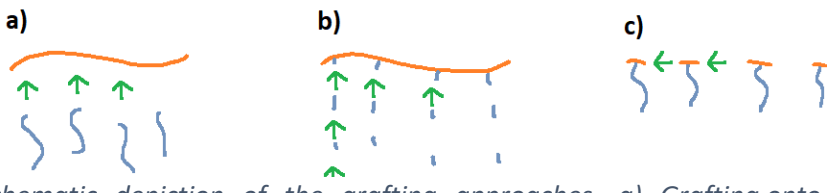

SCHEME 2: *Schematic depiction of the grafting approaches. a) Grafting onto b) grafting from c) grafting through.*

2.2.Polymer Synthesis

There are various polymerization techniques that can be utilized to yield polymers. These can mainly be divided into two classes of polymerization mechanisms, namely step-growth and chain-growth. In the first one a polymer is formed by stepwise combination of monomers, oligomers or two chains of any length. Characteristic for this polymerization is a low average polymer weight throw-out the process, achieving high molecular masses only at the end of the reaction time. A typical example for this technique is polycondensation.

With this said the second polymerization technique will be described more in detail since it is subject of this work. The chain-grow polymerization mechanism depends on monomer addition to the growing chain as sole chain-extension step. The most common example is the free-radical polymerization, where monomer and initiator react without any further controlling agent.[31] This approach leads to a broad molecular-weight dispersity (Đ)[32] due to random chain growth and termination. For most applications this is sufficient, besides high dispersity can be a benefit for the processability.[33]

If the aim is to understand the structure-property-relationship a narrow weight distribution is crucial to understand the explicit role of different structural parameters.

Such defined polymers can be synthesized for example via ionic polymerization, since this technique is not limited by termination reactions like free radical polymerization. For this reason, M. Szwarc also called them “living” polymers when he first introduced ionic polymerization in 1956.[34] Since this polymerization proceeds through ionic reactive centers, it is extremely sensitive to impurities like water, which could terminate the growing chain. Further the technique is not tolerant to all monomers and functional groups.

To overcome these disadvantages and find a middle path between ionic and free radical polymerization, “controlled radical polymerization” methods were developed. Different working groups succeeded with mainly three different approaches. Nitroxide-mediated polymerization (NMP)[35–37] and atom transfer radical polymerization (ATRP)[38,39] were developed to reduce the number of simultaneously propagating chains whereas reversible addition fragmentation chain-transfer (RAFT) polymerization[40,41] focuses on increasing the

number of overall growing chains. Since all of them specialize on certain monomers and ATRP uses metals which might interfere with the application in the battery field, RAFT polymerization was overall found to be most suitable for the purpose of this work.

2.2.1. Reversible Addition Fragmentation Chain Transfer (RAFT) Polymerization

In 1998 Rizzardo et al.[42] firstly described the mechanism of RAFT polymerization which sets itself apart from the principle of NMP and ATRP through a reversible chain-transfer process to obtain a low dispersity. Instead of inhibiting a propagating chain, the RAFT agent instead reversibly can add and release chains and with this exchange between active (propagating) and dormant chain. This results in an overall higher number of simultaneously propagating chains, than initiated. Dispersities of 1.1 are possible with this polymerization technique and since the chain transfer is reversible the reaction time is generally lower than for ATRP and NMP. After an initiating step and the formation of the RAFT adduct radical, this can fragment into the active chain and the polymeric RAFT agent. The active chain carrying the radical propagates before a deactivation step where addition to the RAFT agent happens. The radical is then transferred to again obtain the RAFT adduct radical intermediate which will again fragment. The probability to fragment one chain or the other is equal, leading to a low dispersity.[41,43,44]

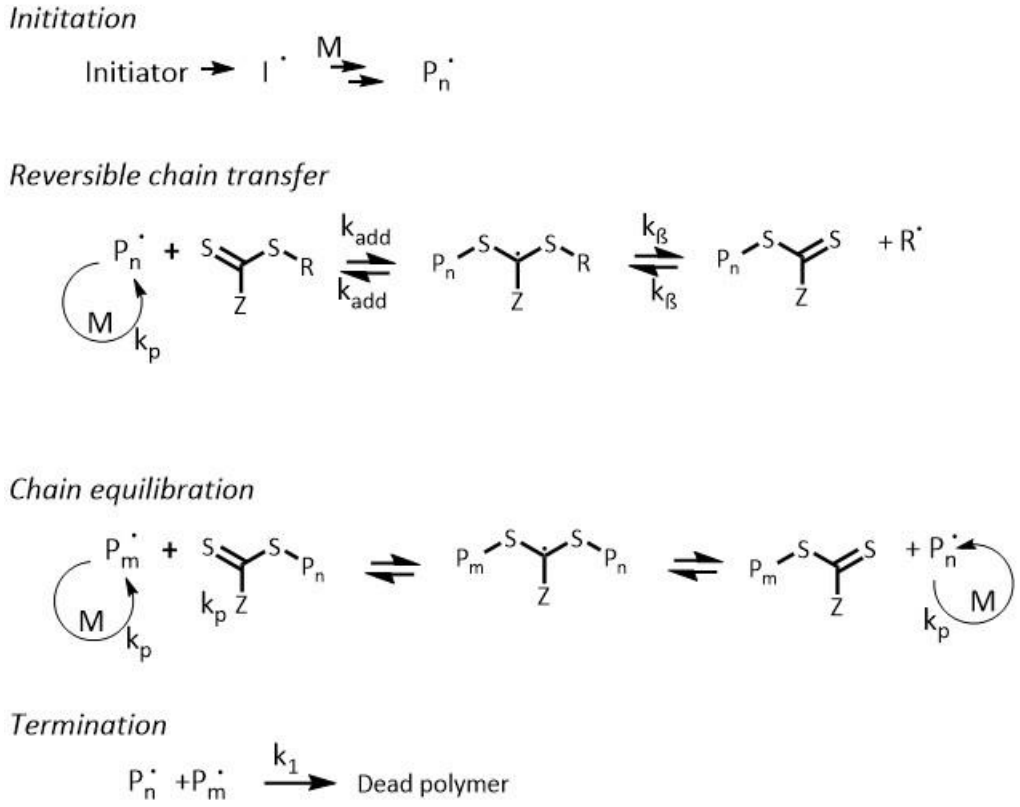

SCHEME 3: *Schematic reaction mechanism of RAFT polymerizations with Initiation, reversible chain transfer, chain equilibration and termination step.*[44]

Typical commercially available RAFT agents are dithioacetates, alkyl dithiobenzoates, dithiocarbamates, trithiocarbonates or xanthates like shown in scheme 3.[40] The most important part of the RAFT agent is the reactive double bond that can easily undergo radical addition, further components are a stabilizing Z group and a rest R which is a leaving group and able to initiate chain growth upon homolytic cleavage.

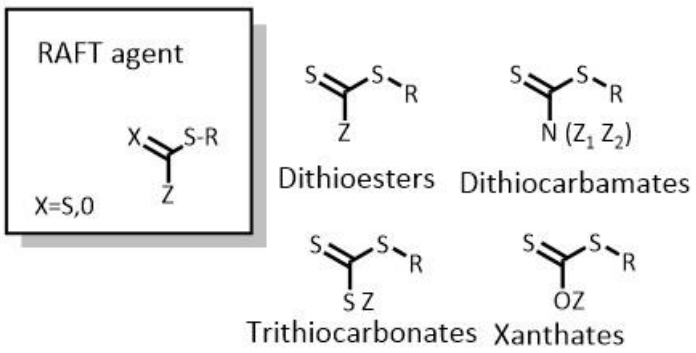

SCHEME 4: *Schematic structure of a RAFT agent and examples for the structure of common RAFT agents.*

The relationship between RAFT agent concentration and molecular weight follows from following equation:

$$M_n = \frac{[M]_0 - [M]_t}{[RAFT]_0 + d\ f\ ([I_2]_0 - [I_2]_0)}\ M_M + M_T$$

[M] = monomer concentration; [RAFT] = concentration of RAFT transfer agent; [I_2] = concentration of the initiator; d = number of formed chains per termination; f = efficiency of the initiator; M_M = molecular mass of the monomer; M_T = mass of the transfer agent

For a successful polymerization the ratio of RAFT agent and initiator plays a great role. The use of too much initiator results in loss of control (free radical mechanism). Also, the above-mentioned equation becomes more trivial if [RAFT] is far greater than [I_2]. If so, the initiator concentration can be neglected, so that the doubling of the RAFT concentration in comparison to the monomer concentration halves the possible molecular weight. The molecular weight for a controlled radical polymerization can be estimated using this formula.

2.3. Lithium-Ion Battery

The development of lithium-ion batteries was awarded with the Nobel Prize in chemistry for J. B. Goodenough, M. S. Whittingham, and A. Yoshino in 2019.[45]

Looking at the general setup of a nowadays commercial battery, it consists out of four main components, namely an anode, a cathode, an electrolyte, and a membrane separating the two electrodes. The foundation for this was laid by Whittingham in 1914, using titanium disulfide (TiS_2) as cathode material.[46] Goodenough replaced TiS_2 with lithium cobalt oxide ($LiCoO_2$, or LCO) in 1980 which offers a higher voltage and significantly improves the safety compared to hydrogen sulfide gas produced by TiS_2 in combination with moisture.[47] Around the same time Yazami showed reversible electrochemical intercalation of Li-ions in graphite.[48] Yoshino then refined Goodenough´s setup by using "soft carbon" instead of lithium metal as an anode, a $LiCoO_2$ cathode and a carbonate ester-based electrolyte and patented the first lithium-ion battery.[49]

The principal working mechanism of a rechargeable lithium-ion battery is as follows: At discharge the lithium intercalated in the anode diffuses through the electrolyte and recombines at the cathode to lithium cobalt oxide. At charge, the other way round, lithium-ions are intercalated in the graphite again.[50]

From the first idea to today's modern batteries over the years many challenges were tackled in more or less successful ways.[51] Some inventions were discarded others were refined. Nowadays some of the not further developed strategies are under reassessment and considered as interesting approach again. In the perspective of revolutionizing the battery field numerous groups are investigating options to improve the state of the art.[52] In this work the electrolyte is the subject of research.

2.3.1. Polymer Electrolytes

The medium in which ion movement between electrodes takes place and which leads to electrochemical conduction is called electrolyte. Most electrolytes in commercially available lithium-ion batteries consist of a liquid in which a Li-salt is dissolved.[53] In this setup bases, acids, and flammable organic liquids can exit the batteries when damage occurs. This means liquid electrolytes as such present a great safety hazard; therefore the high urgency to replace them with other systems.[54] For years research groups have been working on improving electrolytes with very different approaches, e.g. solid electrolytes derived from substance classes like oxides, sulfides or thiosulphates to name prominent ones.[55–57] In laboratory scale and at elevated temperatures astonishing conductivities can be achieved using solid electrolytes like e.g. lithium-rich anti-perovskites.[58] Although solid electrolytes have the notable advantage, that no leakage will occur, they also have their disadvantages. The mainly brittle inorganic materials suffer especially from mechanical damage e.g. originating from significant volume changes that take place while charging and discharging.[59] In fact, losing contact towards the electrodes or crack formation can lower the battery´s capacity tremendously.[60] Using a polymer matrix as electrolyte is providing an obvious solution, resulting firstly in a more flexible and therewith safer battery. Secondly, in comparison to e.g. oxides, solid polymer electrolytes offer enhanced electrode contact properties and are a cost-effective, low weight and easily processible alternative.[61] The drawback so far has been the low conductivity, low chemical stability, and narrow potential window. All these challenges need to be overcome by new ideas and clever combinations of building blocks. The performance of the current generation of lithium polymer batteries has proven to offer a much higher charge and discharge rate for high demanding applications, even if still not outperforming lithium-ion batteries in terms of capacity and cost.[41] Amongst others an important precondition for many successful solid polymer electrolyte systems is good solubility of the lithium salt in the polymer.[20,62,63] The solubility needs to be high, which is determined by the concentration of polar groups, usually oxygen moieties, in each monomer. Polycarbonates (PC) and especially poly(ethylene oxide) (PEO)[4] can be taken as good examples for the latter. One of the disadvantages of polymer electrolytes is their reduced electrochemical stability.[64]

Early on Yazami already experimented with the most prominent example of SPEs: poly(ethylene oxide) (PEO)[48], which is a semi-crystalline polymer with a relatively low glass transition temperature (T_g) of around -56 °C and a melting temperature (T_m) around 65 °C depending on the molecular weight of the PEO[65] in combination with lithium salts. The oxygen moieties of the amorphous segments in the polymer are mainly responsible for the conductivity of the solid polymer electrolytes (SPE).[4] High crystallinity is therefore not desirable, as this leads to slowed down polymer chain dynamics and thus hindering the ion transportation.[24] Unfortunately, back in the early days of lithium-ion batteries all research focused on liquid electrolytes, once there was a promising prototype patented. Nowadays with the knowledge about the limitations of liquid electrolytes researchers are again investigating into promising directions. One of them is to explore novel combinations of copolymers and other architectures based on PEO to overcome for example high crystallization tendencies and enhance the performance of lithium-ion batteries.

3. Results and Discussion

To build up a matrix of similar architectures homo- and copolymers were successfully synthesized via RAFT polymerization from Methoxy(Poly(ethylene oxide))methacrylate (mPEOxMA). In the following the repeating units (ru) of PEO are represented by x with values of 4.5, 9.1 and 19.3 (compare scheme 5) which equals a M_n of the mPEOxMA monomer of 300, 500 and 950 g mol^{-1} respectively.

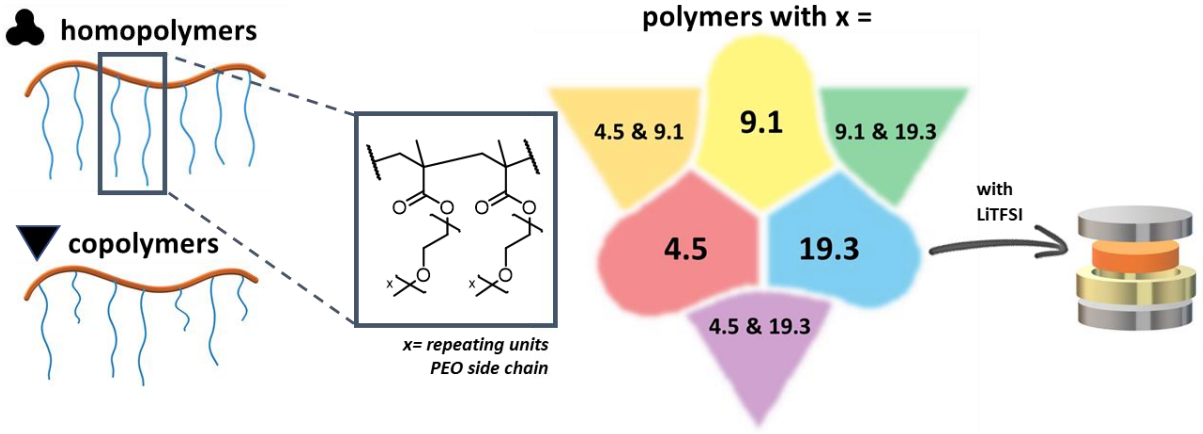

SCHEME 3: *Schematic presentation of the homo- and copolymer structure (left), a zoom into the chemical structure with the assignment x for the ethylene oxide (EO) repeating units (middle left), color code overview graphic for the combinations of x per polymer (middle right) and schematic electrolyte preparation with cell assembly for electrochemical impedance measurements (right).*

To achieve greater understanding over the influence of length and combination of PEO side chains onto ionic conductivities, data from electrochemical impedance spectroscopy (EIS) and differential scanning calorimetry (DSC) data of respective polymers and electrolytes were compared. Therefore, a high degree of control over the obtained polymer by the polymerization technique is of great importance. This is the case because the effect of other molecules than the desired polymer and the influence of dispersity and side products onto ionic conductivities must be minimized.

Therefore, a series of test reactions was carried out to find the optimal reaction conditions and to find a suitable RAFT system. The applicability of the RAFT system for all the given monomers has been tested and the RAFT agent 2-cyanpropan-2-yl-benzodithioat (CPDB) as well as the initiator α,α'-azo-isobutyronitril (AIBN) were chosen. Firstly, both are well-soluble

in the tested solvent-mixtures and perfectly compatible for controlled polymerization of methacrylates.[44,66,67] Secondly, the Z group enables a clear assignment in NMR spectroscopy, due to its characteristic chemical shift. Lastly the end group of polymers directly initiated by AIBN is the same group as the R group provides (compare scheme 6), whereby the characterization is facilitated.

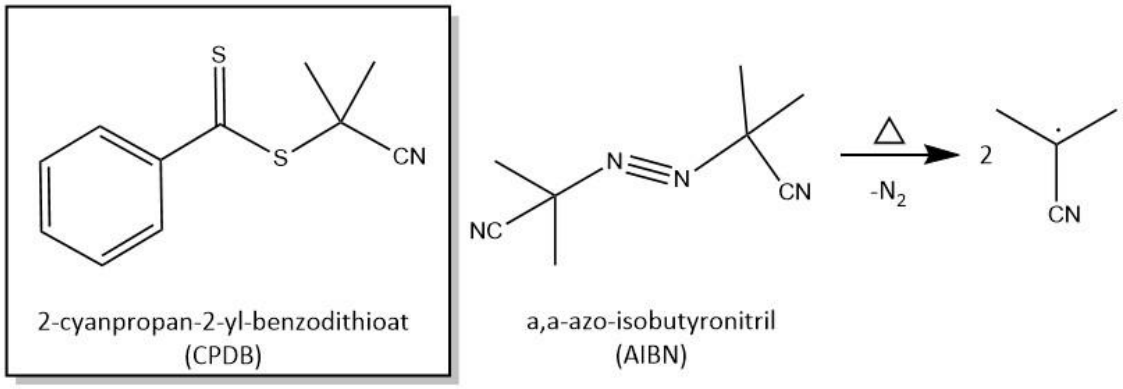

SCHEME 4: *chemical structure of CPDB and AIBN, as well as the mechanism of the initiation reaction of AIBN.*

For the polymerization a mixture from deionized water and 1,4-dioxane (50:50) has proven to be the most suitable solvent. The addition of water is necessary to reduce the required reaction time and more importantly to enable the polymerization of monomers with longer PEO side chains. The solvent enables the PEO chains to extend which provides more accessible double bonds and reactive centers of growing chains.[68] Experiments without addition of water only showed low yields for mPEO9.1MA and nearly no polymer for mPEO19.3MA as monomer. Further the pursued strategy with this solvent mixture also allows uniform copolymerization over the whole range of monomers and maintains direct comparability within the matrix of obtained polymers.

3.1. Homopolymers

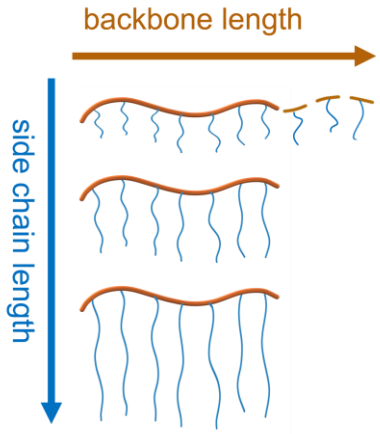

SCHEME 5: *Schematic representation of the variation of the two key-parameters: backbone length in orange and side chain length in blue. In the schematic structure of a brush polymer at the top growth of the backbone is depicted by addition of further monomers*

First of all, homopolymers were synthesized to build up a matrix, which is the basis for subsequent comparisons. A table of the targeted M_n in g mol^{-1} for the synthesized homopolymers is listed in the experimental section (see table 1).

In the following the electrolytes that are discussed were prepared by LiTFSI addition in the ratio of Li-ions to ethylene oxide (EO) repeating units (also written as [Li^+]:[EO]) of 1:10. The ratios 1:15 and 1:20 were also synthesized and are further discussed in chapter 3.4. Effect of Li-salt concentration.

By choosing monomers with different side chain lengths a change in the ionic conductivity of the resulting electrolyte can be observed (see figure 1). When increasing the side chain length from 4.5 to 19.3 repeating units, the ionic conductivity increases one to one and a half orders of magnitude (as shown in figure 1 and denoted by the blue arrow).

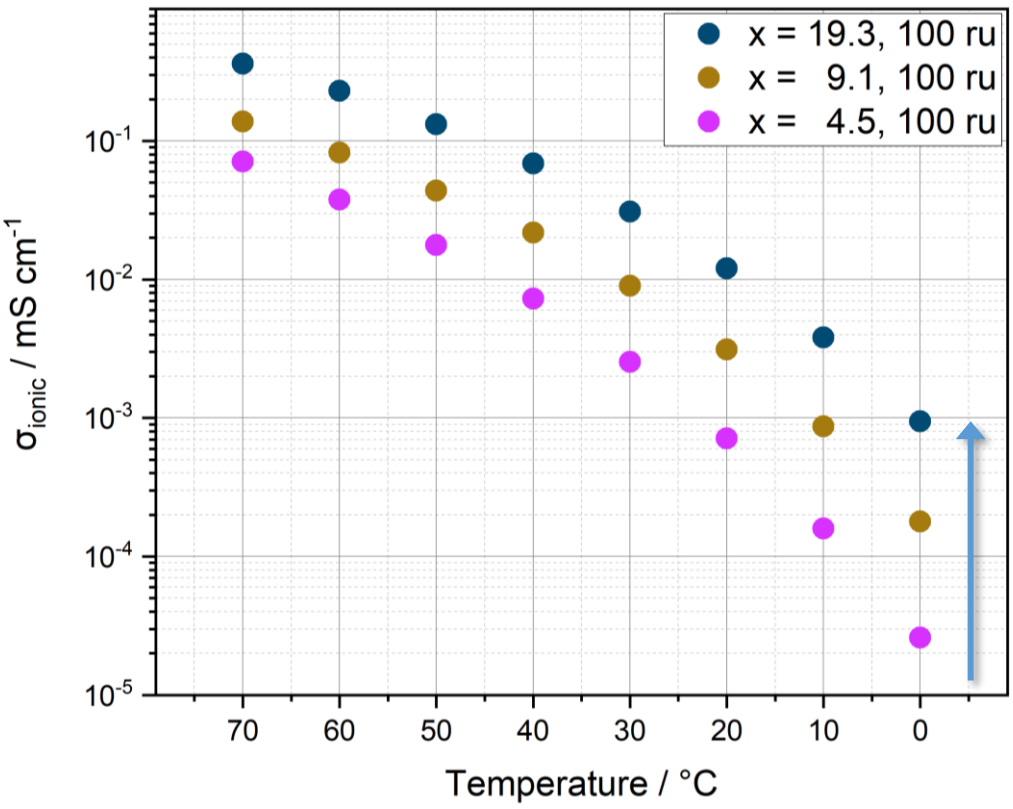

FIGURE 1: *Ionic conductivities of various homopolymers in a temperature range from 0 to 70°C. The graph shows homopolymers with a backbone length of 100 repeating units and the variation of the PEO side chain length. For this measurements, all polymers were mixed with LiTFSI in the ratio [Li⁺]:[EO] of 1:10.*

At lower temperatures the positive effect of longer side chains onto the ionic conductivity is more significant. This is a rather unexpected outcome since for linear PEO a significant decrease in the ionic conductivity (σ_{ionic}) is known for higher molecular weights due to crystallization around 60 °C.[24] This is not the case for the given side chain lengths in the brush polymers at hand. When lowering the operation temperature, the ionic conductivities gradually decrease for all side chain lengths and no drastic drop at a certain temperature can be observed.

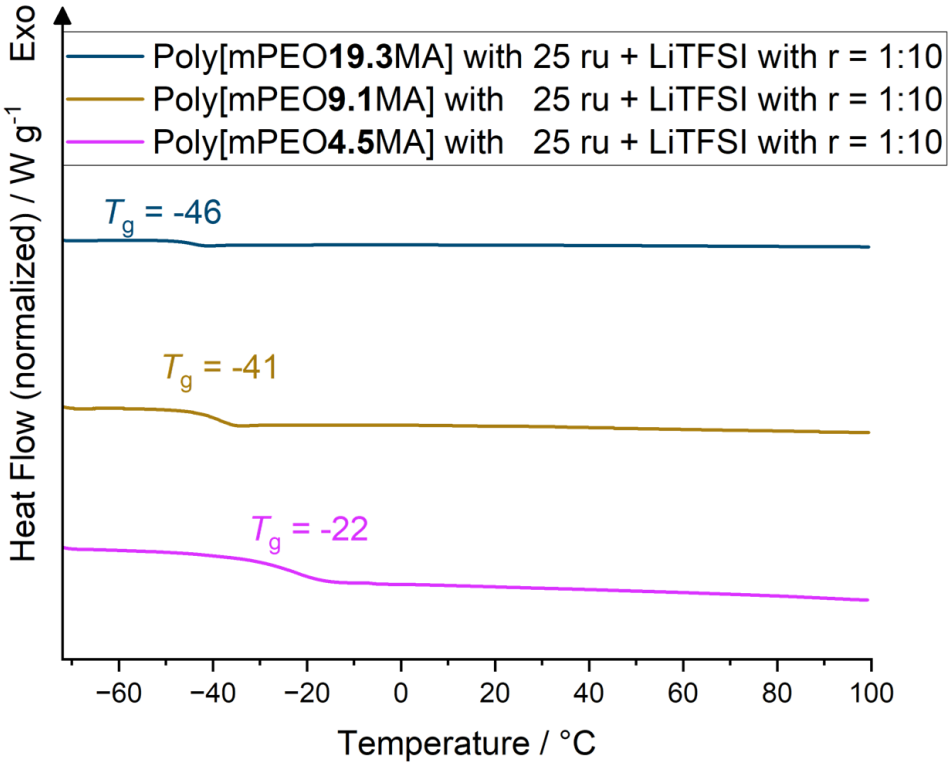

FIGURE 2: *Exothermic heating curves from DSC measurement from electrolytes of polymers with each 25 ru and x = 4.5, 9.1 and 19.3. The respective value for glass transition is noted in the respective color. The ratio [Li⁺]:[EO] is 1:10 for all electrolytes.*

Looking at the data obtained from Differential Scanning Calorimetry (DSC) of the respective polymers a decrease in the glass transition temperature (T_g) with increase of x can be observed (see fig. 2 and table 8). In this figure the DSC heating curves are shown up to a temperature of 100 °C for homopolymers with 25 ru each and a LiTFSI addition in the ratio of 1:10 ([Li⁺]:[EO]). This representative figure for all homopolymer electrolytes clearly shows no melting point for the brush polymer electrolytes in contrast to linear PEO (T_m = 65 °C)[4,24].

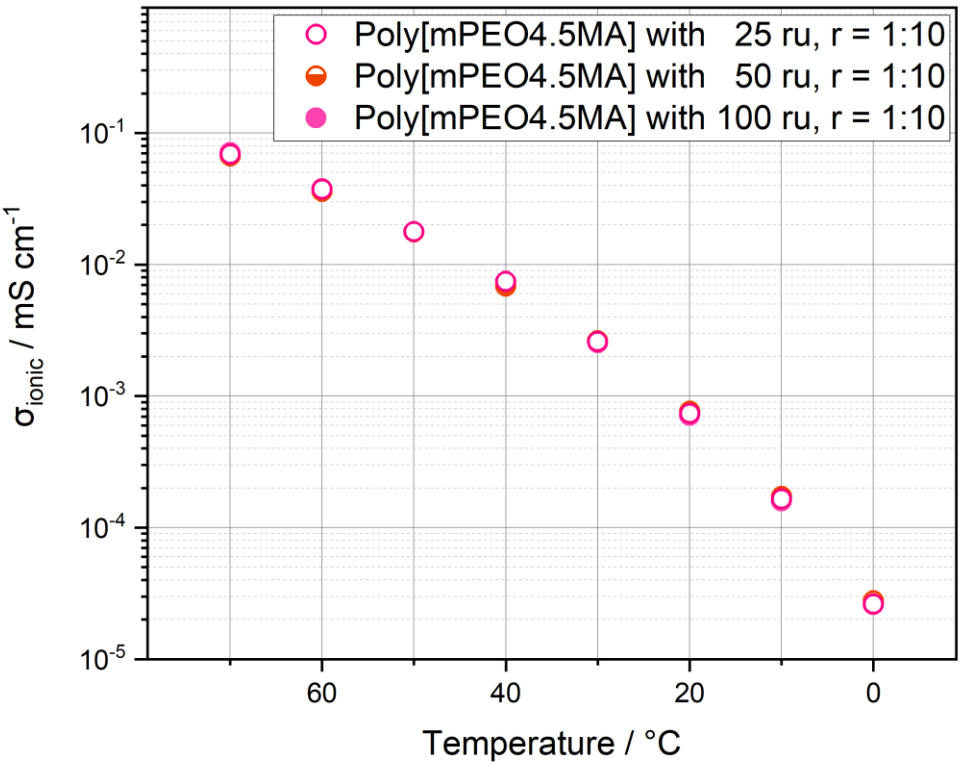

FIGURE 3: *Ionic conductivities of electrolytes from homopolymers in a temperature range from 0 to 70°C. The graph shows homopolymers with different backbone lengths synthesized from mPEOxMA with x = 4.5. For this measurements, all polymers were mixed with LiTFSI in the ratio [Li⁺]:[EO] of 1:10.*

For homopolymers with short PEO side chains, a significant influence of the backbone length for poly(mPEO4.5MA) was not observed (see fig. 3). All conductivity values are quite similar when comparing homopolymers with 25 ru, 50 ru and 100 ru and small deviations might more likely result from small errors while assembling the cells or inaccuracy of the measurement than the polymer architecture itself.

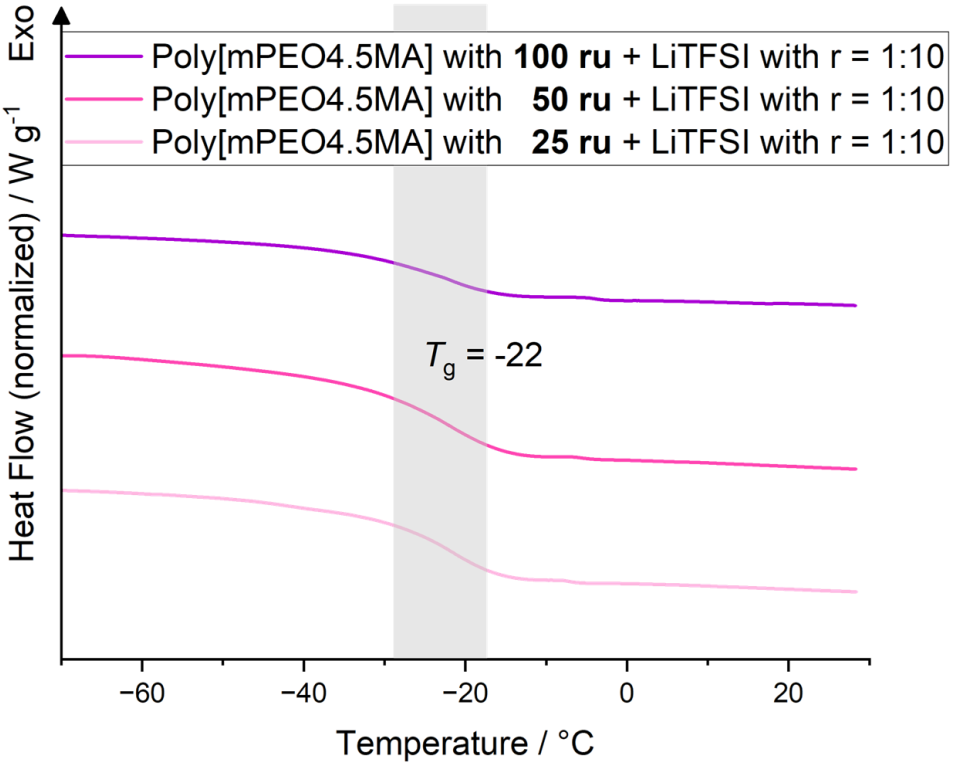

FIGURE 4: *Exothermic heating curves from DSC measurement from electrolytes of polymers with 100, 50 and 25 ru and x = 4.5. The respective value for the glass transition point for all three samples is noted in black color and the temperature range is marked with a grey box. The ratio [Li⁺]:[EO] is 1:10 for all electrolytes.*

Differential scanning calorimetry measurements moreover confirmed a common glass transition point at -22 °C (see figure 4). This higher T_g in comparison to the T_g of homopolymers with longer side chains most likely is a result of stiffness caused by the close distance to the methacrylate backbone. The lose end EO repeating units of longer side chains at some point reach a critical distance from the backbone at some point, which allows them to move more freely afterwards.

For the medium PEO side chain length, the influence of the backbone is still small but detectable (see fig. 5). With increasing the number of repeating units in the backbone the ionic conductivity of the resulting electrolyte decreases at 70 °C from 0.25 mS cm^{-1} (15 ru) to 0.14 mS cm^{-1} (100 ru). At lower temperatures the effect of the backbone length gets less significant. In particular the ionic conductivity at 0 °C is 2.93 x10^{-4} mS cm^{-1} (15 ru) and decreases to a value of 1.78 x10^{-4} mS cm^{-1} (100 ru) when increasing the backbone length.

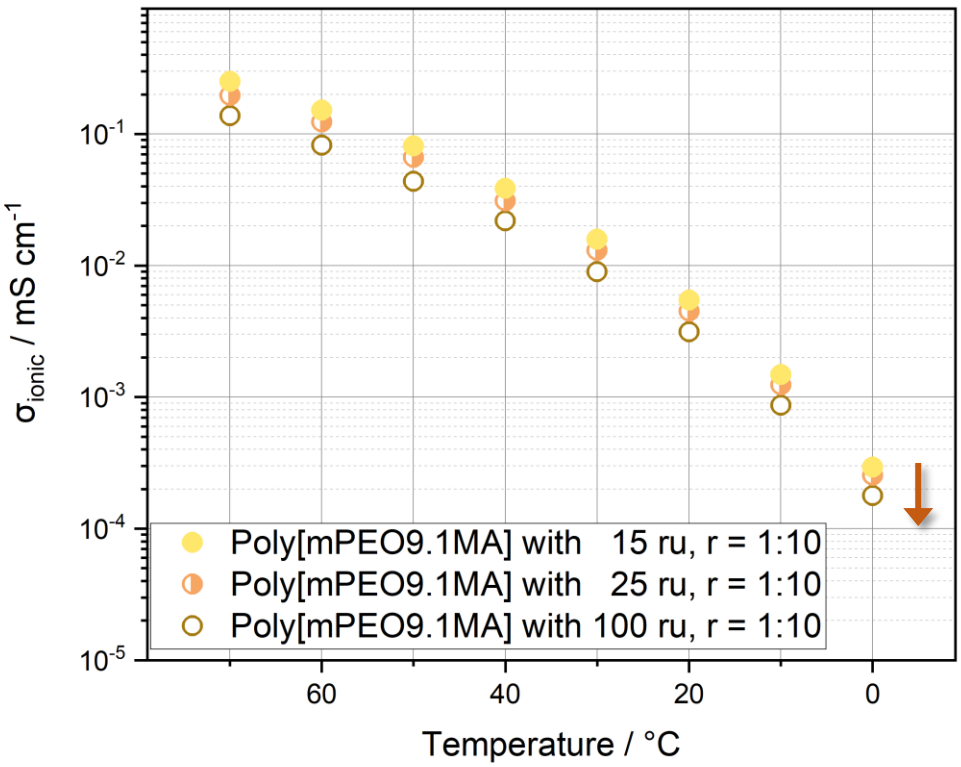

FIGURE 5: *Ionic conductivities of electrolytes from homopolymers in a temperature range from 0 to 70°C. The graph shows homopolymers with different backbone lengths synthesized from mPEOxMA with x = 9.1. For this measurements, all polymers were mixed with LiTFSI in the ratio [Li^+]:[EO] of 1:10.*

Differential scanning calorimetry measurements moreover confirmed a glass transition point varying of -43 °C for the two longer backbones. The difference between them and the -41 °C (for 25 ru) and -42 °C (for 15 ru) are neglectable (see fig. 6). This temperature range lies between homopolymers with longer (T_g = -46 °C) and shorter (T_g = -22 °C) side chains.

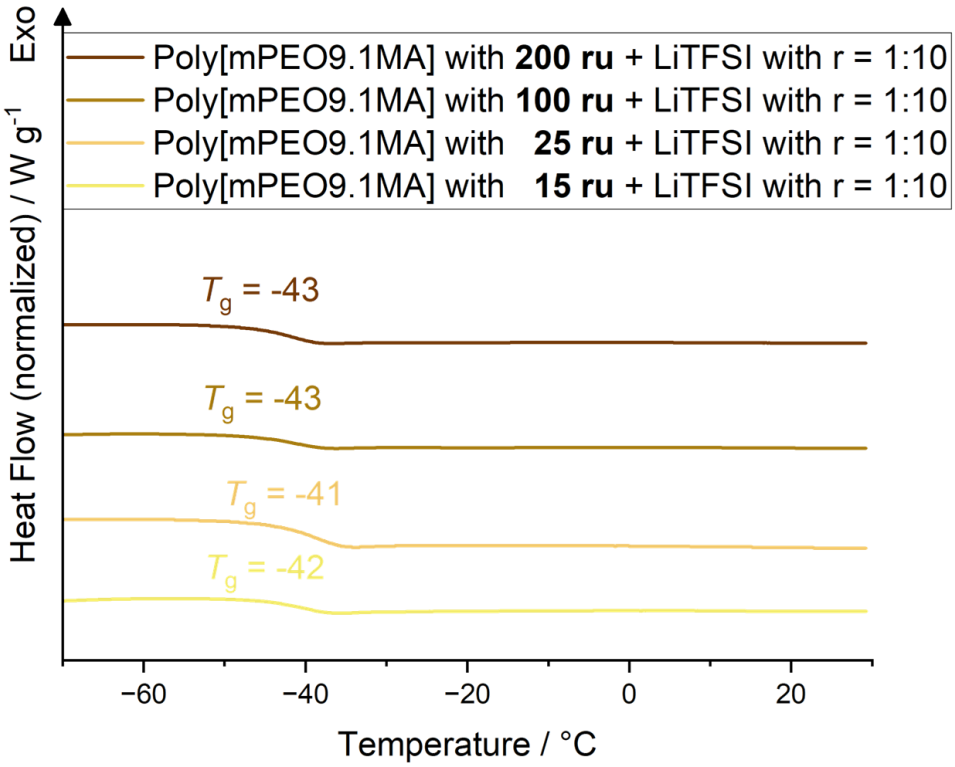

FIGURE 6: *Exothermic heating curves from DSC measurement from electrolytes of polymers with 200, 100, 25 and 5 ru and x = 9.1. The respective value for the glass transition point for each sample is noted in the respective color. The ratio [Li^+]:[EO] is 1:10 for all electrolytes.*

When decreasing the backbone length of the polymers with longer PEO side chains the ionic conductivity increases further (see fig. 7). In other words, to reach the highest possible ionic conductivity for this system, homopolymers with a low number of repeating units in the backbone as well as a long PEO side chains are favorable. If the chemical architecture is optimized accordingly, a total increase of one (at 70°C) up to two orders of magnitude (at 0°C) in the ionic conductivity is possible.

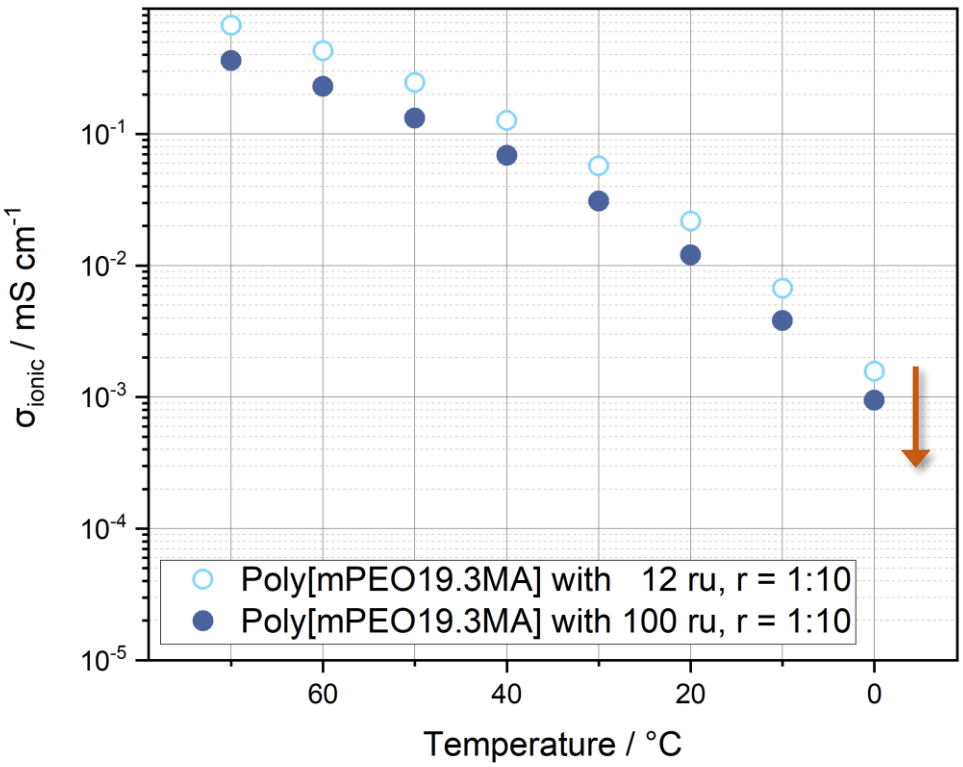

FIGURE 7: *Ionic conductivities of electrolytes from homopolymers in a temperature range from 0 to 70°C. The graph shows homopolymers with different backbone lengths synthesized from mPEOxMA with x = 19.3. For this measurements, all polymers were mixed with LiTFSI in the ratio [Li^+]:[EO] of 1:10.*

Differential scanning calorimetry measurements moreover confirmed a common glass transition point at -46 °C for the electrolytes from homopolymers with the longest side chains (see fig. 8). This T_g lies closest to the T_g of about -60 °C for pure homopolymers with no Li-salt addition.

In conclusion the change of T_g with addition of LiTFSI in the same ratio of $[Li^+]$:[EO] is dependent on the side chain length. A possibility to explain this behavior is with the different solvation capability in different areas of the side chain. If the solvation in close distance to the backbone is less favored and additionally the chain mobility low the Li-ion transport is hindered most in the brush polymer electrolytes with short PEO side chains. This is the case because one side of the PEO chain is attached to the backbone and the degree of freedom to entangle and assemble randomly is very restricted with only 4.5 ethylene oxide repeating units.

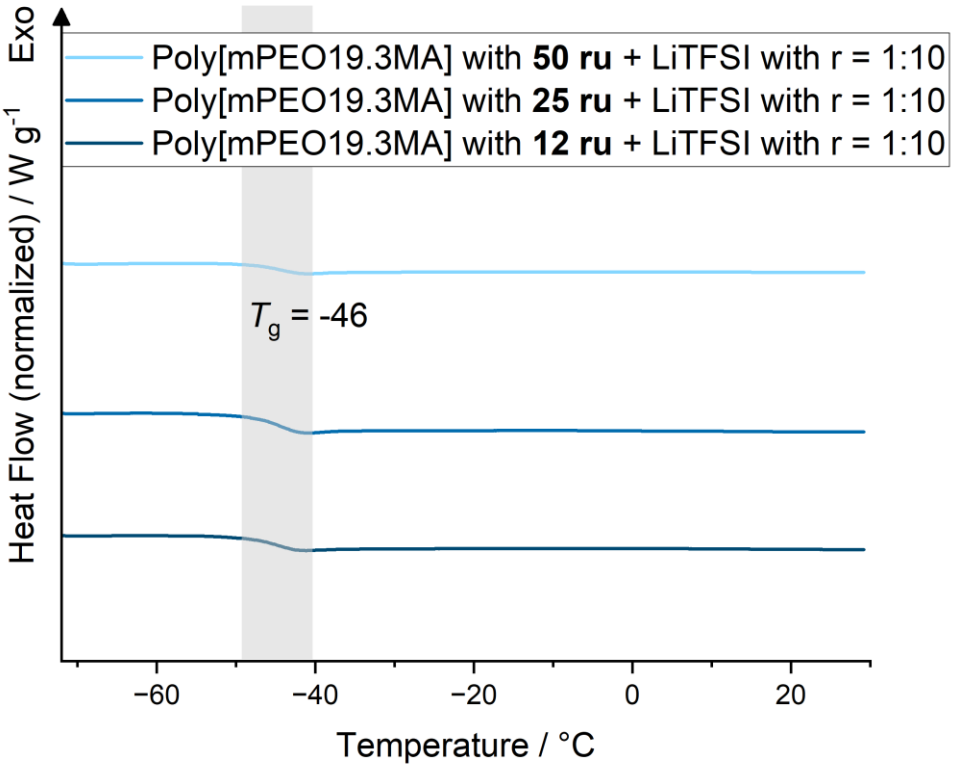

FIGURE 8: *Exothermic heating curves from DSC measurement from electrolytes of polymers with 50, 25 and 12 ru and x = 19.3. The respective value for the glass transition point for all three samples is noted in black color and the temperature range is marked with a grey box. The ratio $[Li^+]$:[EO] is 1:10 for all electrolytes.*

It is common knowledge regarding conductivity of polymers that a higher degree of crystallization leads to larger domains with isolating properties. If we now look at the data given in this chapter this can not be the critical parameter influencing conductivities, since none of the electrolytes showed a T_m and no significant drop at a certain temperature in the ionic conductivity. It seems to be the effect of the mobility of the PEO chain. The finding is that shorter side chains do not contribute much to Li^+ transport and result in low ionic conductivities even if they do not crystallize. The fact that the presence of relatively long chains on a short backbone leads to a higher ionic conductivity also gives a hint that a beneficial higher chain mobility could origin from the orientation of the backbone. Those polymers can align in a more random way relative to each other, since the rigidity of the backbone is only conducing the small amount of attached side chains. The backbones of neighboring polymers can have a different orientation in space and therewith align more beneficial for inter-chain hopping of Li-ions. When attached to long backbones the ionic conductivity of the resulting electrolyte is lower, this could arise from a stricter alignment of PEO chains in the bulk material, where intra-chain hopping is favorized.

It has to be mentioned that this behavior is tightly linked to the amount of Li-salt added to the polymer. The homopolymer with x = 19.3 and without any LiTFSI addition is a solid at room temperature and already can be observe crystallization while cooling down after drying or latest after 24 h. This is a behavior which is also observed in linear PEO by Marzantowicz et al.[69]

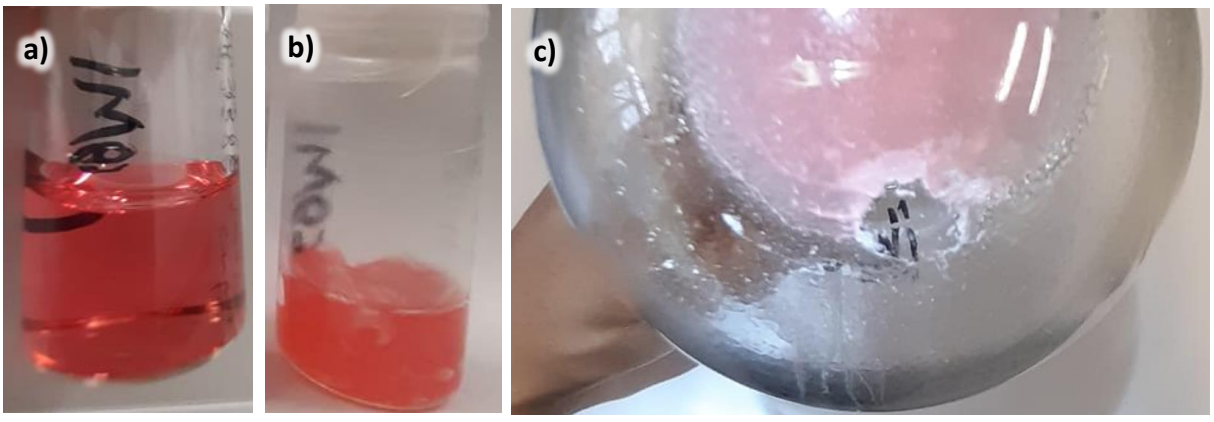

FIGURE 9: *Pictures of poly(mPEO19.3MA) with 100 ru a) right after drying at 60 °C and still fluid b) the same sample; cooled solid polymer at room temperature c) same polymer dried after dialysis also at room temperature with a dotted pattern on the wall of the flask.*

In figure 9 a poly(mPEO19.3MA) sample with 100 repeating units per backbone is shown. The product was therefore washed (several times with cooled n-hexane) for purification and the

solvents were removed under reduced pressure. Picture a) shows the fluid polymer at 60 °C and picture b) the exact same sample in its solidified version at room temperature. The first one (a)) is a viscous fluid and the second one (b)) is brittle upon pressure and circular shapes can be observed in the bulk. After drying of the further purified product (via dialysis) at room temperature, the polymer (c)) shows a dotted pattern throughout the bulk and at the wall of the flask. The polymer chips into circular flakes with different sizes upon applied pressure with a spatula.

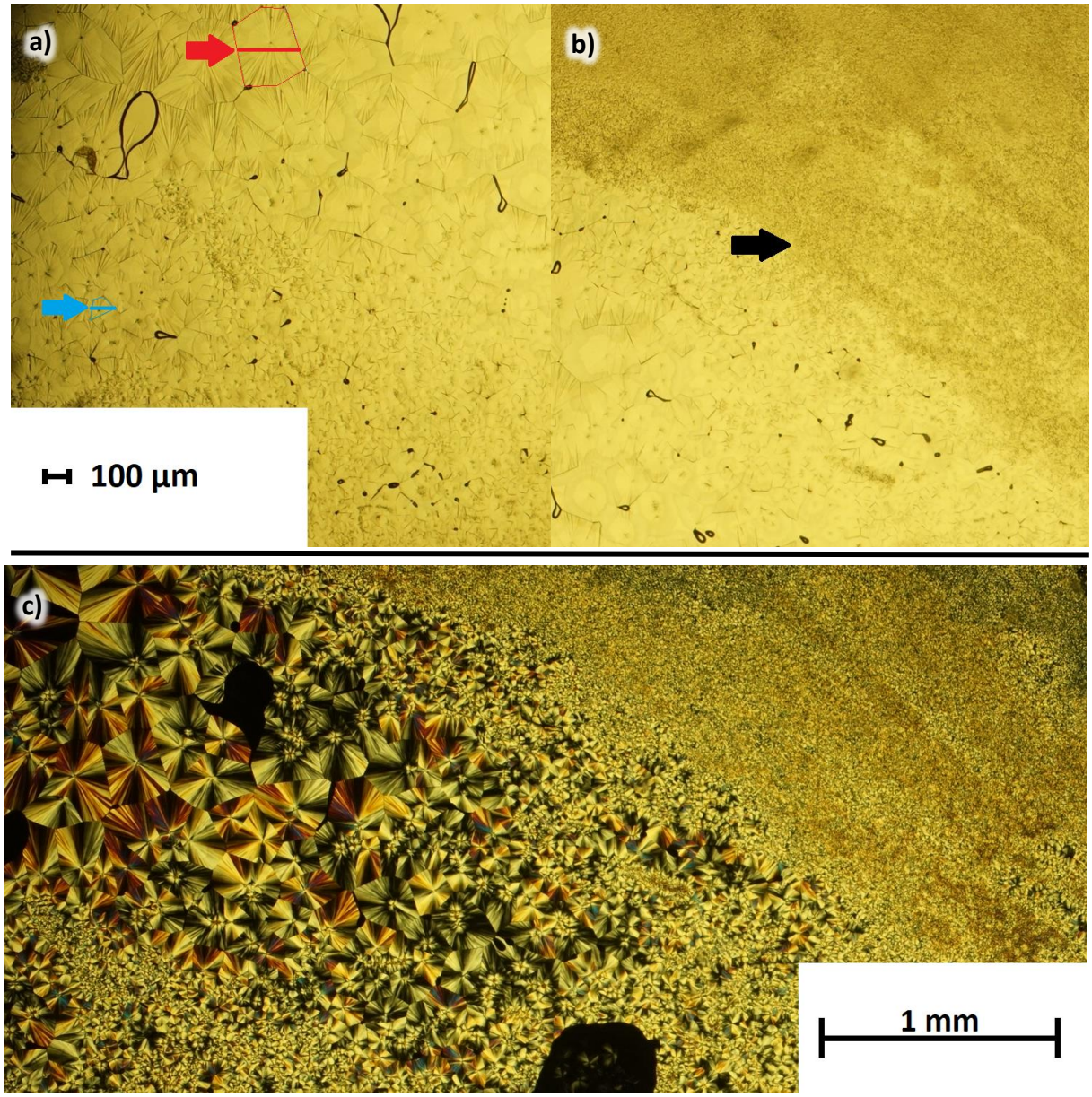

FIGURE 10: *Microscope images of poly(mPEO19.3MA) with 100 ru. a) Two representative spherulites in this crystalline domain are denoted in red and blue. b) The border from the crystalline phase to an area with crystallites in a much smaller size (marked with a black arrow). c) Image of the same area taken with a 90° polarization filter.*

To look at the crystallization pattern more closely the sample was examined under a light microscope (see Fig 10). In the picture a) two representative spherulitic crystallites for the sample are marked in red and blue. The red one is according to optical evaluation 243 µm and the blue one 95 µm wide. In the second picture (see Fig. 10 b)) the border of the crystalline phase to a less ordered area is marked with a black arrow. In the photograph where a polymerization filter was used (see fig. 10 c)) it is visible that also the area on the top right side in b) consists of crystallites with a size about 10 times smaller than the one marked in red in a). This observation confirms an inhomogeneous microstructure containing spherulites of different sizes. For pure PEO a spherulitic crystallization is well-known in literature[69,70] and it stands to reason that they also form for brush polymers with PEO side chains. It applies that the electrolytes from pure PEO and Li-salt still show spherulites which correlates with a significant decrease in ionic conductivity due to crystallization below 30 °C. However, for the PEs from brush polymers at hand this crystallization was not observed. With addition of LiTFSI as described in the experimental section, the crystallization is suppressed. On the other hand, if the polymer and the Li-salt are not dissolved and the combined solutions stirred for hours, but stirred without solvent at elevated temperatures, the spherulites reappear along with colorless Li-salt crystals.

Although no clear drop in ionic conductivity is observed at a certain temperature, the conductivity values decrease slow at high temperatures and faster in the low temperature regime. Generally, when comparing temperature dependent ionic conductivities of polymers with different x the measured values at high temperatures differ only slightly and at lower temperatures these differences become more obvious. The obtained values corresponding to this behavior can be explained with the Vogel-Tammann-Fulcher (VTF) equation which is typically used for PEO-based electrolytes.[71]

3.2. Copolymers with mPEOyMA

Ji et al.[26] stated in 2022 that lower grafting density leads to more free volume to reduce PEO packing and entanglement among side chains to accelerate segmental dynamics and ion transport. They found that decrease of the grafting density by polymerization with MMA as copolymer leads to an overall lower ionic conductivity for mPEOxMA with x < 43.2 compared to the corresponding homopolymer.

This findings are in good accordance with the fact that PMMA hardly conducts lithium ions at all and therefore lowers the lithium-ion conducting mass fraction in the polymer.[72] To prevent a complete drop of ionic conductivity due to isolating PMMA blocks, in this work we focus on distortion of the microstructural order by copolymerization with mPEOxMA with relatively shorter PEO side chains instead (see scheme 8). Specifically the longer PEO side chains which tend to crystallize with one another[69] should rather form amorphous domains or at least keep crystalline domains on smaller range when offered mPEOxMA with shorter side chains as direct neighbors. The segments of the longer side chain that exceed the small side chain neighbor could show accelerated segmental dynamics in the free volume and enhance the ionic conductivity. To investigate this effect on a fundamental level an extensive matrix of copolymers was synthesized. The corresponding approaches are listed in table 2. For all polymers, the given ratio of monomers also represents the targeted number of repeating units per chain.

In the following, copolymers are presented, where the percentage of comonomer and the length of the PEO side chain was varied systematically.

Random copolymers

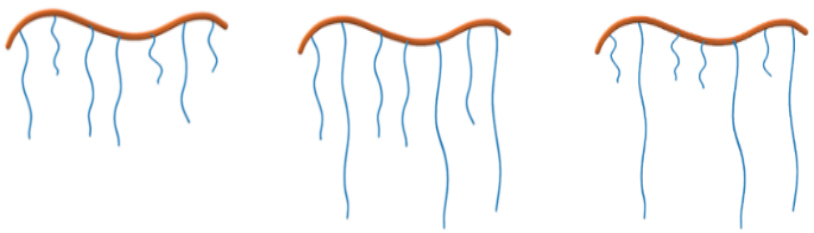

SCHEME 6: *Simplified depiction of general structure of synthesized copolymers with different percentages of monomers with different side chain lengths.*

By varying the composition of the copolymers with different side chain lengths a change in the ionic conductivity of the resulting electrolyte can be observed (see figure 2). In figure 11 the ionic conductivity of the homopolymers of the respective monomers mPEO4.5MA and mPEO19.3MA along with their copolymers in a ratio of 80:20 and reversed is depicted. When comparing the ionic conductivities, it becomes obvious that the electrolyte property is mainly dominated by the conductivity of the longer side chains. As a result, the homopolymer with the longest side chains still shows the best ionic conductivity. At 0 °C the ionic conductivity for the copolymer with 20 equivalents of mPEO4.5MA is approximately the same as for the homopolymer with the long side chains.

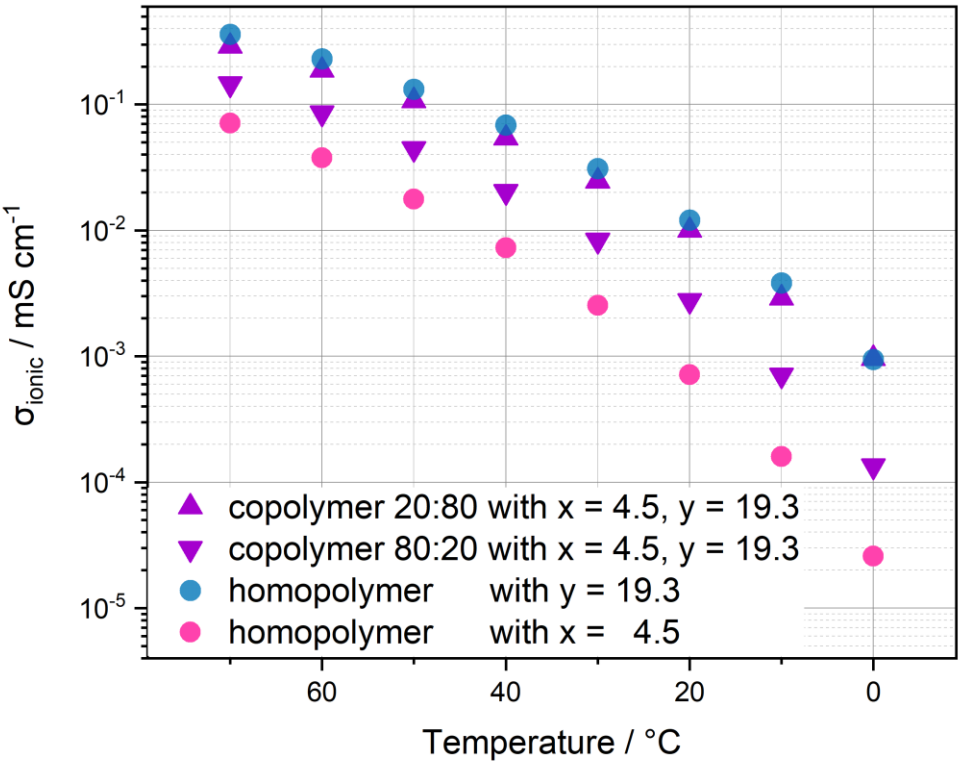

FIGURE 11: *Ionic conductivities of homo- and copolymers with x = 4.5 and y = 19.3 in a temperature range from 0 to 70°C. The copolymers are shown for combinations of 20:80 and 80:20 regarding the ratio of monomers mPEOxMA to mPEOyMA. For this measurements, all polymers were mixed with LiTFSI in the ratio [Li^+]:[EO] of 1:10.*

The measured glass transition points (see fig. 12) for the copolymers Poly(mPEO4.5MA-*co*-mPEO19.3MA) with a molar ratio of the monomers of 80:20 (T_g = -45 °C) and 20:80 (T_g = -44 °C) seem to be counterintuitive, since a higher glass transition for the copolymer with 80 equivalents mPEO4.5MA from 100 equivalents in total (= total number of ru per backbone) would be expected. However, it must be considered, that the weight fraction (w %) of the longer side chains makes up more than half of the total polymer mass (compare table 2).

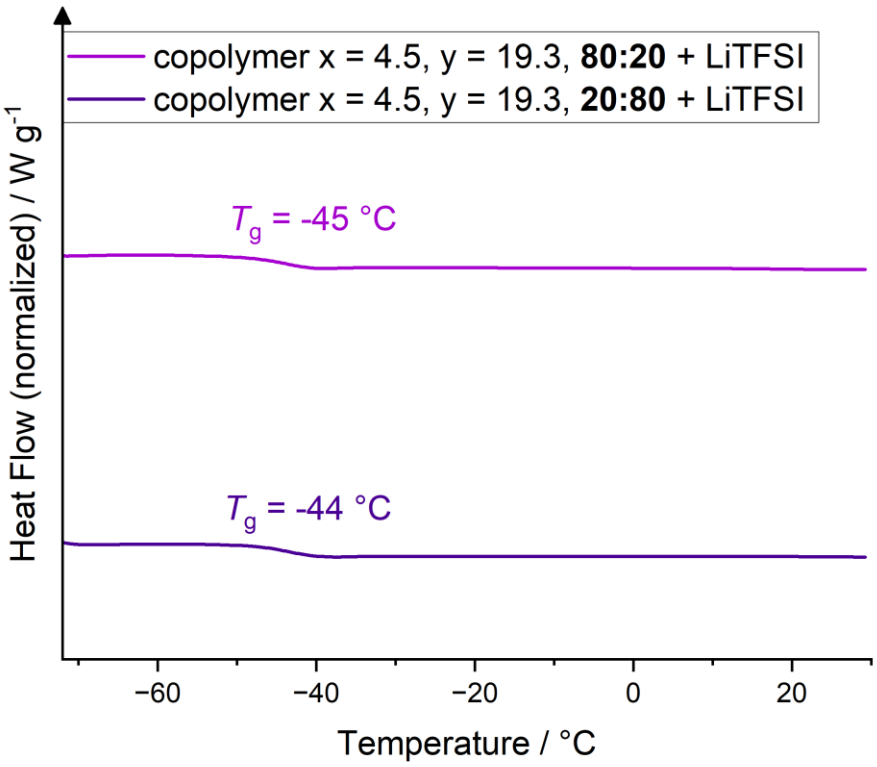

FIGURE 12: *Exothermic heating curves from DSC measurement from electrolytes of copolymers with the ratio 20:80 and reversed with x = 4.5 and y = 19.3. The glass transition points are noted in the respective color. The ratio [Li$^+$]:[EO] is 1:10 for both electrolytes.*

With an increasing mass fraction of long side chains, the ionic conductivity increases and the potential increase in conductivity due to elevated temperatures is smaller. However, there is no significant difference between the homopolymer with long side chains and the copolymer with a molar ratio of 20:80 (93 w % of mPEO19.3MA). The desired positive effect onto the ionic conductivity by reducing the grafting density by shorter neighboring side chains was not observed. On the other hand, the finding that 20 repeating units per backbone can be replaced by the smaller monomer could be interesting for atom economics, cost calculations and processability in the upscaling in industrial battery application.

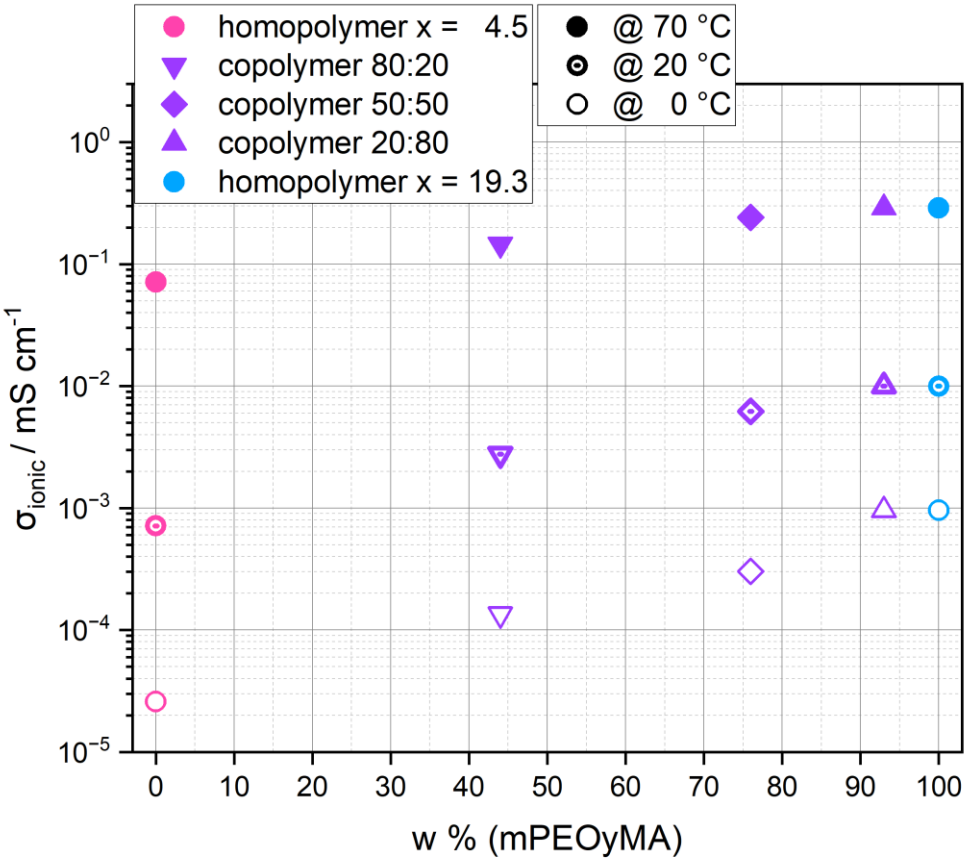

FIGURE 13: *Ionic conductivities of homopolymer poly(mPEO4.5MA), copolymers and poly(mPEO19.3MA) at three different temperatures (0 °C, 20 °C, 70 °C) depending on the weight fraction of mPEO19.3MA in the polymer.*

According to the above discussed data it seems that short side chains do not participate much in the ion transfer and also do not enhance the ion transfer in neighboring long side chains in copolymers by free volume. To the contrary, the ionic conductivity decreases with addition of the short side chain monomer. If this observation results from the short distance from the backbone and the associated disadvantages (e.g., low Li-salt solvation and segmental motion), the ionic conductivity of copolymers with x = 9.1 and y = 19.3 should show values close to or higher than those of the homopolymer with the long side chains.

Unfortunately, this is also not the case (see fig. 14). When comparing all the copolymers with a ratio of 20:80 (with 80 equivalents of the relatively larger monomers) the effect of convergence towards the ionic conductivity of poly(mPEO19.3MA) proves to be true for the two copolymers containing mPEO19.3MA. The T_g for poly(mPEO4.5MA-*co*-mPEO19.3MA)

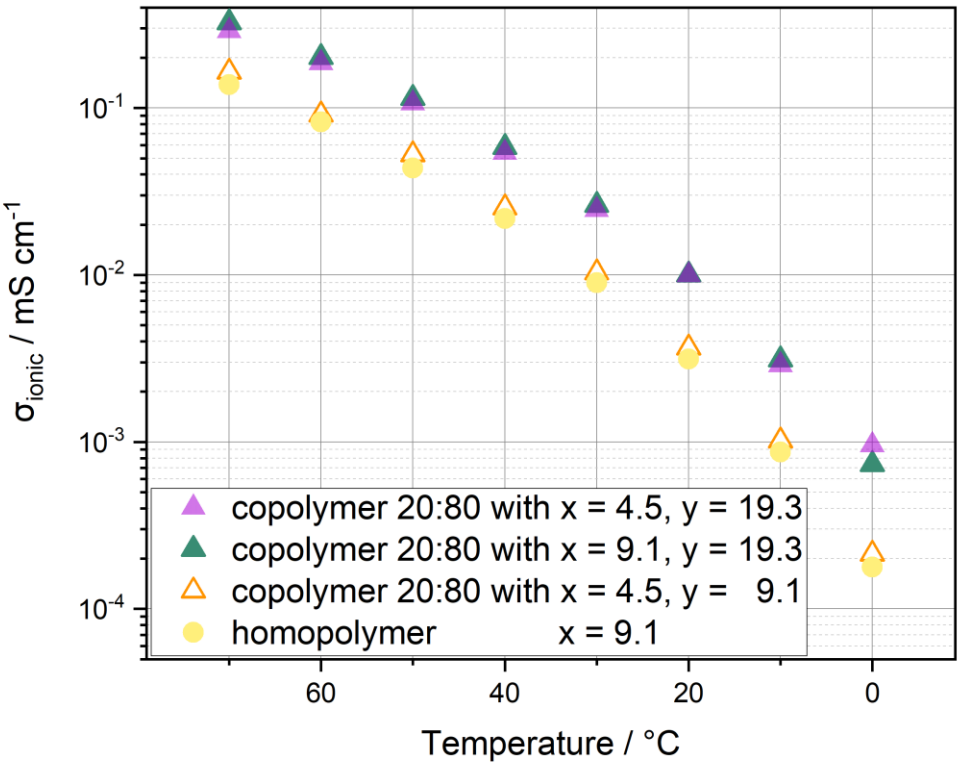

FIGURE 14: *Ionic conductivities of homopolymer with x = 9.1 and copolymers in a ratio of 20:80* regarding the *ratio of monomers mPEOxMA to mPEOyMA* in a temperature range from 0 to 70°C. *For this measurements, all polymers were mixed with LiTFSI in the ratio [Li⁺]:[EO] of 1:10.*

is -44 °C and for poly(mPEO9.1MA-*co*-mPEO19.3MA) -46 °C and unsurprisingly also no melting point was observed (see table 9). The copolymer derived from the two smaller monomers (x = 4.5, y = 9.1) on the other hand delivers higher conductivities (and T_g = -42 °C, see 5) than the corresponding homopolymers shown in fig. 1. This finding cannot be described by the conductivity of one of the contributing monomers dominating the material properties. The increase in the ionic conductivity of poly(mPEO4.5MA-*co*-mPEO9.1MA) could possibly arise from a less complex local self-assembly, less entanglement and therefore higher chain mobility, compared to the longest side chains. Nevertheless, the effect leads to only slightly increased ionic conductivities and is no potential pathway to exceed the performance of poly(mPEO19.3MA) and its copolymers.

In conclusion neither the number of repeating units in the side chain or the weight fraction of long PEO side chains, nor the T_g of the PEs alone is a suitable parameter to predict the influence on the ionic conductivity. This is proof for the complex trade-off between multiple parameters. To clarify if the copolymerization is more beneficial for the microstructure than the blend a reference system was used. The respective homopolymers were blended with each other (in the same percentage as in the copolymer with a backbone repeating unit of 100 for the homopolymers that were blended) and the data reveals slightly higher ionic conductivities for the blends at 70 °C (see fig. 15). At higher temperatures the values exceed those for the copolymer but below 30 °C the copolymer performs better or equally good. This is true for poly(mPEO4.5MA-*co*-mPEO19.3MA).

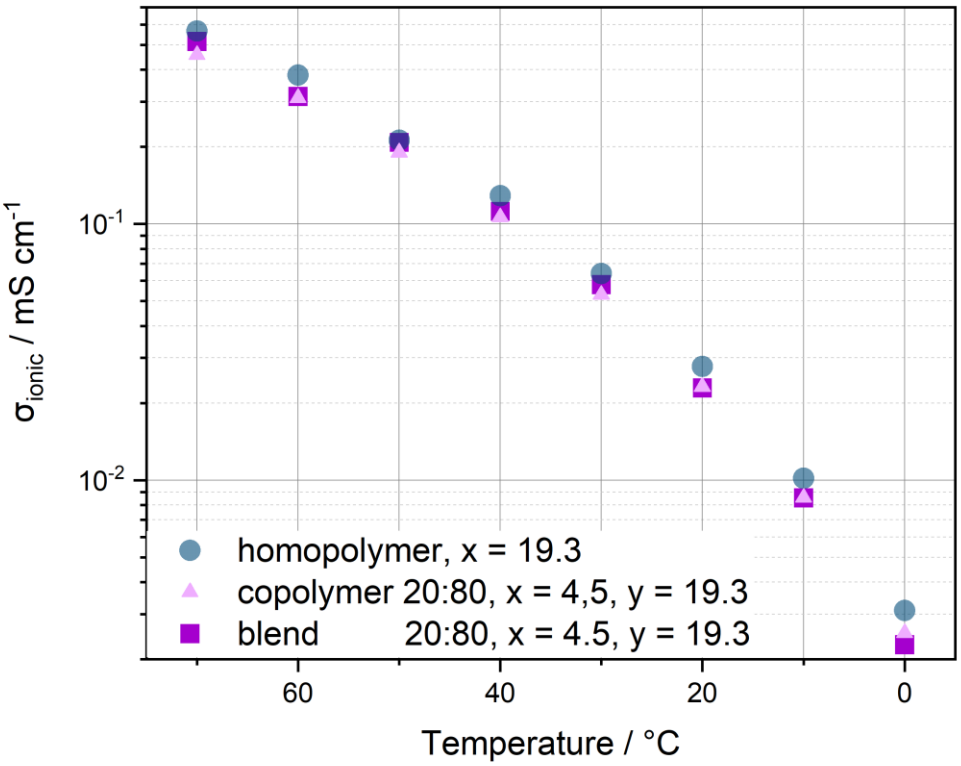

FIGURE 15: *Ionic conductivities of homopolymer and copolymer poly(mPEO4.5MA-co-mPEO19.3MA) as well as blend of the respective homopolymers measured in a temperature range from 0 to 70°C. For this measurements, all polymers were mixed with LiTFSI in the ratio [Li⁺]:[EO] of 1:15.*

For poly(mPEO9.1MA-*co*-mPEO19.3MA) the conductivity of the blend decreases more rapidly at lower temperatures compared to the conductivity of the corresponding copolymer (see fig. 16). Below 40 °C already, the copolymer shows higher conductivities and converges towards the conductivity values of the homopolymer. Although the mentioned differences are extremely low one can observe the trend at lower temperatures. Most likely this is due to a more uniform microstructure characteristic for copolymers due to the fixed chemical structure in comparison to free self-assembly with homopolymers. Since different side chain lengths have different solvation ability it could be the case that domains with homopolymers with shorter side chains locally hinder a small fraction of the lithium transference.

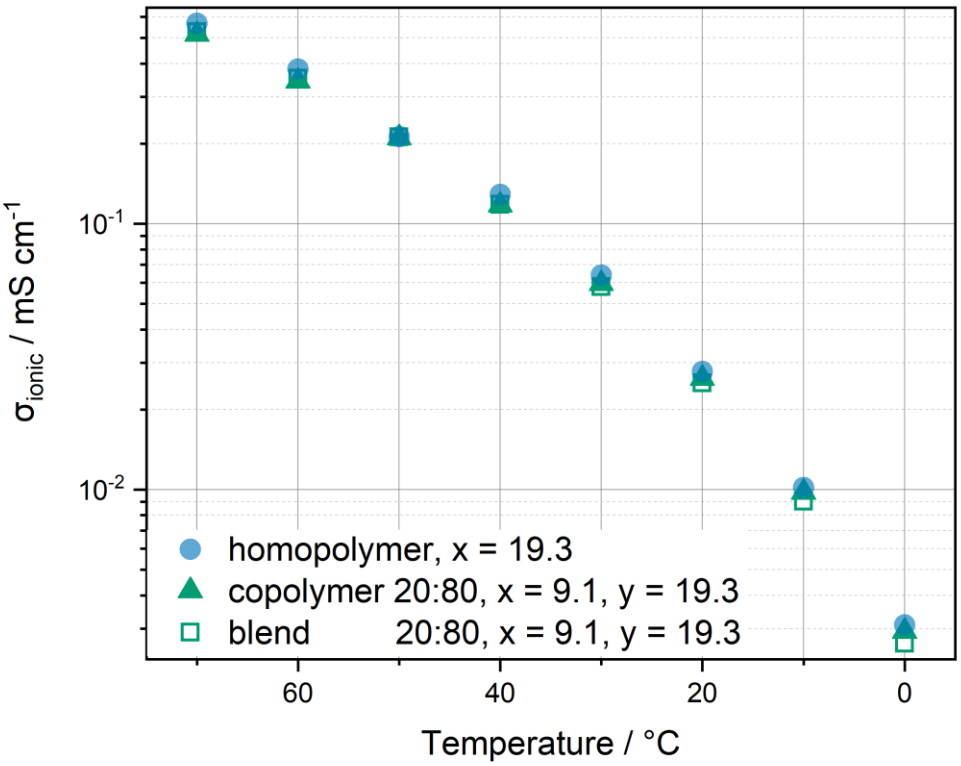

FIGURE 16: *Ionic conductivities of homopolymer and copolymer poly(mPEO9.1MA-co-mPEO19.3MA) as well as blend of the respective homopolymers measured in a temperature range from 0 to 70°C. For this measurements, all polymers were mixed with LiTFSI in the ratio [Li^+]:[EO] of 1:15.*

3.3. Copolymers with 2-ethyl hexyl methacrylate (EHMA)

In literature examples of copolymerization with monomers forming rigid high T_g polymers is widely discussed.[14,16,73] The concept of copolymerization with EHMA was utilized to compare the previously shown copolymers to another type of copolymer with a T_g below the investigated working temperature. In contrast to copolymerization with the PEO-based monomers the viscosity increased but was not sufficient to process the polymer into self-standing PE membranes without further addition of plasticizers. The material shows an interesting mechanical behavior whilst cell assembly. When pressure is applied it tends to break, while without pressure it behaves as a high viscous fluid. Since copolymers can drive phase separation dependent on specific composition, a matrix was synthesized. A possibly favorable phase separation was not achieved according to the measured ionic conductivities. As a result of reducing the conductive volume fraction by replacing PEO chains with non-conductive alkanes the ionic conductivity of the electrolytes drops significantly for all synthesized PEs (compare to temperature depended ionic conductivities for an exemplary copolymer in fig. 17). The notably negative influence onto the ionic conductivity of EHMA as a comonomer points if anything to the participation of short PEO side chains in the ionic conductivity of the bulk material. The results also underline the already well functioning conductive behavior of the PEO-based brush polymers.

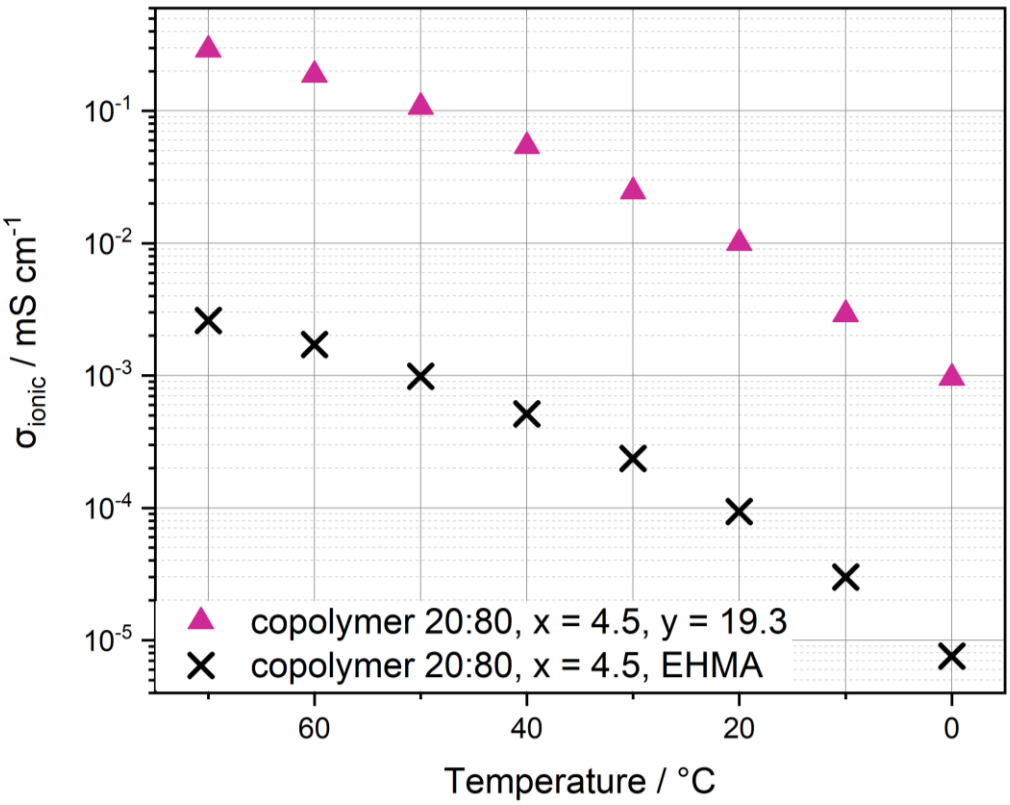

FIGURE 17: *Ionic conductivities of copolymers of mPEO19.3MA with the comonomers mPOE4.5MA or EHMA (in a ratio of 80:20) over a temperature range from 0 to 70°C. For impedance measurements, all polymers were mixed with LiTFSI in the ratio Li^+ to O-moiety in the PEO chain of 1:10.*

3.4. Effect of Li-salt concentration

The amount of LiTFSI added to the SPE and its influence onto the ionic conductivity has been investigated[74]. More in detail molecular dynamic simulations by Hahn et al.[75] reveal insight to the ion solvation and transfer via the crystallization. Within this the mechanical properties are affected. Variation of the ratio of Li^+ to oxygen moieties in the PEO side chain led to following observations of the resulting SPE and its ionic conductivity.

The ionic conductivity of polymer electrolytes with x = 4.5 is not changing significantly depending on Lithium salt concentration. In contrast to the T_g observed, which increases from -22 °C at a ratio of 1:10 (Li^+:EO) over -32 °C (1:15) up to -40 (1:20) approaching the value of -62 °C for polymer without Lithium salt addition (compare heating curves in fig. 18).

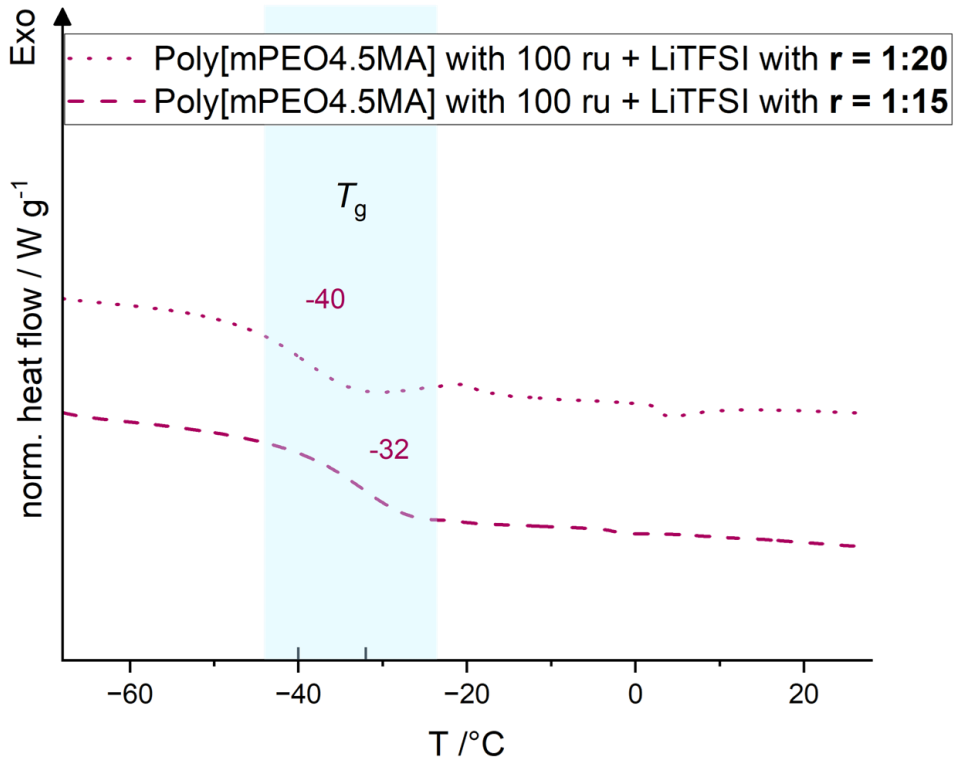

FIGURE 18: *Exothermic heating curves from DSC measurement from electrolytes of homopolymers with x = 4.5. The glass transition points are noted in the respective color. The ratios [Li^+]:[EO] are 1:15 and 1:20 for the depicted electrolytes.*

For the homopolymer with x = 9.1 a LiTFSI addition in a ratio of 1:20 (in comparison to 1:15 and 1:10 for the same polymer) leads to a significant increase of ionic conductivity (see fig. 19) as well as a decrease in T_g of 10 °C to -53 °C (see fig. 20). Further a ratio of 1:15 exceeds the conductivity values for 1:10 up to 50 °C. Above 50 °C electrolytes with a LiTFSI addition of 1:10 results in higher ionic conductivities. The latter is also true for homopolymers with x=19.3 (see fig. 22). In this case by contrast the ratio 1:20 is not favorable, rather a ratio of 1:15 should be chosen to achieve highest possible ionic conductivities.

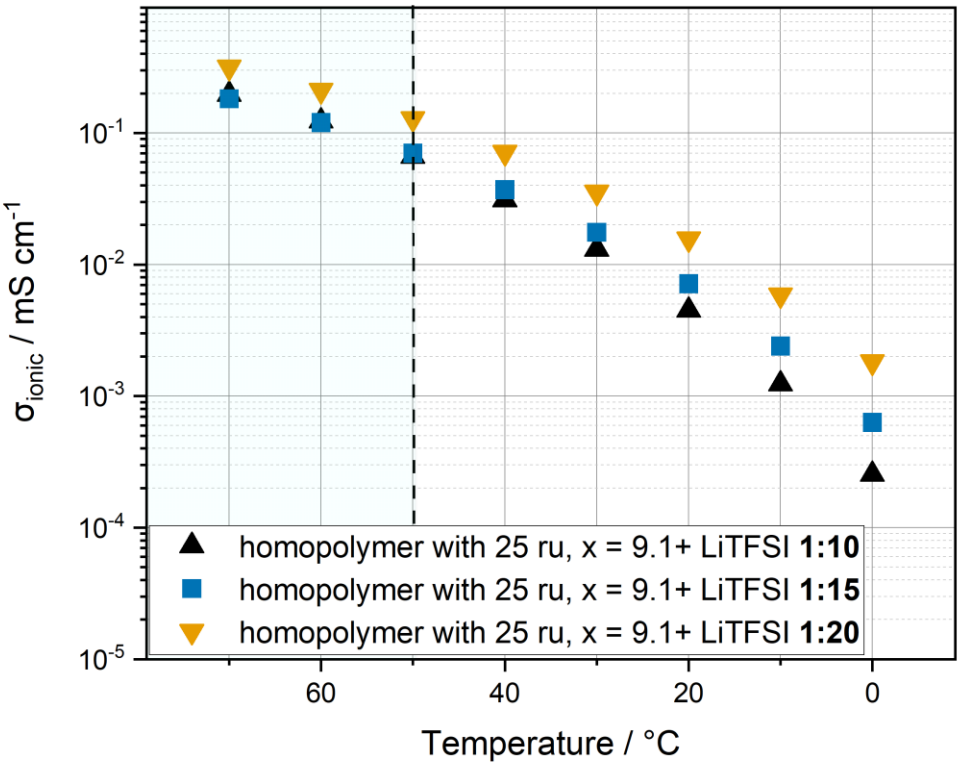

FIGURE 19: *Ionic conductivities of homopolymers with x = 9.1 over a temperature range from 0 to 70°C. For impedance measurements, the polymer was mixed with LiTFSI in the ratios [Li^+]:[EO] of 1:10, 1:15 and 1:20. The blue box symbolizes the temperature range and the dotted line the temperature up to which the PE with a LiTFSI addition of 1:10 outperforms the one with 1:15.*

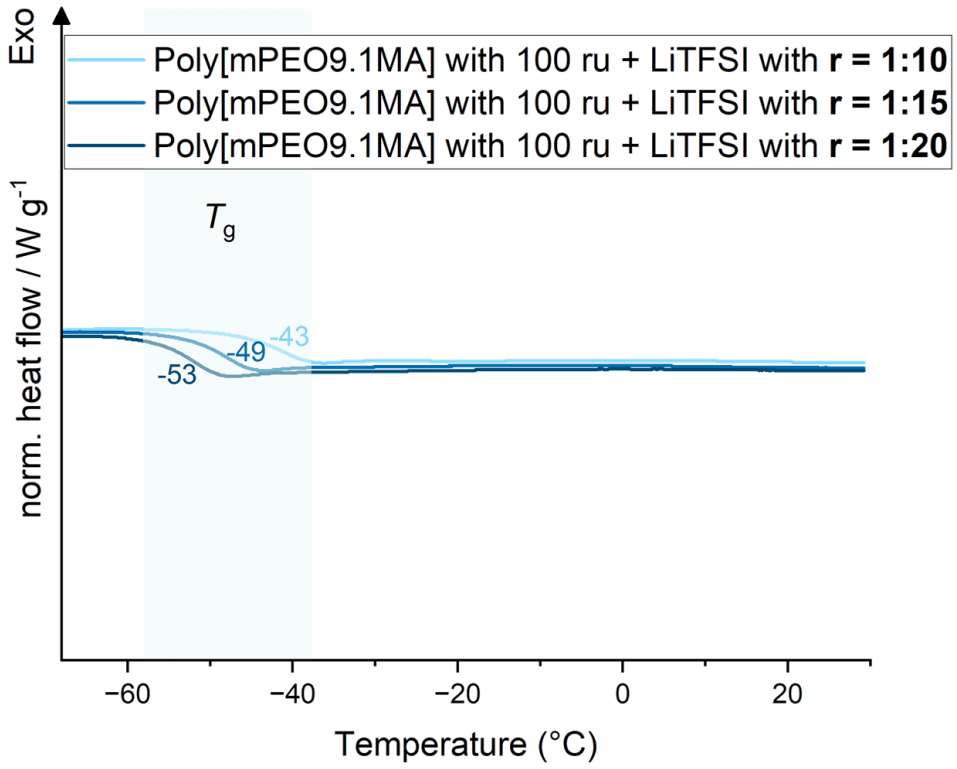

FIGURE 20: *Exothermic heating curves from DSC measurement from electrolytes of homopolymers with x = 9.1. The glass transition points are noted in the respective color. The ratios [Li$^+$]:[EO] are 1:10, 1:15 and 1:20 for the depicted electrolytes.*

The better performance of the PE with a Li-salt addition of 1:15 over the one with 1:10 cannot be explained by crystallization behavior. The latter shows a T_g = -46 °C and no melting point, the PE with less Li-salt (PE with 1:15) in contrary shows a T_g = -52 °C as well as a T_m = 22 °C (see fig. 21) and should therefore deliver lower values (at least below 22 °C) than the firstly mentioned. This complex interplay should rather arise from saturation of the ion-conducting side chains with either badly dissolved LiTFSI. Another possibility are slower segmental dynamics caused by Li-ions coordinated to different chains at the same time. This effect should work like temporary crosslinking in an ionic fashion.

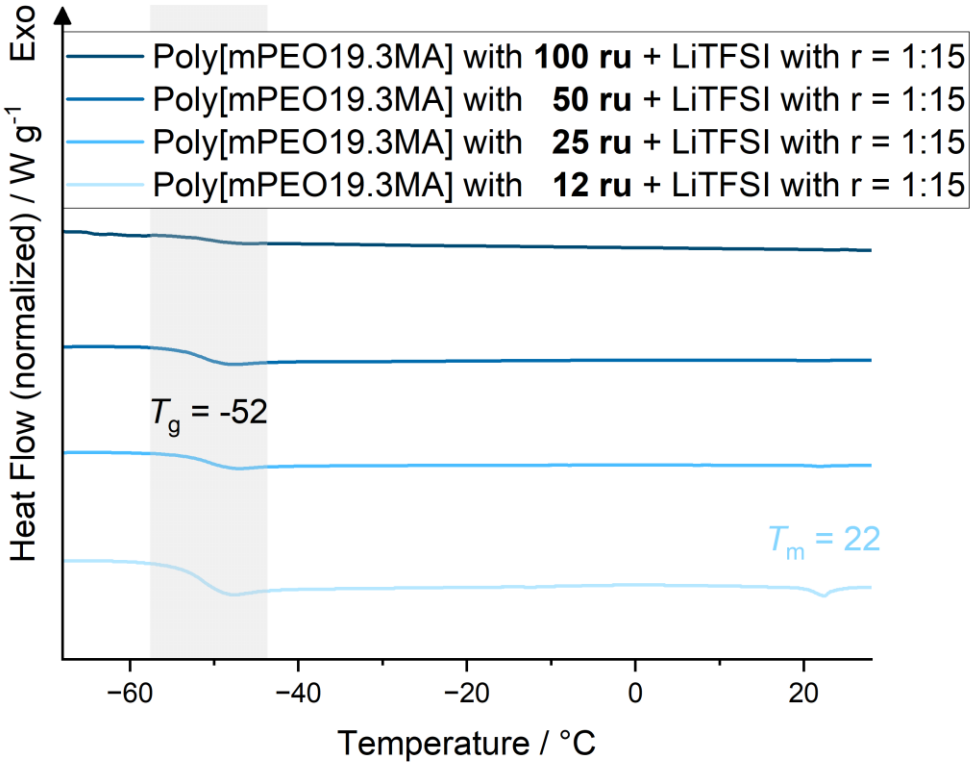

FIGURE 19: *Exothermic heating curves from DSC measurement from electrolytes of homopolymers with x = 19.3 and different repeating units in the backbone. The common glass transition point is noted in black color and the T_m (for the polymer with 12 ru) is noted in the respective color. The ratio [Li^+]:[EO] is 1:15 for the depicted electrolytes.*

Above 50 °C for homopolymers with x=19.3 (see fig. 22), LiTFSI additions of 1:10 as well as 1:15 result in higher ionic conductivities. In this case the ratio 1:20 is not favorable, rather a ratio of 1:15 should be chosen to in average over all temperatures achieve highest possible ionic conductivities.

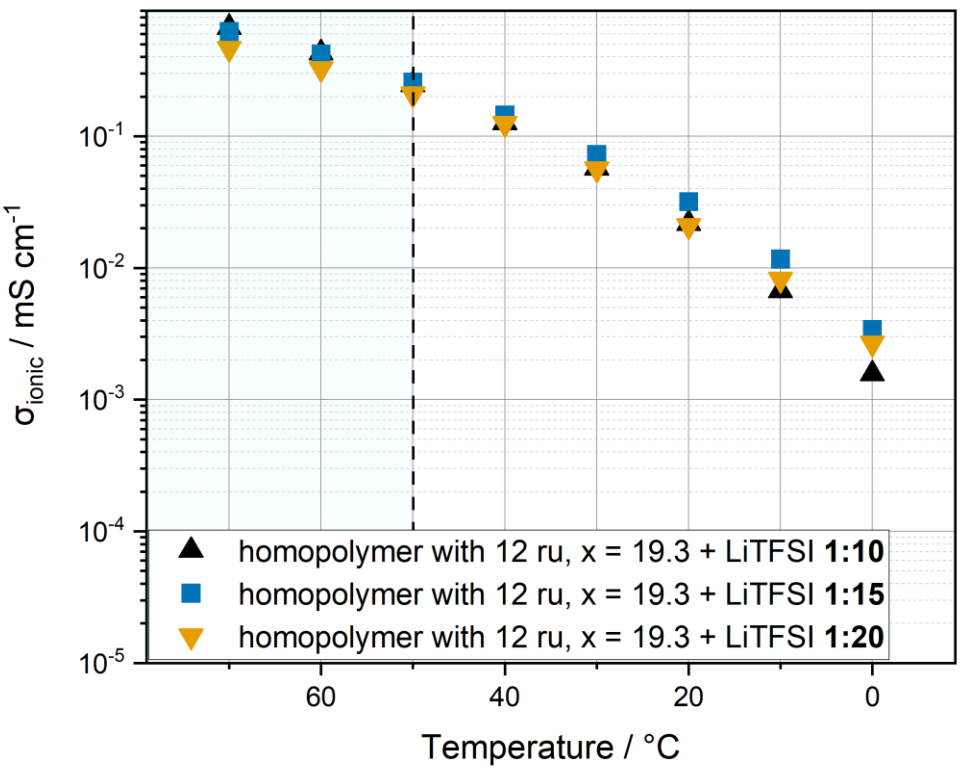

FIGURE 20: *Ionic conductivities of homopolymers with x = 19.3 over a temperature range from 0 to 70°C. For impedance measurements, the polymer was mixed with LiTFSI in the ratios [Li^+] to [EO] of 1:10, 1:15 and 1:20. The blue box symbolizes the temperature range and the dotted line the temperature up to which the PE with LiTFSI additions of 1:10 and 1:15 outperform the one with 1:12.*

The lower performance of the PE with a Li-salt addition of 1:20 can on one hand be easily explained with the respective DSC data that show an explicitly significant T_m at 27 °C (see Fig. 23) in comparison to the less concise melting point of the PE with a higher amount of LiTFSI. On the other hand, the decrease in ionic conductivity could be caused by the simple fact that there are not enough Li-ions available to maintain proper ionic conductivities. More in detail, domains with different concentrations of dissolved Li-salt could coexist and further the optimal morphology (comparable to transfer channels) is not formed throughout the bulk material. The resulting Li-ion transfer is slowed down when passing through less optimal domains. Most probably in reality both described effects exist next to each other. In the data for poly(mPEO19.3MA) with a lithium addition of 1:15 and 1:20 the trend can be observed that with a lower number of backbone repeating units and a lower LiTFSI content, the brush polymer behaves more and more like linear PEO with regard to crystallization.

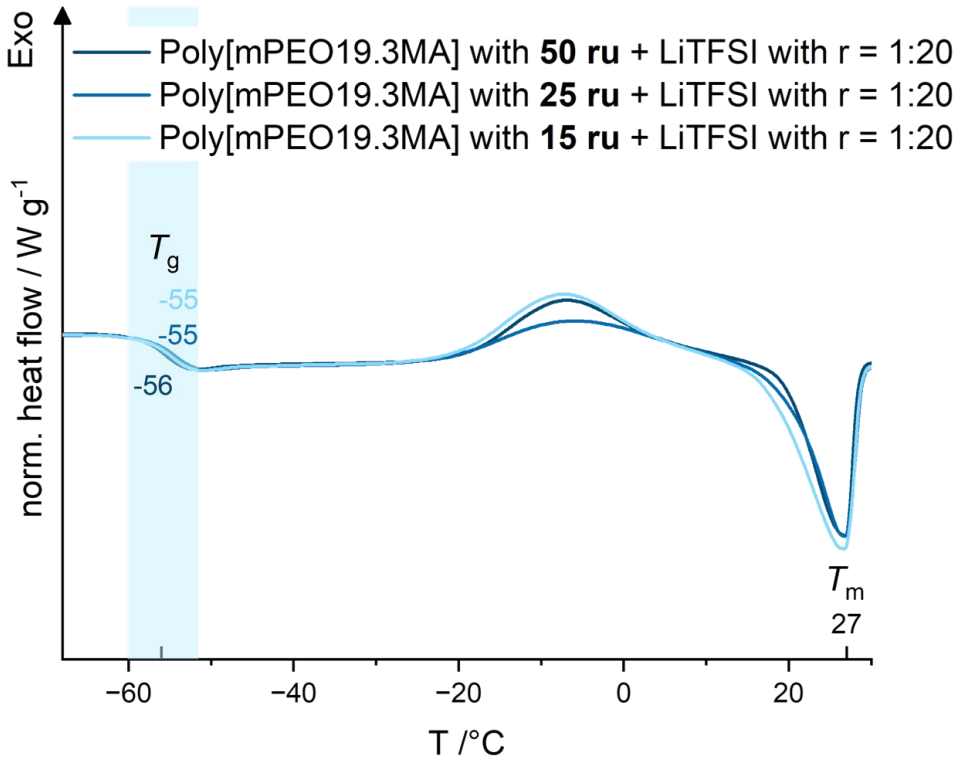

FIGURE 21: *Exothermic heating curves from DSC measurement from electrolytes of homopolymers with x = 19.3 and different repeating units in the backbone. The glass transition points are noted in the respective color and the common T_m is noted in black color. The ratio [Li^+]:[EO] is 1:20 for the depicted electrolytes.*

In this example it becomes obvious how complex the Li-salt addition affects the tendency for crystallization and the segmental motion of the brush polymers. An LiTFSI addition in the ratio 1:15 seems most beneficial with regard to the ionic conductivity, whereas a higher or lower amount of LiTFSI is not profitable. If looking at two extreme temperatures (0 °C and 70 °C, see fig. 24) it seems more likely that the accelerated chain dynamics at 70 °C (for the 1:20 PE) is not enough to overcome blocked ion pathways by segmental motion. In conclusion for the 1:20 ratio the reason for lower ionic conductivities can be a lack of enough Li-ions.

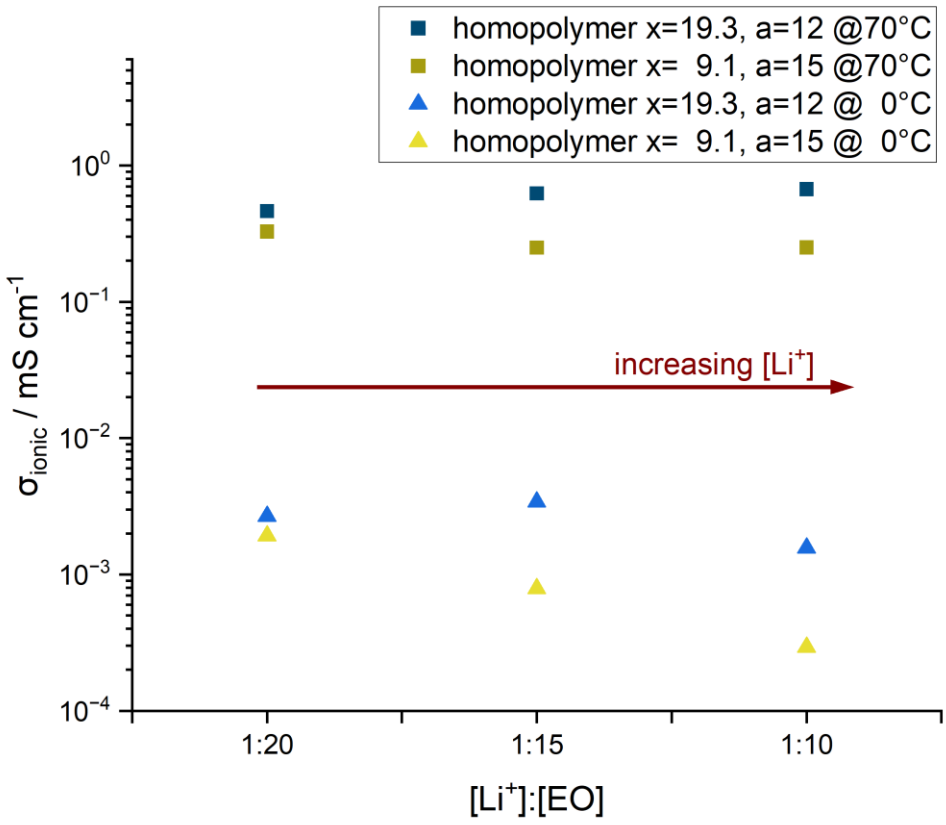

FIGURE 22: *Li-salt amount-dependent comparison of ionic conductivities of homopolymer poly(mPEO9.1MA) with 15 backbone repeating units and poly(mPEO19.3MA) with 12 backbone repeating units at 0 °C and 70 °C.*

When comparing the data for the copolymer Poly((mPEO4.5MA)-co-(mPEO19.3MA)) in the ratios of composition of 80:20 and 20:80 (compare figures 25 and 26) it is apparent, that a LiTFSI addition of 1:20 is beneficial for those copolymers dominated by mPEO19.3MA. The ratio 1:10 consistently shows the lowest possible values for ionic conductivity (see fig. 25). It is interesting though that the ionic conductivities for PE with a ratio of 1:15 converges to the highest measured values at low temperatures and the values for a ratio of 1:10 are significantly lower at all temperatures. This observation underlines the theory, that the solvation ability of mPEO4.5MA is lower. Therefore, the phase with longer PEO chains can dissolve more Li-ions itself (compared to a PE from the poly(mPEO19.3MA) homopolymer where 1:20 is not a sufficient ratio) and the ion transference is high. At temperatures below 20 °C the segmental motion is not sufficient anymore and the PE with 1:20 is outperformed

by the PE with 1:15. At ratios or 1:10 the copolymer is saturated and Li-ion transference is hindered by the inhomogeneous phase.

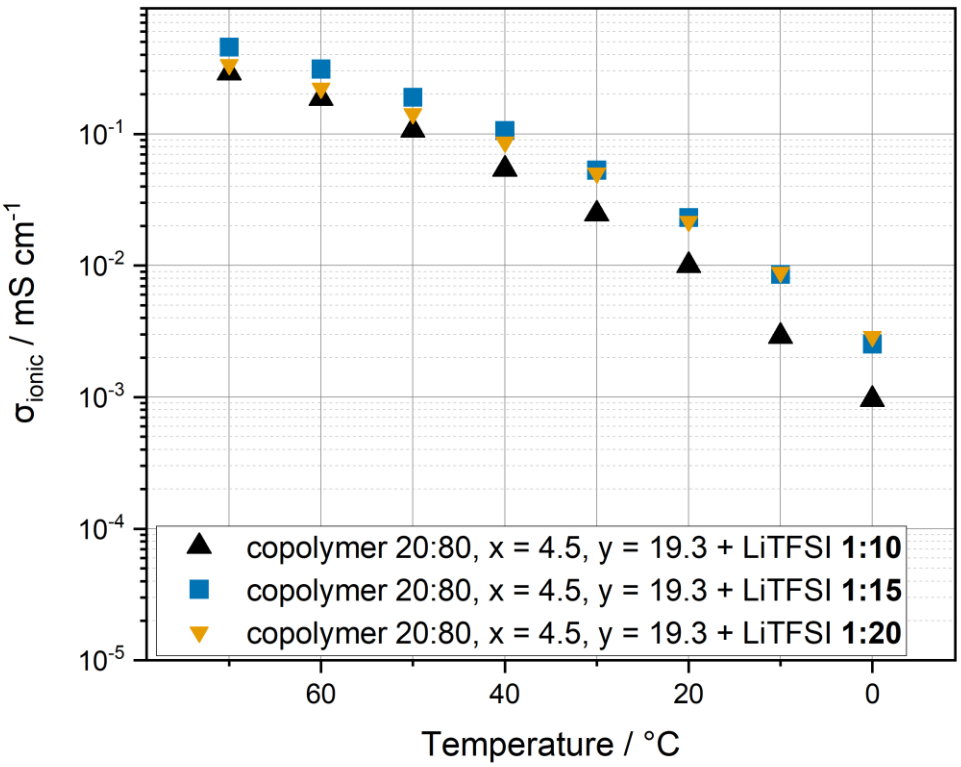

FIGURE 23: *Ionic conductivities of copolymers with x = 4.5 and y = 19.3 in a ratio of 20:80 over a temperature range from 0 to 70°C. For impedance measurements, the polymers were mixed with LiTFSI in the ratios [Li⁺] to [EO] of 1:10, 1:15 and 1:20.*

When comparing the data for the copolymer Poly((mPEO4.5MA)-co-(mPEO19.3MA)) in the ratio of composition of 80:20 (see fig. 26) it is apparent, that a LiTFSI addition of 1:20 is beneficial for the copolymer with mainly shorter side chains. It must be considered that the ionic conductivities for this copolymer combination is lower than for those dominated by mPEO19.3MA. At high temperatures the ionic conductivity is two times lower and at low temperatures the difference between the values of 80:20 and 20:80 is nearly in the range of one order of magnitude.

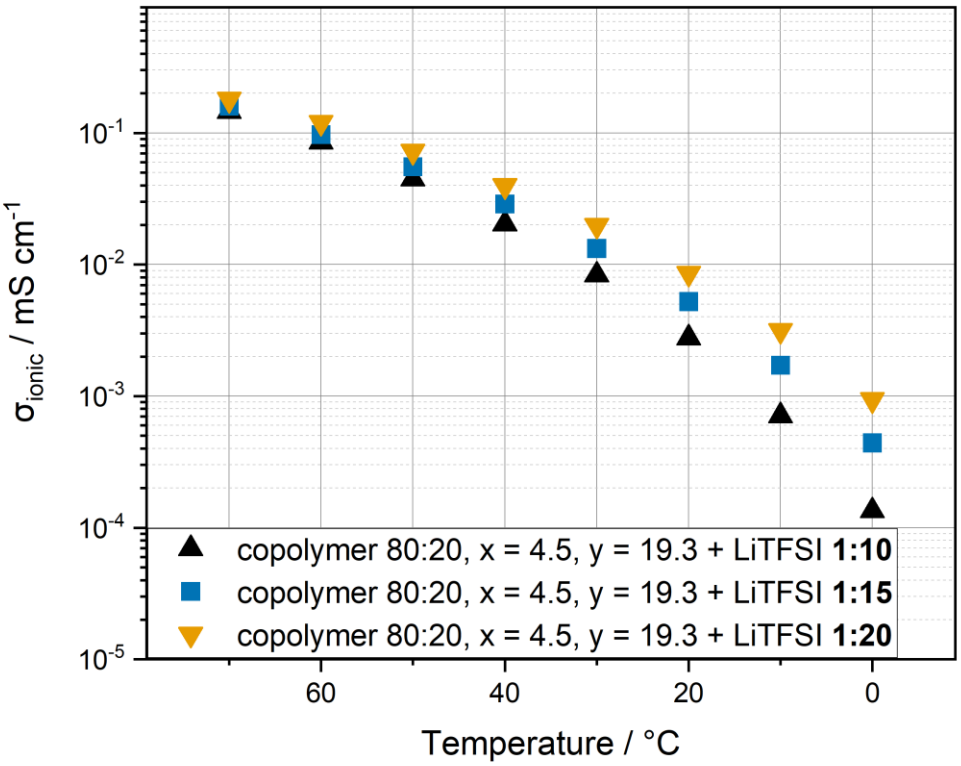

FIGURE 24: *Ionic conductivities of copolymers with x = 4.5 and y = 19.3 in a ratio of 80:20 over a temperature range from 0 to 70°C. For impedance measurements, the polymers were mixed with LiTFSI in the ratios [Li⁺] to [EO] of 1:10, 1:15 and 1:20.*

Further the transference number of the best performing homopolymer poly(mPEO19.3MA)$_{12}$ with a ratio of Li^+ to O-moiety of 1:15 was measured in a lithium symmetrical cell assembly. Resulting in a Li^+ transference number of 0.1 for the given electrolyte. This lays within the range of transference numbers reported for PEO-based electrolytes in literature.

3.5. Copolymers with Solketal methacrylate (SMA) – Anion Trapping

Sun and Angell[76] presented in 2001 the potential of borates and other boron containing derivatives to enhance the performance of polymer electrolytes. Also other groups investigated in borates and other approaches for (quasi) single-ion conduction[77,78]. Two interesting concepts to accelerate ion conduction are single-ion conductors or to immobilize the anion of Li-salts via anion trapping sites. For polymer electrolytes there are a few examples of polyanions where the polymer chain itself carries the negative charge[79]. For this approach it is mostly necessary to utilize a step in the synthesis where the ion is exchanged for the Li-ion. This was also done by our group but is not part of this work (therefore one example is only roughly shown in grey color in scheme 9)

The second approach the anion trapping certain moieties in the polymer have the ability to coordinate the TFSI-anion. Therefore, the respective polymer is simply prepared with Li-salt as for the other polymers in this work (see scheme 9). The step for ion-exchange is not necessary. In detail copolymers in different ratios from mPEOxMA with SMA were synthesized that can easily be functionalized with boronic acids.

By utilizing solketal methyl methacrylate (SMA) as comonomer, the possibility of enhanced ion conduction can be combined with the poly(PEOxMA) under investigation. Therefore, the monomer was synthesized beforehand and then polymerized with mPEOxMA via the grafting through approach. Afterwards the solketal on the polymer was hydrolyzed to form a diol.

From there on in a further step of post-polymerization-modification the free diol groups were then crosslinked with boronic acid ($B(OH)_3$) and lithium hydroxide (Li(OH)). By this crosslinking technique the resulting polyanion together with the Lithium cation can act as single ion conducting material (see scheme 9, grey arrow).

As a second possibility boronic acids with an aromatic rest can be used to react in a condensation reaction with the diol groups. Under certain circumstances the polymer can then act as an electrolyte by mixing it with LiTFSI.

The anion of LiTFSI can then coordinate to the boron and will be hindered to participate in ion transfer. In this manner the boron acts as an ion trap (compare scheme 9, center, blue arrows), which leads to an effect similar to the first single ion conduction mechanism.

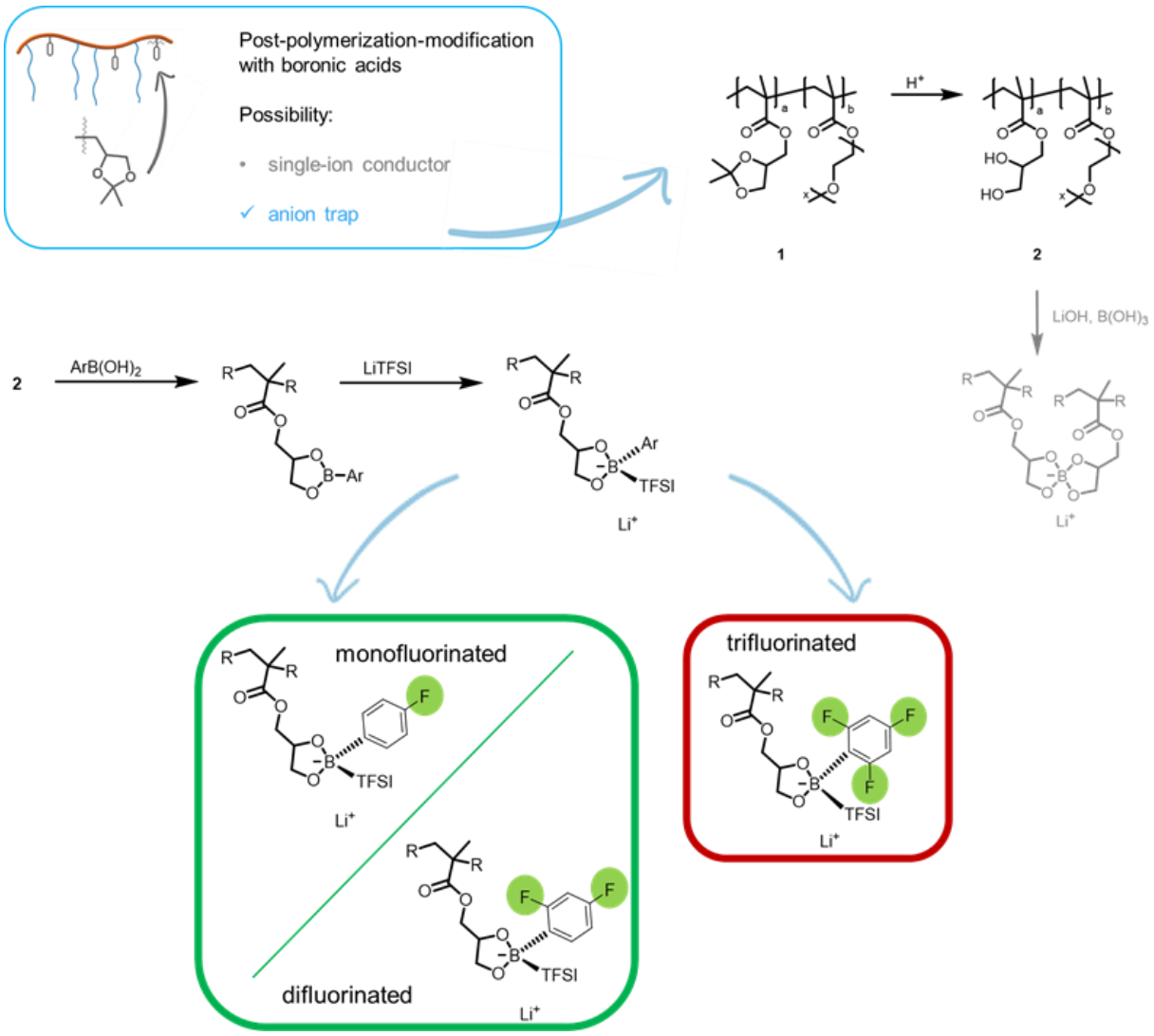

SCHEME 7: *Schematic depiction of the copolymer structure and the idea for anion trapping in the box at the top. To the right and below the blue box the route for on post-polymerization-modification to form an anion trap in black color. At the bottom two successfully synthesized anion trapping polymers in the green box next to the not achieved structure in the red box. In grey the alternative route to yield a single-ion conductor.*

The two copolymers with anion trapping sites were synthesized successfully according to NMR (see figures 27 and 28) and Infrared spectroscopy (IR) (compare figure 29).

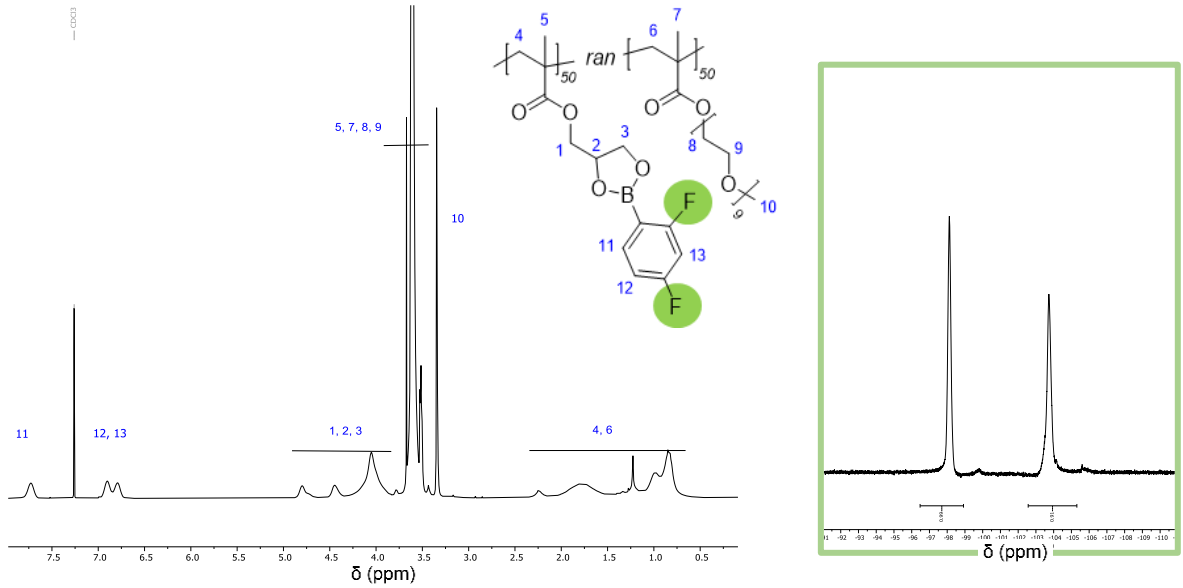

FIGURE 25: *^{1}H-NMR spectrum (left) and ^{19}F-NMR spectrum (right) of the copolymers with the anion trapping site of the difluorinated species.*

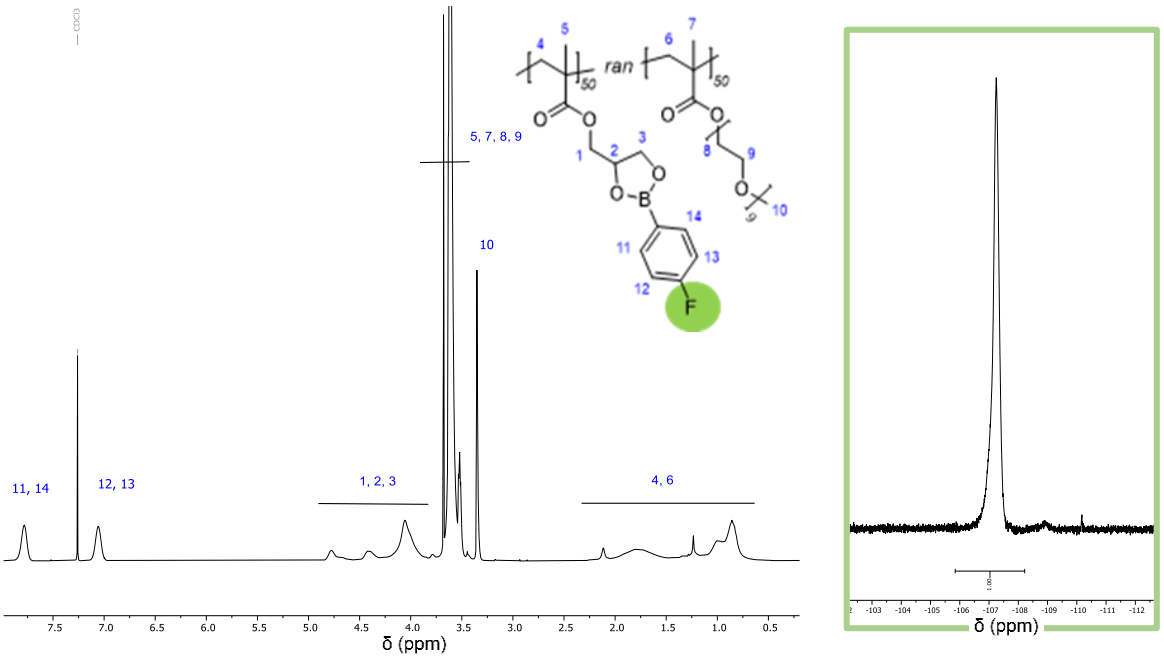

FIGURE 26: *^{1}H-NMR spectrum (left) and ^{19}F-NMR spectrum (right) of the copolymers with the anion trapping site of the difluorinated species.*

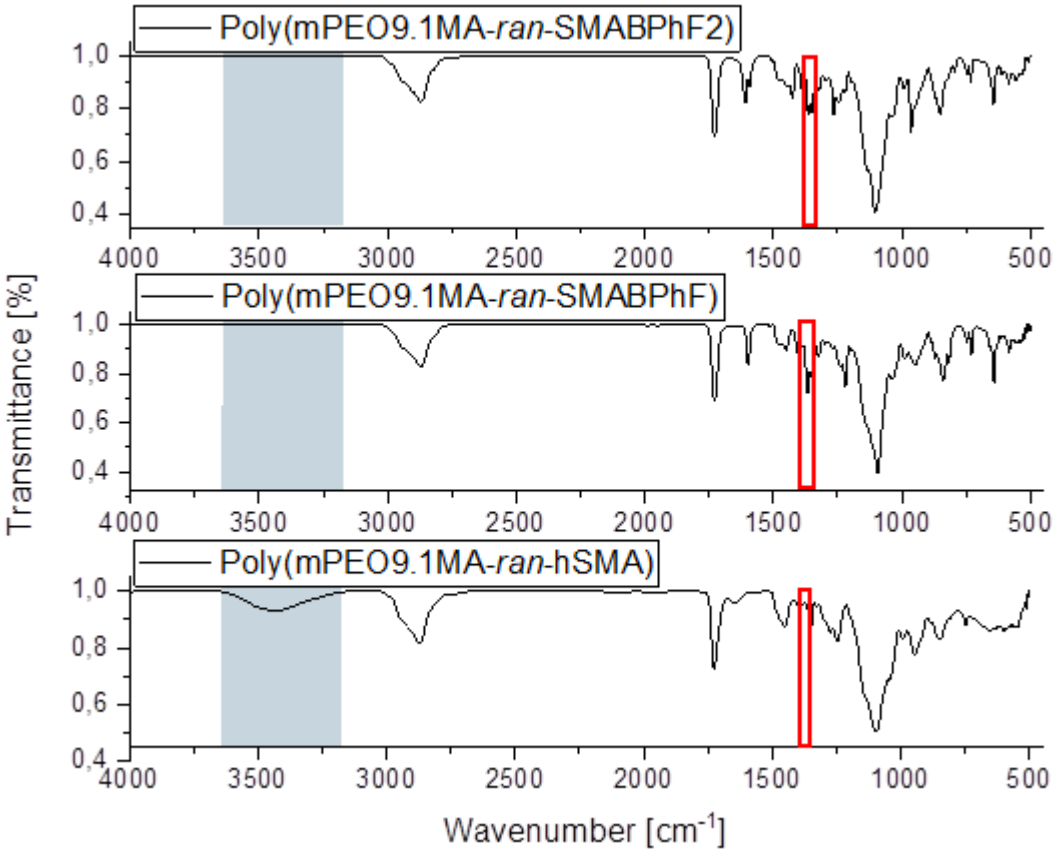

FIGURE 27: *Representative IR spectra of (from top to bottom) the di- and monofluorinated anion trap copolymers for mPEO9.1MA and lastly poly(mPEO9.1MA-co-hSMA) as the diol form before addition of the boronic acids. The blue box marks the O-H vibration band and the red box the range of the B-O vibration.*

The appearance of the B-O vibration bands and disappearance of the O-H vibration bands in the spectra of the post-polymerization-modified copolymers in comparison to the diol bearing copolymer confirms the successful functionalization (see figure 29). The obtained polymers were handled under inert conditions to prevent the reversion of the esterification while electrolyte preparation and then dried in a Büchi®-oven for two days at 65 °C. The data for ionic conductivity (see fig. 30) for the anion trap copolymers show significant differences regarding the copolymer composition. A clear trend due to the now incorporated anion trap is not observed, but a drop in ionic conductivity of one and a half orders of magnitude. The best performing copolymer from this selection is the one in a ratio of 50:50 with mPEO19.3MA. This result is not surprising since the already proven trend of best ion

conduction in poly(mPEO19.3MA) is visible once again. Second best performing is the 50:50 copolymer from the mPEOxMA with the shorter side chain.

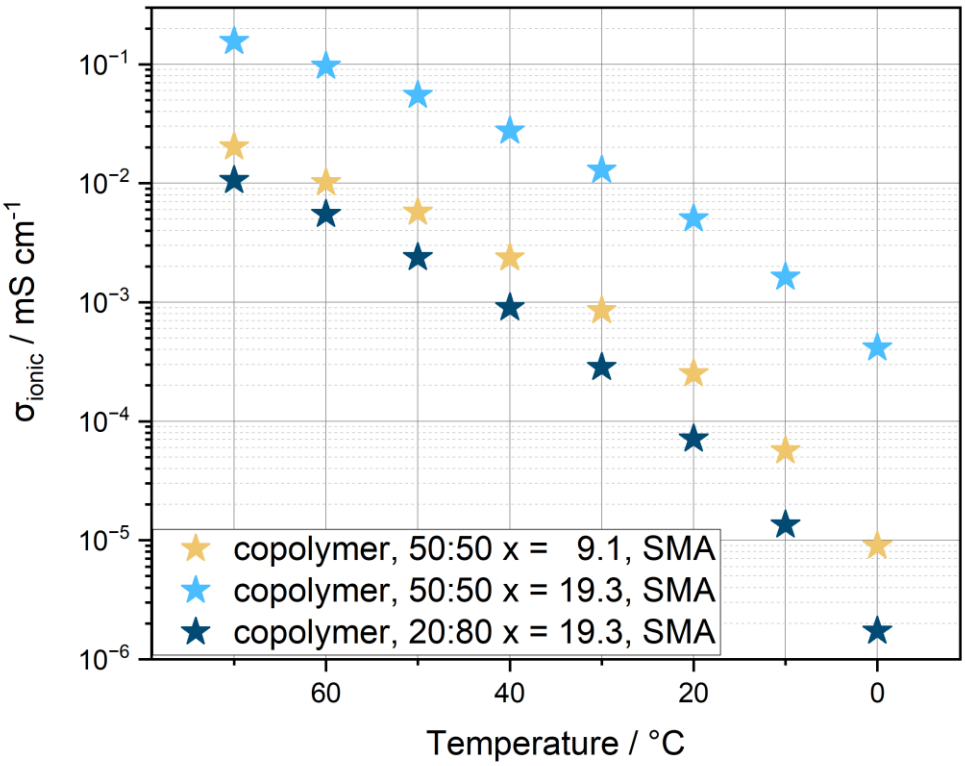

FIGURE 28: *Ionic conductivities of copolymers from mPEOxMA with x = 9.1 and 19.3 to SMA in a ratio of 50:50 and 20:80 over a temperature range from 0 to 70°C. For impedance measurements, the polymers were mixed with LiTFSI in the ratios [Li$^+$] to [EO] of 1:10, 1:15 and 1:20.*

To conclude the approach was not resulting in an increase of ionic conductivity. Hence the mechanical stability was improved up until the point of flexible and also brittle self-standing membranes depending on the monomer ratio. Besides, the measured conductivity is still quite high considering the very low content of PEO in the electrolyte. For better insights further investigations are needed by measuring the copolymer in a brush polymer matrix instead of in pure form.

4. Conclusion and Outlook

Numerous homo- and copolymers were successfully synthesized in a controlled manner. RAFT polymerization was therefore optimized to yield high conversions and equal applicability for all monomers. Further, polymer electrolytes were prepared by mixing with different amounts of LiTFSI and assembled with no further use of additives or solvents in a steel symmetrical cell assembly. Especially with the copolymerization of mPEOxMA of different side chain lengths, common drawbacks of PEO-based electrolytes, namely crystallization tendencies and with that low ion conductivities below 40°C, could be investigated. The brush polymers in contrast to PEO do not show much crystallization if mixed with LiTFSI and with well-chosen parameters the conductivities of the obtained electrolytes can be increased by up to two orders of magnitude. The highest ionic conductivities could be observed for poly(mPEO19.3MA) with a number of backbone repeating units of 12. Starting from, this further disturbance by copolymerization with shorter side chains to yield higher ionic conductivities was investigated. The copolymerization did not yield in higher conductivities and the positive effect from available free volume due to short neighboring PEO chains could not be proven for the system with x = 4.9 and y = 19.3. Nevertheless, this approach led to the interesting finding, that the ionic conductivity for poly(mPEO4.5MA-co-mPEO9.1MA) exceeded the conductivities of the respective homopolymers. Copolymerization with EHMA as a reference system for higher mechanical stability with a still relatively low T_g resulted in a significant decrease of ionic conductivity, showing the benefit of copolymerization with a PEO-based comonomer.

The impact of different ratios of LiTFSI addition was also addressed, showing that a $[Li^+]$:[EO] ratio of 1:15 for longer side chains with around 19 EO repeating units and 1:20 for shorter PEO chains exhibited the highest possible ionic conductivity for the given polymer architecture.

To conclude, the approach to generate more free volume for the side chains with x = 19.3 by copolymerization with relatively shorter side chains was not successful regarding an increase in ionic conductivity. Although this type of copolymerization also did not lead to a drastic drop in conductivity values.

The anion trapping approach to overcome the limited conductivity was not resulting in an increase of ionic conductivity. Hence the mechanical stability was improved up until brittle self-standing membranes and the conductivity is still quite high considering the very low

content of PEO in the electrolyte. For better insights further investigations are needed by measuring the copolymer in a brush polymer matrix instead of in pure form.

5. Experimental Part

5.1. Materials

RAFT agent 2-(2'-cyanopropyl)dithiobenzoate (CPDB, abcr), 1,4-dioxane (Roth), n-hexane (Roth) and diethyl ether (Et_2O, Fisher), dichloromethane (DCM, Fisher), were used as received without further purification. The inhibitor from monomer Methoxy(poly(ethylene oxide)) methacrylate (mPEO xMA with x = 4.5, 9.1 and 19.3; representing the number of ethylene oxide repeating units, Sigma Aldrich) and 2-ethylhexyl methacrylate (EHMA, Fisher) was removed before polymerization by a short column of basic alumina (50 – 200 µm, 60 Å, ACROS Organics). For mPEO19.3MA the monomer was therefore dissolved in DCM as an eluent. Azobisisobutyronitrile (AIBN, Sigma Aldrich) was recrystallized from ethanol previous to use. Deionized water was purified with a Garnsted GenPure Pro system. Bis(trifluoromethanesulfonyl)imide lithium salt (LiTFSI, 99.95%, Sigma Aldrich) was dried at 80°C and 10^{-3} mbar for 2 days and subsequently stored under argon atmosphere (inside a glovebox MBraun Unilab, < 0.1 - 2 ppm H_2O, < 0.1 - 2 ppm O_2). All solvents and reagents were of analytical grade or higher if not further specified.

5.2. Experimental Procedures

5.2.1. SYNTHESIS OF HOMOPOLYMER Poly(mPEO19.3MA) via RAFT POLYMERIZATION

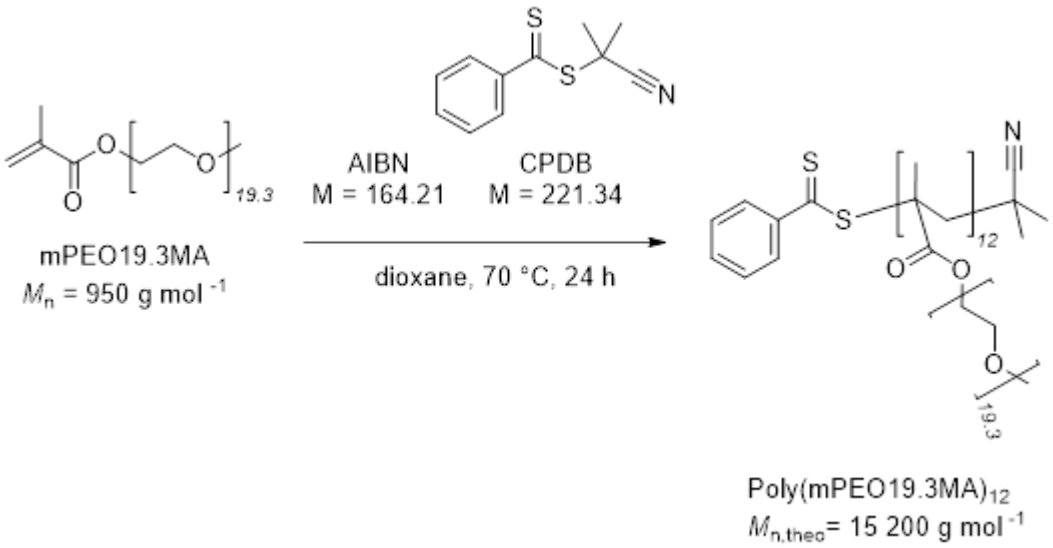

FIGURE 29: *Representative reaction mechanism for the synthesis of poly(mPEOxMA). Namely poly(mPEO19.3MA) with 12 repeating units per backbone.*

Methoxy (poly(ethylene oxide)) methacrylate (4.75 g, 5.00 mmol, 1.00 eq)) was dissolved in 5 mL of a mixture of water and 1,4-dioxane (50:50) in a Schlenk-tube equipped with a stirring bar. Stock solutions of AIBN (6.60 mg, 0.04 mmol, 0.008 eq) and CPDB (88.5 mg, 0.40 mmol, 0.08 eq) in 1,4-dioxane were prepared and added at room temperature (rt). The reaction mixture was degassed via at least three freeze-pump-thaw cycles. The Schlenk-tube was then placed into a preheated oil bath at 70°C under N_2 atmosphere and stirred for 24h. The reaction mixture was quenched by cooling and poured into an excess of n-hexane and washed several times for purification. To remove unreacted monomer dialysis of the polymer was performed in water at rt for 2 to 4 days. The water was changed 6 times and Spectra/Por®membrane tubing with a molecular weight cut off (MWCO) of 3.5 kDa was utilized. The obtained pink product was dried for 2 days at 60°C and ~10^{-3} mbar in a vacuum oven to a constant weight (see 5.2.7. Drying). ^{1}H- and ^{13}C NMR signals were in good accordance to literature.

All other homo- and copolymers were synthesized accordingly. The ratios of RAFT agent to initiator ([CPDB]:[AIBN]) were kept constant to 10:1 for all syntheses, the ratios of monomer to RAFT agent were varied in order to modify the backbone length and are listed in table 1 for homopolymers.

TABLE 1: *Assignment of the names of the synthesized polymers to the initial ratios and the M_n of the monomers and polymers (theoretical value and determined by size exclusion chromatography (SEC)).*

polymer	M_n(mPEOxMA) /g mol^{-1}	initial ratios [M1] : [RAFT] : [I]	$M_{n,theo}$(polymer) /g mol^{-1}	$M_{n,SEC}$(polymer)
Poly(mPEO4.5MA)$_{25}$	300	100 : 4.00 : 0.40	7 500	7 500
Poly(mPEO4.5MA)$_{50}$	300	100 : 2.00 : 0.20	15 000	13 000
Poly(mPEO4.5MA)$_{100}$	300	100 : 1.00 : 0.10	30 000	20 500
Poly(mPEO9.1MA)$_{15}$	500	100 : 6.50 : 0.65	7 600	10 500
Poly(mPEO9.1MA)$_{25}$	500	100 : 4.00 : 0.40	12 500	13 200
Poly(mPEO9.1MA)$_{50}$	500	100 : 2.00 : 0.20	25 000	20 300
Poly(mPEO9.1MA)$_{100}$	500	100 : 1.00 : 0.10	50 000	42 800
Poly(mPEO9.1MA)$_{200}$	500	100 : 0.50 : 0.05	100 000	85 500
Poly(mPEO19.3MA)$_{12}$	950	100 : 8.00 : 0.80	10 900	15 200
Poly(mPEO19.3MA)$_{25}$	950	100 : 4.00 : 0.40	23 800	22 100
Poly(mPEO19.3MA)$_{50}$	950	100 : 2.00 : 0.20	47 500	32 700
Poly(mPEO19.3MA)$_{100}$	950	100 : 1.00 : 0.10	95 000	-

Depending on the targeted molecular weight Spectra/Por®membrane tubing with a MWCO of 3.5 / 6 / 8 kDa were utilized for purification of the product.

The TGA curves for poly(mPEO9.1MA)$_{100}$ and poly(mPEO19.3MA)$_{100}$ exhibit one main weight loss region while the temperature differs with respect to the PEO side chain length. The TGA curve of poly(mPEO9.1MA)$_{100}$ shows a weight loss of only about 1 % until 301 °C. This could be attributed to dehydration of traces of water in the highly hygroscopic sample. The weight loss is shown in the temperature range of 301 – 383 °C.

The TGA curve of poly(mPEO19.3MA)$_{100}$ shows a weight loss of only about 0.8 % until 360 °C. This could be attributed to dehydration of traces of water in the highly hygroscopic sample. The major weight loss is shown in the temperature range of 360 – 405 °C.

For both samples no further weight loss steps were observed.

The TGA curve of poly(mPEO4.5MA)$_{100}$ shows a weight loss of about 4 % until 230 °C and a second one of about 16 % until 290 °C. This could be attributed remaining solvent and water in the sample, due to insufficient drying, the second step could arise from side chain cleavage, due to overheating while handling. The main weight loss of 80 % is shown in the temperature range of 290 – 369 °C.

5.2.2. SYNTHESIS OF COPOLYMER Poly(mPEO19.3MA-*co*-mPEO4.5MA) via RAFT POLYMERIZATION

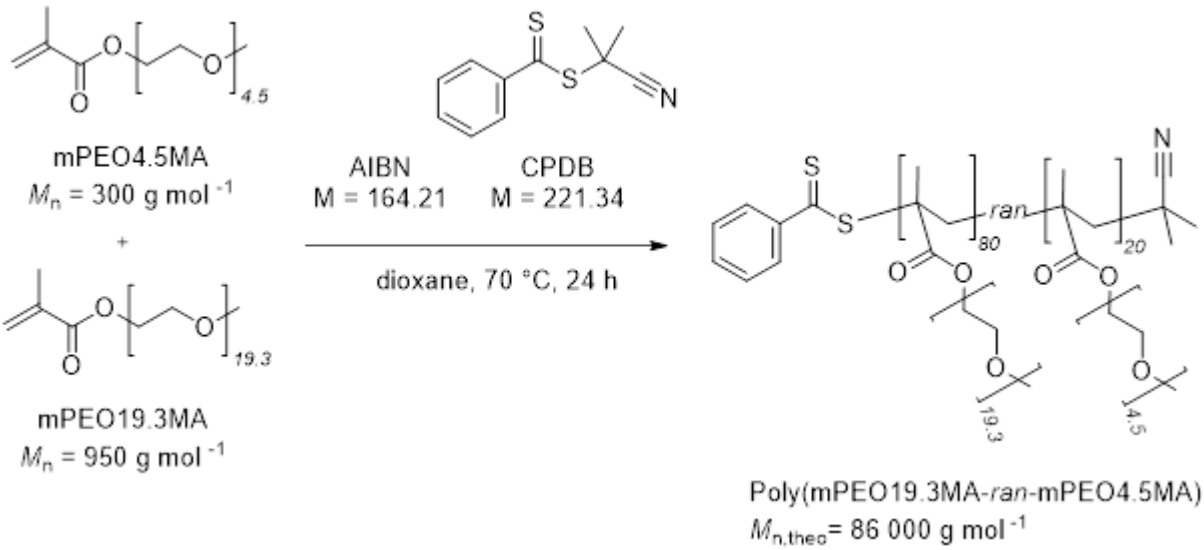

FIGURE 30: *Representative reaction mechanism for the synthesis of copolymers of mPEOxMA. Namely poly(mPEO19.3MA-co-mPEO4.5MA) in a molar ratio of mPEOxMA with x = 4.5 and y = 19.3 of 20:80.*

The monomers methoxy (poly(ethylene oxide)) methacrylate (mPEOxMA) with x = 4.5 (0.40 g, 1.33 mmol, 20.00 eq) and mPEOyMA with y = 19.3 (5.07 g, 5.33 mmol, 80.00 eq) were dissolved in 6 mL of a mixture of water and 1,4-dioxane (50:50) in a Schlenk-tube equipped with a stirring bar. Stock solutions of AIBN (1.09 mg, 0.006 mmol, 0.10 eq) and CPDB (14.8 mg, 0.06 mmol, 1.00 eq) in 1,4-dioxane were prepared and added at room temperature (rt). The reaction mixture was degassed via at least three freeze-pump-thaw cycles. The Schlenk-tube was then placed into a preheated oil bath at 70°C under N_2 atmosphere and stirred for 24h. The reaction mixture was quenched by cooling and poured into an excess of n-hexane and washed several times for purification. To remove unreacted monomer dialysis of the polymer was performed in water at rt for 2 to 4 days. The water was changed 6 times and Spectra/Por®membrane tubing with a molecular weight cut off (MWCO) of 3.5 kDa was utilized. The obtained pink product was dried for 2 days at 60°C and ~10^{-3} mbar in a vacuum oven to a constant weight (see 5.2.7. Drying). ^{1}H- and ^{13}C NMR signals were in good accordance to literature.

All other copolymers were synthesized accordingly. The ratios of RAFT agent to initiator ([CPDB]:[AIBN]) were kept constant to 10:1 for all syntheses, the ratios of monomer to RAFT

agent were varied in order to modify the backbone length and are listed in table 2 for copolymers of type Poly(mPEOxMA-*co*-mPEOyMA).

TABLE 2: *Assignment of the names of the synthesized copolymers to the initial ratios and the M_n of the respective monomers and copolymers along with the weight fraction of the larger monomer.*

polymer	M1	M2			
	M_n(mPEOxMA) /g mol^{-1}	M_n(mPEOyMA) /g mol^{-1}	initial ratios [M1] : [M2] : [RAFT] : [I]	$M_{n,theo}$(P) /g mol^{-1}	w% (M2)
Poly(mPEO4.5MA-*co*-mPEO9.1MA)	300	500	80:20:1.00:0.10	34 000	29
Poly(mPEO4.5MA-*co*-mPEO9.1MA)			50:50:1.00:0.10	40 000	63
Poly(mPEO4.5MA-*co*-mPEO9.1MA)			20:80:1.00:0.10	46 000	87
Poly(mPEO4.5MA-*co*-mPEO19.3MA)	300	950	80:20:1.00:0.10	43 000	44
Poly(mPEO4.5MA-*co*-mPEO19.3MA)			50:50:1.00:0.10	62 500	76
Poly(mPEO4.5MA-*co*-mPEO19.3MA)			20:80:1.00:0.10	82 000	93
Poly(mPEO9.1MA-*co*-mPEO19.3MA)	500	950	80:20:1.00:0.10	59 000	32
Poly(mPEO9.1MA-*co*-mPEO19.3MA)			50:50:1.00:0.10	72 500	66
Poly(mPEO9.1MA-*co*-mPEO19.3MA)			20:80:1.00:0.10	86 000	88

Initial ratios are given in concentration ratios. M1 and M2 stand for monomer 1 and monomer 2, RAFT for RAFT agent, I for initiator namely AIBN, squared brackets symbolize concentrations of the respective reactants.

Depending on the targeted molecular weight Spectra/Por®membrane tubing with a MWCO of 3.5 / 6 / 8 kDa were utilized for purification of the product.

5.2.3. SYNTHESIS OF COPOLYMER Poly(mPEO19.3MA-*co*-EHMA) via RAFT POLYMERIZATION

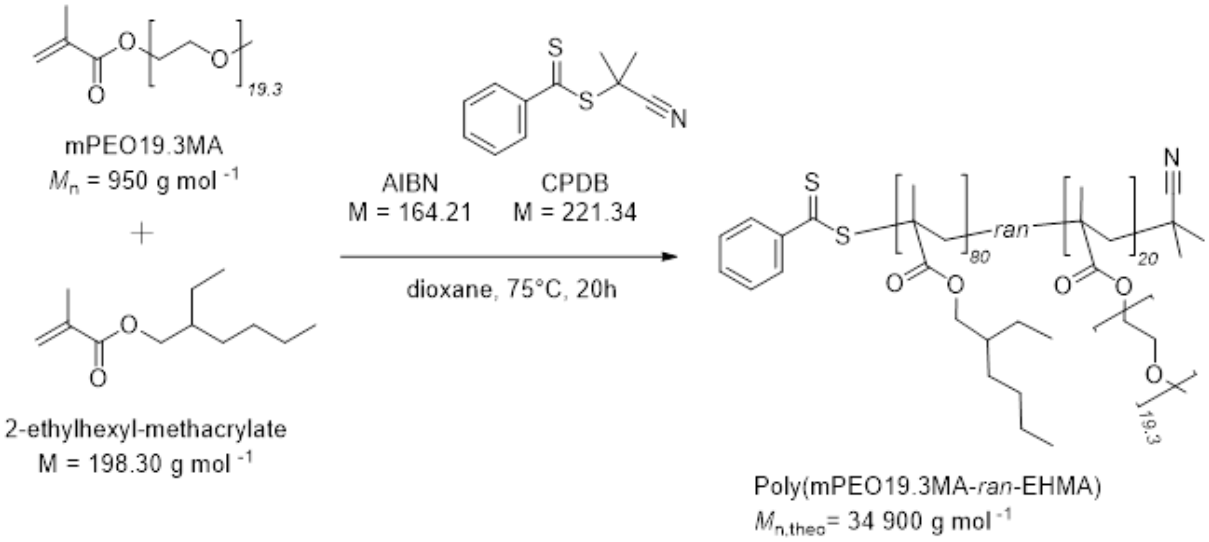

FIGURE 31: *Representative reaction mechanism for the copolymerization of mPEOxMA with EHMA. Namely poly(mPEO19.3MA-co-EHMA) in a molar ratio of mPEOxMA to EHMA of 20:80.*

The monomers methoxy (poly(ethylene oxide)) methacrylate (mPEOxMA) with x = 19.3 (2.80 g, 2.95 mmol, 20.00 eq) and EHMA (2.34 g, 11.8 mmol, 80.00 eq) were dissolved in 6 mL 1,4-dioxane in a Schlenk-tube equipped with a stirring bar. Stock solutions of AIBN (2.42 mg, 0.015 mmol, 0.10 eq) and CPDB (32.6 mg, 0.15 mmol, 1.00 eq) in 1,4-dioxane were prepared and added at room temperature (rt). The reaction mixture was degassed via at least three freeze-pump-thaw cycles. The Schlenk-tube was then placed into a preheated oil bath at 75°C under N_2 atmosphere and stirred for 20h. The reaction mixture was quenched by cooling and poured into an excess of diethyl ether and washed several times for purification. To remove unreacted monomer dialysis of the polymer was performed in water at rt for 2 to 4 days. The water was changed 6 times and Spectra/Por®membrane tubing with a molecular weight cut off (MWCO) of 3.5 kDa was utilized. The obtained pink product was dried for 2 days at 60°C and ~10^{-3} mbar in a vacuum oven to a constant weight (see 5.2.7. Drying). ^{1}H- and ^{13}C NMR signals were in good accordance to literature.

The polymers were synthesized analogous to 5.2.2 but with pure 1,4-dioxane as solvent and longer reaction times of 48h. Also, the polymer was precipitated in an excess of cold diethylether for copolymers with a high EHMA content and in n-hexane for copolymers with

a high PEO content. Since the copolymers show amphiphilic character, a precipitation was not easily achieved. The main purification was dialysis against water with dialysis tubing a MWCO of 3.5 kDa. The ratios of monomer to RAFT agent were varied in order to modify the backbone length and are listed in table 3 for copolymers of type Poly(mPEOxMA-*co*-EHMA).

TABLE 3: *Assignment of the names of the synthesized copolymers to the initial ratios and the M_n of themPEOxMA monomers and copolymers along with the weight fraction of the larger monomer.*

polymer	M1			
	M_n(mPEOxMA) /g mol^{-1}	initial ratios [M1] : [EHMA] : [RAFT] : [I]	$M_{n,theo}$(polymer) /g mol^{-1}	w% (mPEOxMA)
Poly[mPEO4.5MA-*ran*-EHMA]	300	10:90:1.00:0.10	20 800	14
Poly[mPEO4.5MA-*ran*-EHMA]		20:80:1.00:0.10	21 900	27
Poly[mPEO4.5MA-*ran*-EHMA]		50:50:1.00:0.10	24 900	60
Poly[mPEO9.1MA-*ran*-EHMA]	500	20:80:1.00:0.10	25 900	39
Poly[mPEO9.1MA-*ran*-EHMA]		30:70:1.00:0.10	28 900	52
Poly[mPEO19.13MA-*ran*-EHMA]	950	20:80:1.00:0.10	34 900	54
Poly[mPEO19.13MA-*block*-EHMA]		20:80:1.00:0.10	34 900	54
Poly[mPEO19.13MA-*ran*-EHMA]		50:50:1.00:0.10	57 400	83
Poly[mPEO19.13MA-*block*-EHMA]		50:50:1.00:0.10	57 400	83
Poly[mPEO19.13MA-*ran*-EHMA]		20:80:1.00:0.10	80 000	95

5.2.4. SYNTHESIS OF COPOLYMER Poly(mPEO19.3MA-*co*-SMA) via RAFT POLYMERIZATION

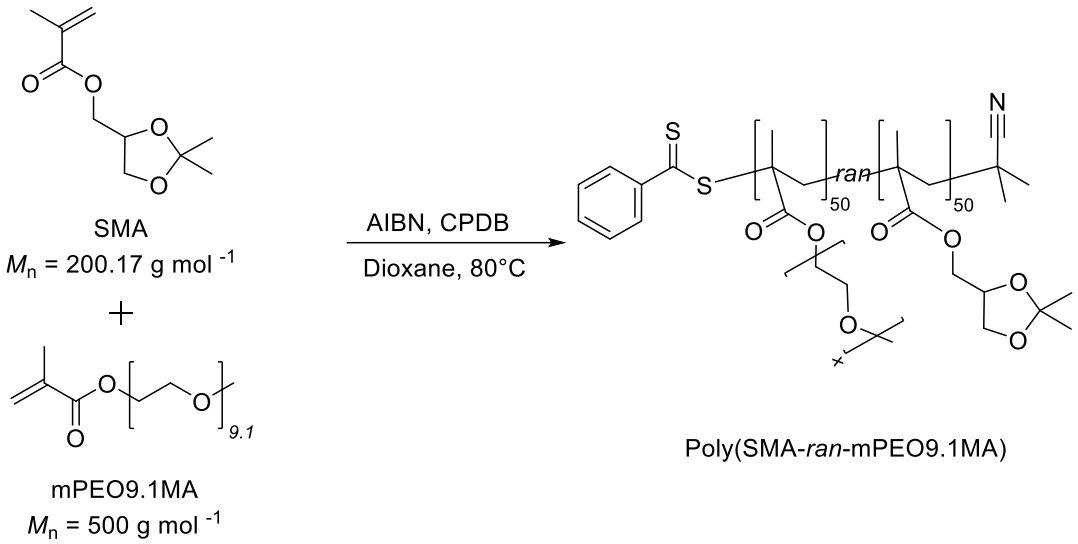

FIGURE 32: *Representative reaction mechanism for the copolymerization of mPEOxMA with SMA. Namely poly(SMA-co-mPEO9.1MA) in a molar ratio of mPEOxMA to SMA of 50:50.*

The monomers methoxy (poly(ethylene oxide)) methacrylate (mPEOxMA) with x = 9.1 (4.60 g, 9.20 mmol, 50.00 eq) and SMA (1.84 g, 9.20 mmol, 50.00 eq) were dissolved in 7 mL 1,4-dioxane in a Schlenk-tube equipped with a stirring bar. Stock solutions of AIBN (6.65 mg, 0.07 mmol, 0.22 eq) and CPDB (45.2 mg, 0.20 mmol, 1.11 eq) in 1,4-dioxane were prepared and added at room temperature (rt). The reaction mixture was degassed via at least three freeze-pump-thaw cycles. The Schlenk-tube was then placed into a preheated oil bath at 80 °C under N_2 atmosphere and stirred for 24 h. The reaction mixture was quenched by cooling and poured into an excess of n-hexane and washed several times for purification. The obtained pink product was dried to a constant weight (obtained yield of 93%). ^{1}H-NMR signals were in good accordance to literature.

Post-polymerization-modification

Step 1: hydrolysis of SMA containing polymer

To obtain the diol form of the copolymer, hydrolysis was performed in acetonitrile and HCl (1 molar) at room temperature for 12 h (see figure 35).

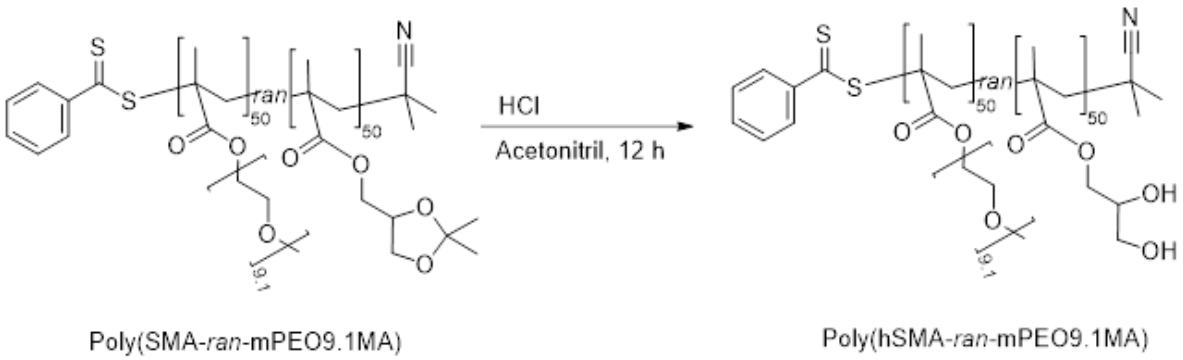

FIGURE 33: *reaction mechanism of the hydrolysis of the copolymer yielding the diol form.*

Step 2: functionalization of the diol with boronic acid

The esterification of the copolymer with the respective boronic acid was conducted in dry dioxane at room temperature for 24 h.

5.2.5. Calculation of the yield and the number of repeating units from NMR

Calculating the degree of polymerization from NMR data:

When using the raw product NMR, the remaining doble bond proton signals of the monomer can be set to 1 each and utilized to calculate the conversion in good approximation. To calculate the number of repeating units per chain, the aromatic proton signals of the RAFT agent are in summary set to 5 and correlated to the signals of the methoxy end group of mPEO.

When the product was purified via dialysis the calculation is more complex, since the signals of the RAFT group are weaker. The integral of the CH_3 end group proton signal is first corrected by removing the CH_3 groups from remaining monomer from the integral. Same procedure is conducted with the PEO repeating unit signal. Therefore, the average number of PEO side chain protons is calculated, and the proton signal fraction of remaining monomer is removed from the integral. By dividing the integral after correction by the average number of protons per PEO side chain, the number of backbone repeating units per macromolecule can be obtained.

This is done since SEC results for M_n are not reliable even though regularly, they would be the easier option to obtain *the degree of polymerization*.

Challenge regarding SEC measurements:

Reliable SEC data for poly(mPEO19.3) is not easily obtained for the PEO-graft brush polymers. Realistically obtained values are nonrealistic or show a dispersity of over 10 and a multimodal elution diagram. The in the group available SEC column combinations (for THF and water) are not appropriate to separate PEO side chain polymers of higher molecular weights. Most likely the used technique for characterization is insufficient due to the behavior of PEO side chain polymers in column chromatography with extremely broadened retention times.

5.2.6. Electrolyte Preparation

Prior to electrolyte preparation the polymer was dried for 2 days at 65°C and ~10^{-3} mbar. In order to prepare the electrolyte, the polymer and LiTFSI in predefined ratios of [Li^+]:[EO] 1:10, 1:15 and 1:20 were dissolved separately in acetone. After combining the two solutions, the mixture was stirred for at least 8 hours to ensure complete mixing and a uniform distribution of the dissolved salt. Afterwards, the solvent was slowly removed under reduced pressure to a constant weight (beginning from 600 mbar to 10^{-3} mbar at 65°C for at least 2 days). The polymer electrolytes (PEs) were subsequently stored and handled under argon atmosphere (inside a glovebox MBraun Unilab, < 0.1 - 2 ppm H2O, < 0.1 - 2 ppm O2).

Samples for the anion trapping project were beyond this dried in a Büchi® glass oven before electrolyte preparation as well as after mixing with Lithium salt and before cell assembly.

Moreover, membranes were also additionally dried in a prior to cell assembly.

5.2.7. Drying

The obtained polymers were dried for 2 days at 60°C and a pressure ≥ 10^{-3} mbar in a vacuum oven to a constant weight. It as to be noted that the samples need to be dried in a flask that maximizes the surface area to ensure complete drying as well as to prevent the spillage of sample.

The following procedure was utilized:

TABLE 4: *Overview and description of the drying procedure for the polymers.*

Drying Step	Description of Task	Temperature [°C]	Pressure [bar]	Time [h]
Step 1	Placing the sample into vacuum oven, equilibrate temperatures	65 °C	1	0.5
Step 2	Stir the sample			
Step 3	Reduce pressure	65 °C	6 10^{-1}	2
Step 4	Stir the sample			
Step 5	Reduce pressure	65 °C	2 10^{-1}	2
Step 6	Stir the sample			
Step 7	Reduce pressure	65 °C	1 10^{-3}	44

Only by following this procedure the drying process was successful. Meaning that also no inhomogeneities (e.g., dried top layer on the surface of the sample, whereas bulk of the sample remained fluid) were observed.

Samples dried less than 2 days still contained remaining water in the bulk. Even if dried at 70°C and under reduced pressure the weight was not yet constant.

Dried samples were sealed with Parafilm and transferred into a glovebox (O2 level and moisture level in a range of < 0.1 to maximal 2 ppm) and stored under Argon atmosphere.

5.2.8. Cell Assembly

For assembling cells, the dry electrolytes were transferred into a glovebox and handled under Argon atmosphere while keeping O_2- and moisture levels below 2 ppm.

FIGURE 34: LEFT AND MIDDLE: *Representative pictures of an electrolyte membrane* **RIGHT:** *Schematic representation of the cell assembly showing the stainless-steel electrodes in metallic color and the membrane in orange color.*

Self-standing membranes as shown in figure 36 were sandwiched in a symmetrical setup between two stainless-steel electrodes (with a thickness of d = 1 mm and a diameter of 15 mm) (compare fig. 37 right).

FIGURE 35: LEFT: *Representative pictures of a fluid electrolyte in a glass vial* **MIDDLE:** *Picture of the lower cell case with one stainless-steel electrode, the ring spacer and a drop of electrolyte.* **RIGHT:** *Schematic representation of the cell assembly showing the stainless-steel electrodes in metallic color, the ring spacer in yellow color and the fluid sample in orange color.*

Fluid electrolyte samples were dripped onto the center of a stainless-steel electrode (thickness d = 1 mm, outer diameter = 15 mm) equipped with a ring spacer out of Mylar® foil (thickness d = 100 µm, outer diameter = 16 mm, inner diameter = 8 mm) then another stainless-steel electrode (thickness d = 1 mm, outer diameter = 15 mm) was stacked on top and coin cell-type cells (CR2032) were assembled manually (see fig. 37 middle and right).

The ring spacer setup was used to prevent the electrodes from touching due to displacement of sample, as known in literature.[80] To ensure full contact between electrodes and solid electrolytes the assembled cells were stored at 70 °C for 12 h previous to electrochemical impedance spectroscopy (EIS) measurement.

The cells for measurement of the transference number (t_+) were assembled in a lithium symmetrical setup. Fluid electrolyte samples were dripped onto the center of a lithium disk with a diameter of 12 mm and a thickness of 0.5 µm. Then a ring spacer out of Mylar® foil (thickness d = 100 µm, outer diameter = 16 mm, inner diameter = 8 mm) was added, followed by another disk out of metallic lithium. This assembly was put between two stainless-steel blocking electrodes (two different electrodes; thickness of first electrode = 1 mm, thickness of second electrode = 500 µm, both with the same outer diameter = 15 mm) and coin cell-type cells (CR2032) were assembled manually (see fig 38). Again, the ring spacer setup was used to prevent the electrodes from touching due to displacement of sample.

FIGURE 36: *Schematic representation of the cell assembly for t_+ measurement showing the stainless-steel electrodes in metallic color, the lithium discs in grey color, the ring spacer in yellow color and the electrolyte in orange color.*

Since this was not always sufficient to prevent the lithium disks from touching (compare fig. 39 top right) some samples were assembled with a Celgard® membrane impregnated with electrolyte and two stainless steel electrodes with a thickness of d = 500 µ (see fig. 39 bottom left). Others were assembled with only an additional Celgard® membrane to the original cell assembly (shown in fig. 39 bottom right). This was necessary to be able to measure over a long enough time range without cell failure due to short circuit.

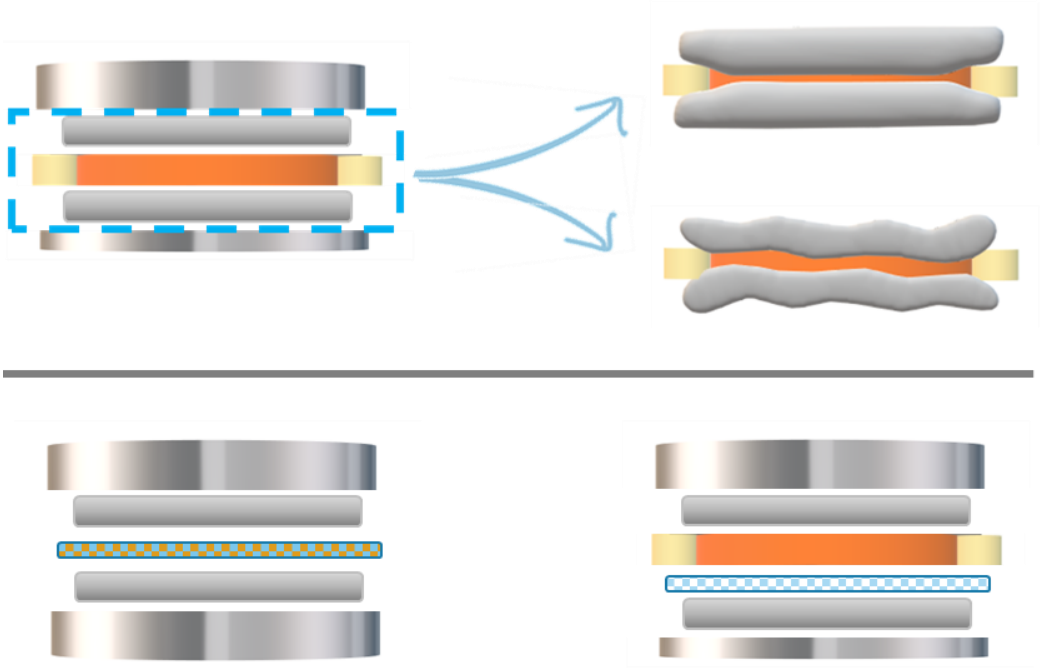

FIGURE 37 TOP: *Schematic representation of the ideal cell assembly on the left side showing the stainless-steel electrodes in metallic color, the lithium discs in grey color, the ring spacer in yellow color and the electrolyte in orange color. On the right side are two schematic representations shown, in which the lithium discs might touch each other after applying pressure when closing the cell case.* **BOTTOM, LEFT:** *Schematic representation of the cell assembly with the stainless-steel electrodes in metallic color, the lithium discs in grey color and the impregnated membrane in orange and blue colored check.* **BOTTOM, RIGHT:** *Schematic representation of the cell assembly with the stainless-steel electrodes in metallic color, the lithium discs in grey color, the membrane in white and blue colored check, the ring spacer in yellow color and the electrolyte in orange color.*

The usage of stainless-steel electrodes with different thickness has its cause in the desire of assemble the cells with the same amount of pressure. Since the cells are closed manually the overall thickness of the stack and the addition of steal feathers are the only options to maintain similar pressure values. That means with the addition of two lithium discs the setup of the stack would be thicker than for the regular impedance measurement. To solve this issue a smaller second stainless-steel spacer is used. This does not apply to the setup with only the impregnated membrane, since the membrane is thinner than the ring spacer.

5.3. Instrumentation

5.3.1. Nuclear Magnetic Resonance (NMR) Spectroscopy

Nuclear Magnetic Resonance (NMR) Spectroscopy was performed on a Bruker Ascend 400 MHz NMR in Chloroform-d if not otherwise mentioned. The chemical shifts were reported in parts per million (ppm) referenced to the characteristic solvent signal.

The results were utilized for calculation of conversion by comparison of end group signals to signals of CH_2 in the backbone or signals of double bond protons respectively. Further for the copolymers polymerized from different mPEOxMAs a distinction of the proton signals assigned to the different monomers was not possible due to the similar chemical shift. In this case it was considered that both monomers were consumed uniformly and the ratio in the product is according to the theoretical value.

5.3.2. Size-Exclusion Chromatography (SEC)

Size Exclusion Chromatography (SEC) was carried out in THF on a TosoH Bioscience HLC 8320GPC EcoSEC system equipped with three PSSSDV columns of 5 µm (100 Å, 1000 Å, 100000 Å) (8 x 300 mm), as well as a UV and a differential refractive index (IR) detector. The operation temperature was set to 35 °C and the flow rate was set to 1 mL min^{-1}. The system was calibrated using PMMA standards ranging from 800 to 2.2 x 106 g mol^{-1}. The concentration of the sample solution was 2.0 mg mL^{-1} from which a volume of 50 µL was injected onto the columns.

It must be mentioned that SEC was not sufficient to deliver exact results with the given column combination and THF at 35 °C as eluent.

5.3.3. Differential Scanning Calorimetry (DSC)

Differential Scanning Calorimetry (DSC) was carried out on a DSC Q200 (TA Instruments) in a range from -75 °C to 130 °C, with a scan rate of 5 K min^{-1}. The pans holding the samples were initially heated to 130 °C followed by two cycles of cooling to -75 °C and heating to 100 °C. To determine T_g of selected polymers as well as electrolytes values of the second heating curves were considered. After start and end point identification the T_g was delivered via the midpoint method.

5.3.4. Fourier-Transform Infrared Spectroscopy (FTIR)

Fourier-Transform Infrared Spectroscopy (FTIR) was performed on a Bruker VERTEX 80 equipped with a PIKE MIRacle™ Universal ATR adapter. The pure dry sample was applied onto a diamond prism at ambient temperature and measured from 400 to 4000 cm^{-1}. The raw data was handled with OPUS software.

5.3.5. Thermo Gravimetric Analysis (TGA)

Thermal Gravimetric Analysis (TGA) was carried out using a TGA 5500 (TA Instruments) at a heating rate of 10 K min^{-1} up to 800 °C. Samples were prepared as 5 to 10 mg equivalents on an aluminum pan. The two utilized operation gases were nitrogen and air.

5.3.6. Electrochemical Impedance Spectroscopy (EIS)

Ionic conductivities were analyzed using a VMP-300 from biologic using EIS option and a CCH-8 cell holder inside a Binder Climate chamber to control the temperature over a temperature range from 0 to 70 °C. Therefore, the samples were heated to 70 °C then cooled to 0 °C and from there on heated in steps of 10 °C up to 70 °C and cooled back to 0 °C accordingly. The cells were thermally equilibrated for 1 h each prior to the measurement. It was measured over a frequency range from 100 mHz to 1 MHz with an amplitude of 10 mV. For each temperature step 4 measurements were conducted (2 on the heating as well as 2 on the cooling cycle) and the average bulk resistance was utilized to calculate the ionic conductivity as followed:

$$\sigma_i = \frac{1}{R_{bulk}} \times \frac{d}{A}$$

With R_{bulk} as the bulk electrolyte resistance

d as the thickness of the electrolyte (d= 100 µm for fluid samples or the membrane thickness for solid samples)

A the surface area of the electrode that is in direct contact with the electrolyte

The values for R_{bulk} were extracted from the respective Nyquist plots.

5.3.7. Transference numbers (t_+)

Transference numbers (t_+) were also obtained using a VMP-300 from biologic using a CCH-8 cell holder inside a Binder Climate chamber to ensure a fixed temperature of 40°C or 60 °C. Therefore, the samples were assembled in a Lithium symmetric cell setup, closed manually and prior to the measurement heated to the measuring temperature accordingly. Transference number for Li^+:

$$t_+ = \frac{I_{ss} * (U - I_i * R_i)}{I_{i,exp} * (U - I_{ss} * R_{ss})}$$

with

I_{ss} steady state current

I_{exp} experimental current

I_{in} initial current

R_{ss} steady state resistance

R_i steady state resistance

U constant voltage

5.3.8. Polarization microscope

The crystallization patterns were observed with an optical Zeiss Axiophot microscope at an applied voltage of 3.8 V with digital video camera (and an optional polarizer orientated at 90 degrees to the illumination). Therefore, the respective dried samples were tempered to 60 °C and one drop of the fluid sample was applied to a 1 mm Epredia™ microscope slide and sandwiched with a second slide. The prepared hygroscopic samples were stored in an air and moisture tight container under nitrogen atmosphere for 12 hours to keep them dry while cooling and then were directly measured (t < 5 min, open to air and moisture). Pictures were taken with the camera model ILCE-5100 from SONY with an exposure time of 1/4000 s. The camera was directly attached to the microscope setup. A magnification of 25x and 200x was achieved by 10x ocular lens and 2.5x or 20x objective lenses.

6. Abbreviations

A	Area
AIBN	Azobisisobutyronitrile
ATRP	Atom transfer radical polymerization
-b-	Indicates a block copolymer from the monomers written to its left and right
CV	Cyclic voltammetry
-co-	Indicates a copolymer from the monomers written to its left and right
CPDB	2-Cyan-2-propylbenzodithionat
d	thickness
DCM	Dichloromethane
DSC	Differential Scanning Calorimetry
DVB	Divinylbenzene
e.g.	For example
EHMA	2-ethyl-hexyl methacrylate
EIS	electrochemical impedance spectroscopy
EO	Ethylene oxide
et al.	Et alii/aliae/alia. lat.: and others
EV	Electric vehicle
GPC	Gel permeation chromatography
I_i	Initial current
$I_{i,exp}$	Experimental value for initial current
I_{ss}	Steady state current
Li^+	Lithium cation
LiTFSI	Lithium bis(trifluoromethanesulfonyl)imide
MMA	Methyl methacrylate
M_n	Number average molar mass; ordinary arithmetic mean or average of the molecular masses of the individual macromolecules
NMC	Nickel-mangan-cobalt-oxide
NMP	Nitroxide-mediated polymerization
NMR	Nuclear magnetic resonance
mPEOxMA	Methoxy(poly(ethylene oxide)$_x$) methacrylate, with x representing the number of EO ru
PEO	Poly(ethylene) oxide
PS	Poly styrene
PMMA	Poly(methyl methacrylate)
RAFT	Reversible addition-fragmentation chain-transfer
R_{bulk}	Resistance of the bulk material
R_i	Initial resistance
R_{ss}	Steady state resistance
-ran-	Indicates a random copolymer from the monomers written to its left and right
ru	Repeating unit
SEC	Size exclusion chromatography

SMA	Solketal methacrylate, IUPAC name: (2,2-Dimethyl-1,3-dioxolan-4-yl)methyl methacrylate
hSMA	Hydrolysed Solketal methacrylate, IUPAC name: 2,3-dihydroxypropyl methacrylate
SSE	Solid-state electrolyte
t_+	Transference number
T_c	Crystallization temperature
T_g	Glass transition temperature
TGA	Thermogravimetric analysis
T_m	Melting temperature
U	Voltage
vs.	Versus
σ_{ionic}	Ionic conductivity, also σ_i

7. List of symbols

Å	Angström
°C	Degree Celsius
Đ	Dispersity
eq	Equivalents
g	Gram
l	Liter
m	Meter
ppm	Parts per million
®	Registered trademark
S	Siemens
™	Unregistered trade mark
t	Time
δ	Chemical shift in NMR spectroscopy
σ	Conductivity

References

1. Leadbetter, J. & Swan, L. Battery storage system for residential electricity peak demand shaving. *Energy and Buildings* **55,** 685–692; 10.1016/j.enbuild.2012.09.035 (2012).
2. Lightfoot, P., Mehta, M. A. & Bruce, P. G. Crystal Structure of the Polymer Electrolyte Poly(ethylene oxide)3:LiCF3SO3. *Science (New York, N.Y.)* **262,** 883–885; 10.1126/science.262.5135.883 (1993).
3. Zhang, H. *et al.* Lithium bis(fluorosulfonyl)imide/poly(ethylene oxide) polymer electrolyte. *Electrochimica Acta* **133,** 529–538; 10.1016/j.electacta.2014.04.099 (2014).
4. Xue, Z., He, D. & Xie, X. Poly(ethylene oxide)-based electrolytes for lithium-ion batteries. *J. Mater. Chem. A* **3,** 19218–19253; 10.1039/C5TA03471J (2015).
5. Fenton, D. E., Parker, J. M. & Wright, P. V. Complexes of alkali metal ions with poly(ethylene oxide). *Polymer* **14,** 589; 10.1016/0032-3861(73)90146-8 (1973).
6. Berthier, C. *et al.* Microscopic investigation of ionic conductivity in alkali metal salts-poly(ethylene oxide) adducts. *Solid State Ionics* **11,** 91–95; 10.1016/0167-2738(83)90068-1 (1983).
7. Ponam & Singh, P. Effect of PEO Concentration on Electrochemical and Mechanical Properties of PVDF, PEO and LATP Blended Solid Polymer Electrolyte. In *Computational and Experimental Methods in Mechanical Engineering,* edited by V. V. Rao, A. Kumaraswamy, S. Kalra & A. Saxena (Springer Singapore, Singapore, 2022), Vol. 239, pp. 67–76.
8. Pradeepa, P., Edwin raj, S., Sowmya, G., Kalaiselvimary, J. & Ramesh Prabhu, M. Optimization of hybrid polymer electrolytes with the effect of lithium salt concentration in PEO/PVdF-HFP blends. *Materials Science and Engineering: B* **205,** 6–17; 10.1016/j.mseb.2015.11.009 (2016).
9. Wu, Y. *et al.* Incorporating multifunctional LiAlSiO4 into polyethylene oxide for high-performance solid-state lithium batteries. *Journal of Energy Chemistry* **53,** 116–123; 10.1016/j.jechem.2020.04.070 (2021).
10. Xu, L. *et al.* Boosting the ionic conductivity of PEO electrolytes by waste eggshell-derived fillers for high-performance solid lithium/sodium batteries. *Mater. Chem. Front.* **5,** 1315–1323; 10.1039/D0QM00541J (2021).
11. Erabhoina, H., Rosenbach, D., Mohanraj, J. & Thelakkat, M. Solid polymer nanocomposite electrolytes with improved interface properties towards lithium metal battery application at room temperature. *Electrochimica Acta* **387,** 138455; 10.1016/j.electacta.2021.138455 (2021).
12. Zhou, Z., Zou, R., Liu, Z. & Zhang, P. Deciphering the role of tetrahydrofuran residue in the poly(ethylene oxide)/LiTFSI hybrid used for secondary battery electrolyte. *Giant* **6,** 100056; 10.1016/j.giant.2021.100056 (2021).
13. Butzelaar, A. J. *et al.* A Systematic Study of Vinyl Ether-Based Poly(Ethylene Oxide) Side-Chain Polymer Electrolytes. *ACS Appl. Polym. Mater.* **3,** 1573–1582; 10.1021/acsapm.0c01398 (2021).
14. Butzelaar, A. J. *et al.* Styrene-Based Poly(ethylene oxide) Side-Chain Block Copolymers as Solid Polymer Electrolytes for High-Voltage Lithium-Metal Batteries. *ACS applied materials & interfaces* **13,** 39257–39270; 10.1021/acsami.1c08841 (2021).
15. Krause, C. H. *et al.* Quasi-solid single ion conducting polymer electrolyte membrane containing novel fluorinated poly(arylene ether sulfonimide) for lithium metal batteries. *Journal of Power Sources* **484,** 229267; 10.1016/j.jpowsour.2020.229267 (2021).

16. Panday, A. *et al.* Effect of Molecular Weight and Salt Concentration on Conductivity of Block Copolymer Electrolytes. *Macromolecules* **42,** 4632–4637; 10.1021/ma900451e (2009).

17. Teran, A. A. & Balsara, N. P. Thermodynamics of block copolymers with and without salt. *The journal of physical chemistry. B* **118,** 4–17; 10.1021/jp408079z (2014).

18. Yang, G. *et al.* Selective Plasticization of Poly (ethylene oxide) (PEO) Block in Nanostructured Polystyrene− PEO− Polystyrene Triblock Copolymer Electrolytes. *J. Electrochem. Soc.* **169,** 50506; 10.1149/1945-7111/ac6a18 (2022).

19. Wright, P. V. Recent Trends in Polymer Electrolytes Based on Poly(Ethylene Oxide). *Journal of Macromolecular Science: Part A - Chemistry* **26,** 519–550; 10.1080/00222338908051991 (1989).

20. Sanchez, J.-Y., Alloin, F., Benrabah, D. & Arnaud, R. Polymer and salt selection for lithium polymer batteries. *Journal of Power Sources* **68,** 43–51; 10.1016/S0378-7753(97)02573-1 (1997).

21. Wright, P. V. Developments in Polymer Electrolytes for Lithium Batteries. *MRS Bull.* **27,** 597–602; 10.1557/mrs2002.194 (2002).

22. Diddens, D., Heuer, A. & Borodin, O. Understanding the Lithium Transport within a Rouse-Based Model for a PEO/LiTFSI Polymer Electrolyte. *Macromolecules* **43,** 2028–2036; 10.1021/ma901893h (2010).

23. Borodin, O. & Smith, G. D. Mechanism of Ion Transport in Amorphous Poly(ethylene oxide)/LiTFSI from Molecular Dynamics Simulations. *Macromolecules* **39,** 1620–1629; 10.1021/ma052277v (2006).

24. Marzantowicz, M. *et al.* Crystallization and melting of PEO:LiTFSI polymer electrolytes investigated simultaneously by impedance spectroscopy and polarizing microscopy. *Electrochimica Acta* **50,** 3969–3977; 10.1016/j.electacta.2005.02.053 (2005).

25. Volel, M., Armand, M. & Gorecki, W. Influence of Sample History on the Morphology and Transport Properties of PEO−Lithium Salt Complexes. *Macromolecules* **37,** 8373–8380; 10.1021/ma0490404 (2004).

26. Ji, X. *et al.* Unveiling the Side-Chain Effect on Ionic Conductivity of Poly(ethylene oxide)-Based Polymer-Brush Electrolytes. *ACS Appl. Energy Mater.* **5,** 8410–8418; 10.1021/acsaem.2c00962 (2022).

27. Gold, V. *The IUPAC Compendium of Chemical Terminology* (International Union of Pure and Applied Chemistry (IUPAC), Research Triangle Park, NC, 2019).

28. Bates, F. S. Polymer-polymer phase behavior. *Science (New York, N.Y.)* **251,** 898–905; 10.1126/science.251.4996.898 (1991).

29. Milner, S. T. Polymer brushes. *Science (New York, N.Y.)* **251,** 905–914; 10.1126/science.251.4996.905 (1991).

30. Feng, C. *et al.* Well-defined graft copolymers: from controlled synthesis to multipurpose applications. *Chemical Society reviews* **40,** 1282–1295; 10.1039/B921358A (2011).

31. Odian, G. G. *Principles of polymerization* (Wiley, Hoboken, N.J, 2010).

32. Stepto, R. F. T. Dispersity in polymer science (IUPAC Recommendations 2009). *Pure and Applied Chemistry* **81,** 351–353; 10.1351/PAC-REC-08-05-02 (2009).

33. Kalinchev, E. L. Controlling the Processability of Polymeric Materials. *International Polymer Science and Technology* **29,** 55–62; 10.1177/0307174X0202900513 (2002).

34. SZWARC, M. ‘Living’ Polymers. *Nature* **178,** 1168–1169; 10.1038/1781168a0 (1956).

35. Moad, G., Rizzardo, E. & Solomon, D. H. Selectivity of the reaction of free radicals with styrene. *Macromolecules* **15,** 909–914; 10.1021/MA00231A042 (1982).

36. Rizzardo, E. & Solomon, D. H. On the Origins of Nitroxide Mediated Polymerization (NMP) and Reversible Addition–Fragmentation Chain Transfer (RAFT). *Aust. J. Chem.* **65,** 945; 10.1071/CH12194 (2012).

37. Rizzardo, E. & Solomon, D. H. A new method for investigating the mechanism of initiation of radical polymerization. *Polymer Bulletin* **1,** 529–534; 10.1007/BF00254480 (1979).

38. Wang, J.-S. & Matyjaszewski, K. Controlled/"living" radical polymerization. atom transfer radical polymerization in the presence of transition-metal complexes. *J. Am. Chem. Soc.* **117,** 5614–5615; 10.1021/ja00125a035 (1995).

39. Kato, M., Kamigaito, M., Sawamoto, M. & Higashimura, T. Polymerization of Methyl Methacrylate with the Carbon Tetrachloride/Dichlorotris- (triphenylphosphine)ruthenium(II)/Methylaluminum Bis(2,6-di-tert-butylphenoxide) Initiating System: Possibility of Living Radical Polymerization. *Macromolecules* **28,** 1721–1723; 10.1021/ma00109a056 (1995).

40. Matyjaszewski, K. Discovery of the RAFT Process and Its Impact on Radical Polymerization. *Macromolecules* **53,** 495–497; 10.1021/acs.macromol.9b02054 (2020).

41. Barner-Kowollik, C. *Handbook of RAFT Polymerization* (Wiley, 2008).

42. Chiefari, J. *et al.* Living Free-Radical Polymerization by Reversible Addition−Fragmentation Chain Transfer: The RAFT Process. *Macromolecules* **31,** 5559–5562; 10.1021/ma9804951 (1998).

43. Moad, G., Rizzardo, E. & Thang, S. H. Radical addition–fragmentation chemistry in polymer synthesis. *Polymer* **49,** 1079–1131; 10.1016/j.polymer.2007.11.020 (2008).

44. Moad, G., Rizzardo, E. & Thang, S. H. Living Radical Polymerization by the RAFT Process. *Aust. J. Chem.* **58,** 379; 10.1071/CH05072 (2005).

45. *The Nobel Prize in Chemistry 2019* (Su. 2019).

46. Whittingham, M. S. Electrical energy storage and intercalation chemistry. *Science (New York, N.Y.)* **192,** 1126–1127; 10.1126/science.192.4244.1126 (1976).

47. Mizushima, K., Jones, P. C., Wiseman, P. J. & Goodenough, J. B. LixCoO2 (0<x<-1): A new cathode material for batteries of high energy density. *Materials Research Bulletin* **15,** 783–789; 10.1016/0025-5408(80)90012-4 (1980).

48. Yazami, R. & Touzain, P. A reversible graphite-lithium negative electrode for electrochemical generators. *Journal of Power Sources* **9,** 365–371; 10.1016/0378-7753(83)87040-2 (1983).

49. Akira Yoshino, Kenichi Sanechika, Takayuki Nakajima. *Secondary battery* (1985).

50. Winter, M. & Brodd, R. J. What are batteries, fuel cells, and supercapacitors? *Chemical reviews* **104,** 4245–4269; 10.1021/cr020730k (2004).

51. Winter, M., Barnett, B. & Xu, K. Before Li Ion Batteries. *Chemical reviews* **118,** 11433–11456; 10.1021/acs.chemrev.8b00422 (2018).

52. Grey, C. P. & Hall, D. S. Prospects for lithium-ion batteries and beyond-a 2030 vision. *Nature communications* **11,** 6279; 10.1038/s41467-020-19991-4 (2020).

53. Blomgren, G. E. Liquid electrolytes for lithium and lithium-ion batteries. *Journal of Power Sources* **119-121,** 326–329; 10.1016/S0378-7753(03)00147-2 (2003).

54. Wang, Q. *et al.* Thermal runaway caused fire and explosion of lithium ion battery. *Journal of Power Sources* **208,** 210–224; 10.1016/j.jpowsour.2012.02.038 (2012).

55. Kim, K. J., Balaish, M., Wadaguchi, M., Kong, L. & Rupp, J. L. M. Solid-State Li–Metal Batteries: Challenges and Horizons of Oxide and Sulfide Solid Electrolytes and Their Interfaces. *Adv. Energy Mater.* **11**; 10.1002/aenm.202002689 (2021).

56. Chen, S. *et al.* Sulfide solid electrolytes for all-solid-state lithium batteries: Structure, conductivity, stability and application. *Energy Storage Materials* **14,** 58–74; 10.1016/j.ensm.2018.02.020 (2018).

57. Wang, S. *et al.* Influence of Crystallinity of Lithium Thiophosphate Solid Electrolytes on the Performance of Solid-State Batteries. *Adv. Energy Mater.* **11**; 10.1002/aenm.202100654 (2021).

58. Zhao, Y. & Daemen, L. L. Superionic conductivity in lithium-rich anti-perovskites. *J. Am. Chem. Soc.* **134,** 15042–15047; 10.1021/ja305709z (2012).

59. Budiman, B. A. *et al.* Mechanical damages in solid electrolyte battery due to electrode volume changes. *Journal of Energy Storage* **52,** 104810; 10.1016/j.est.2022.104810 (2022).

60. Boaretto, N. *et al.* Lithium solid-state batteries: State-of-the-art and challenges for materials, interfaces and processing. *Journal of Power Sources* **502,** 229919; 10.1016/j.jpowsour.2021.229919 (2021).

61. Zhao, Y. *et al.* Solid Polymer Electrolytes with High Conductivity and Transference Number of Li Ions for Li-Based Rechargeable Batteries. *Advanced science (Weinheim, Baden-Wurttemberg, Germany)* **8,** 2003675; 10.1002/advs.202003675 (2021).

62. Manuel Stephan, A. & Nahm, K. S. Review on composite polymer electrolytes for lithium batteries. *Polymer* **47,** 5952–5964; 10.1016/j.polymer.2006.05.069 (2006).

63. Long, L., Wang, S., Xiao, M. & Meng, Y. Polymer electrolytes for lithium polymer batteries. *J. Mater. Chem. A* **4,** 10038–10069; 10.1039/C6TA02621D (2016).

64. Mindemark, J., Lacey, M. J., Bowden, T. & Brandell, D. Beyond PEO—Alternative host materials for Li + -conducting solid polymer electrolytes. *Progress in Polymer Science* **81,** 114–143; 10.1016/j.progpolymsci.2017.12.004 (2018).

65. Vrandečić, N. S., Erceg, M., Jakić, M. & Klarić, I. Kinetic analysis of thermal degradation of poly(ethylene glycol) and poly(ethylene oxide)s of different molecular weight. *Thermochimica Acta* **498,** 71–80; 10.1016/j.tca.2009.10.005 (2010).

66. Mayadunne, R. T. A. *et al.* Living Radical Polymerization with Reversible Addition−Fragmentation Chain Transfer (RAFT Polymerization) Using Dithiocarbamates as Chain Transfer Agents. *Macromolecules* **32,** 6977–6980; 10.1021/ma9906837 (1999).

67. Moad, G., Chong, Y. K., Postma, A., Rizzardo, E. & Thang, S. H. Advances in RAFT polymerization: the synthesis of polymers with defined end-groups. *Polymer* **46,** 8458–8468; 10.1016/j.polymer.2004.12.061 (2005).

68. Klimkevicius, V. & Makuska, R. Successive RAFT polymerization of poly(ethylene oxide) methyl ether methacrylates with different length of PEO chains giving diblock brush copolymers. *European Polymer Journal* **86,** 94–105; 10.1016/j.eurpolymj.2016.11.026 (2017).

69. Marzantowicz, M. *et al.* Crystalline phases, morphology and conductivity of PEO:LiTFSI electrolytes in the eutectic region. *Journal of Power Sources* **159,** 420–430; 10.1016/j.jpowsour.2006.02.044 (2006).

70. Marzantowicz, M., Krok, F., Dygas, J. R., Florjańczyk, Z. & Zygadło-Monikowska, E. The influence of phase segregation on properties of semicrystalline PEO:LiTFSI electrolytes. *Solid State Ionics* **179,** 1670–1678; 10.1016/j.ssi.2007.11.035 (2008).

71. Ikeda, M. & Aniya, M. Understanding the Vogel–Fulcher–Tammann law in terms of the bond strength–coordination number fluctuation model. *Journal of Non-Crystalline Solids* **371-372,** 53–57; 10.1016/j.jnoncrysol.2013.04.034 (2013).

72. Bennington, P. *et al.* Role of solvation site segmental dynamics on ion transport in ethylene-oxide based side-chain polymer electrolytes. *J. Mater. Chem. A* **9,** 9937–9951; 10.1039/D1TA00899D (2021).

73. Jones, J. A. *et al.* Thermoresponsive copolymers of methacrylic acid and poly(ethylene glycol) methyl ether methacrylate. *J. Polym. Sci. A Polym. Chem.* **43,** 6095–6104; 10.1002/pola.21099 (2005).

74. Rosenbach, D. *et al.* Synthesis and Comparative Studies of Solvent-Free Brush Polymer Electrolytes for Lithium Batteries. *ACS Appl. Energy Mater.* **2,** 3373–3388; 10.1021/acsaem.9b00211 (2019).

75. Hahn, M. *et al.* Investigating solid polymer and ceramic electrolytes for lithium-ion batteries by means of an extended Distribution of Relaxation Times analysis. *Electrochimica Acta* **344,** 136060; 10.1016/j.electacta.2020.136060 (2020).

76. Sun, X. & Austen Angell, C. “Acid-in-chain” versus “base-in-chain” anionic polymer electrolytes for electrochemical devices. *Electrochimica Acta* **46,** 1467–1473; 10.1016/S0013-4686(00)00741-6 (2001).

77. Hong, D. G., Baik, J.-H., Kim, S. & Lee, J.-C. Solid polymer electrolytes based on polysiloxane with anion-trapping boron moieties for all-solid-state lithium metal batteries. *Polymer* **240,** 124517; 10.1016/j.polymer.2022.124517 (2022).

78. Mazor, H., Golodnitsky, D., Peled, E., Wieczorek, W. & Scrosati, B. A search for a single-ion-conducting polymer electrolyte: Combined effect of anion trap and inorganic filler. *Journal of Power Sources* **178,** 736–743; 10.1016/j.jpowsour.2007.09.056 (2008).

79. Ma, Q. *et al.* Impact of the functional group in the polyanion of single lithium-ion conducting polymer electrolytes on the stability of lithium metal electrodes. *RSC Adv.* **6,** 32454–32461; 10.1039/C6RA01387B (2016).

80. Homann, G. *et al.* Poly(Ethylene Oxide)-based Electrolyte for Solid-State-Lithium-Batteries with High Voltage Positive Electrodes: Evaluating the Role of Electrolyte Oxidation in Rapid Cell Failure. *Sci Rep* **10,** 4390; 10.1038/s41598-020-61373-9 (2020).

8. Appendix

8.1. TGA data

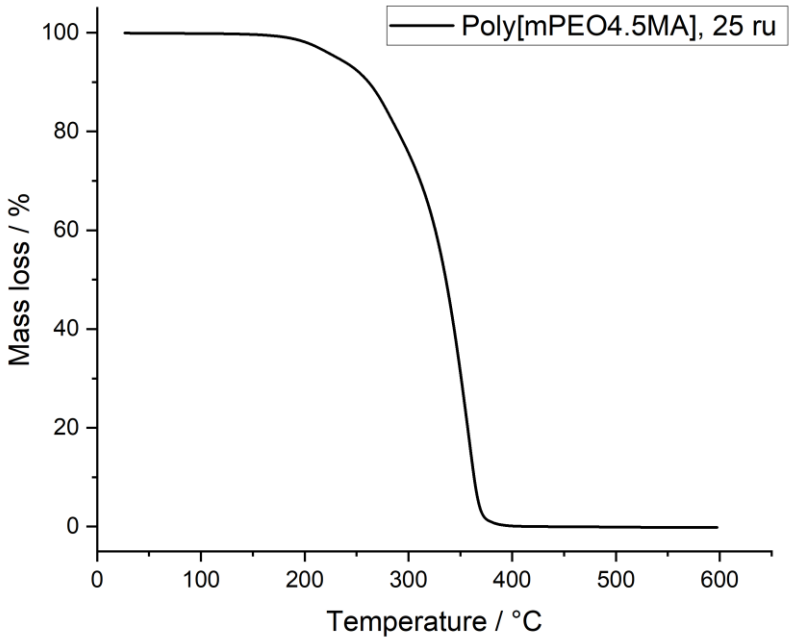

FIGURE 39: *TGA curve of the homopolymer from mPEO4.5MA with 25 ru.*

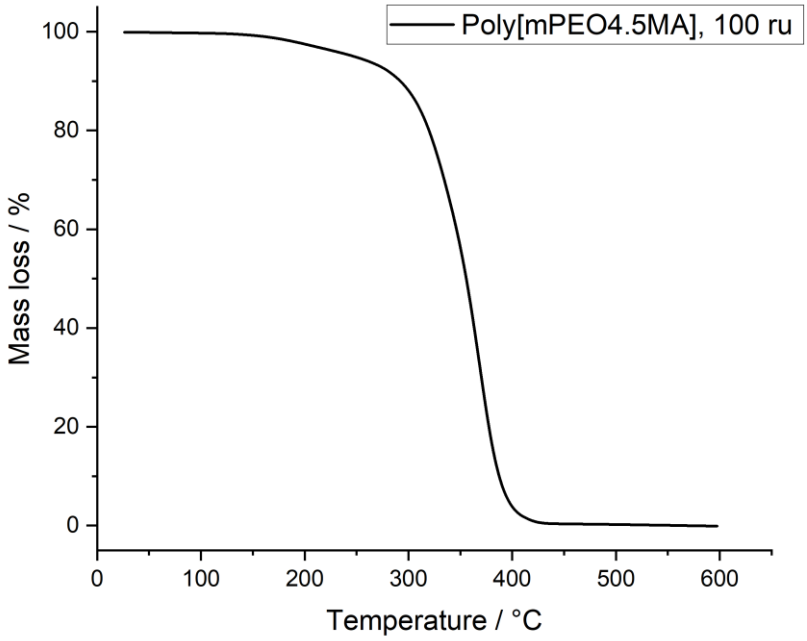

FIGURE 38: *TGA curve of the homopolymer from mPEO4.5MA with 100 ru.*

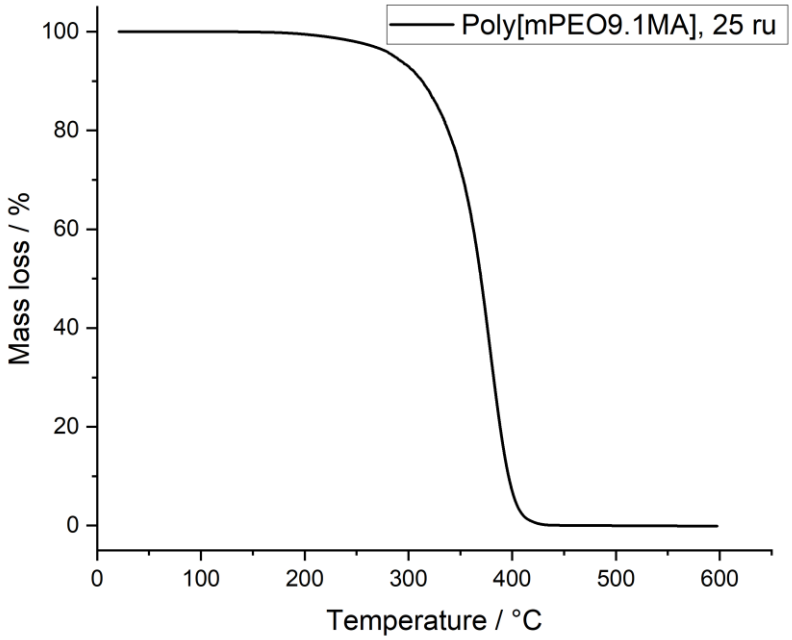

FIGURE 40: *TGA curve of the homopolymer from mPEO9.1MA with 25 ru.*

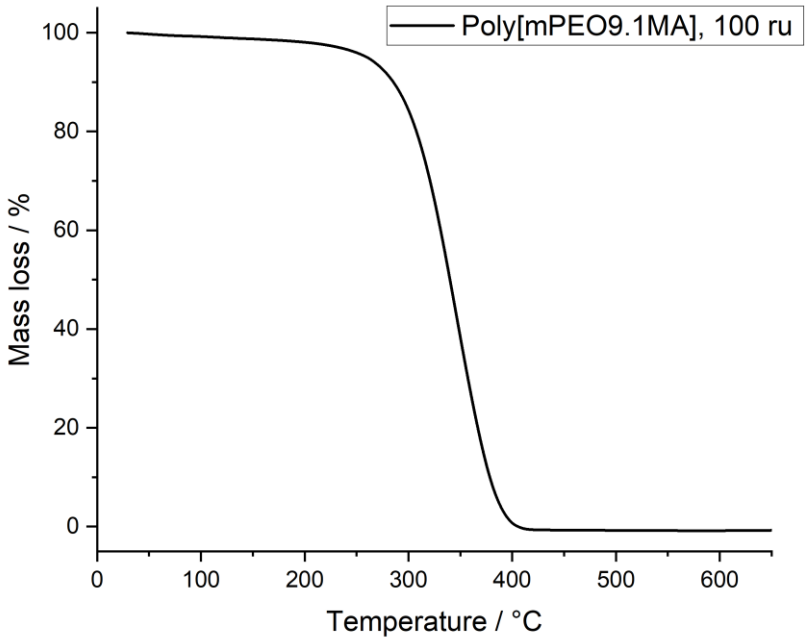

FIGURE 41: *TGA curve of the homopolymer from mPEO9.1MA with 100 ru.*

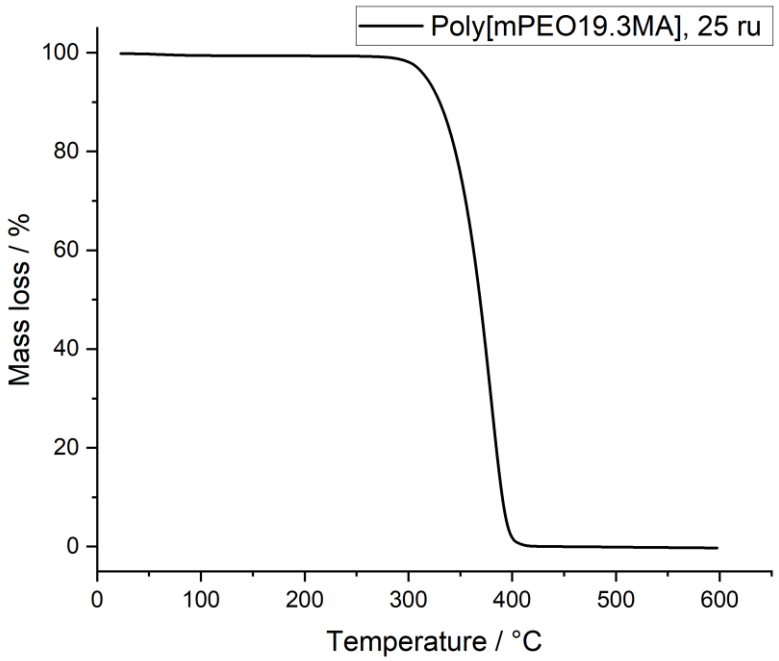

FIGURE 42: *TGA curve of the homopolymer from mPEO19.3MA with 25 ru.*

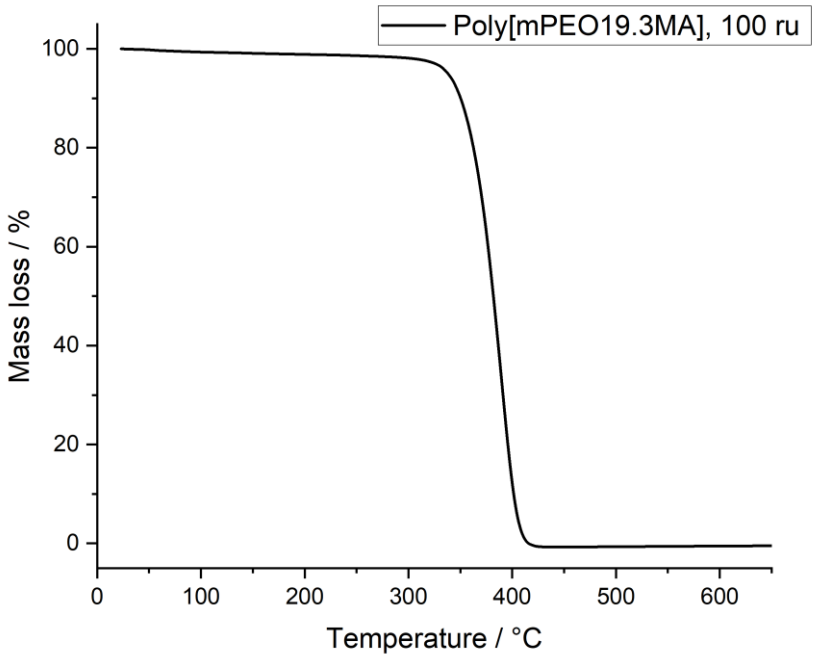

FIGURE 43: *TGA curve of the homopolymer from mPEO19.3MA with 100 ru.*

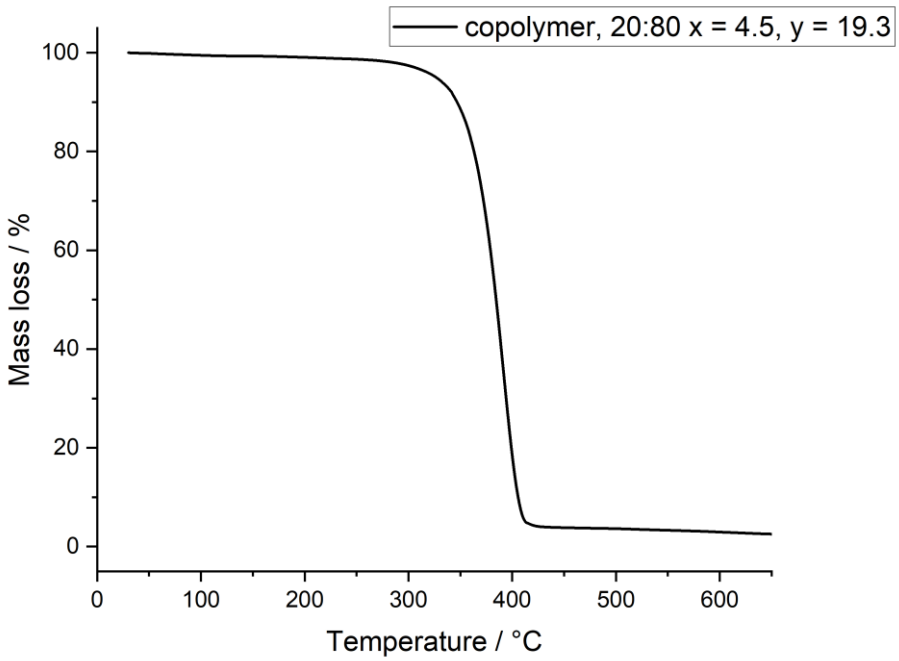

FIGURE 44: *TGA curve of the copolymer from mPEO4.5MA and mPEO19.3MA in a ratio of 20:80.*

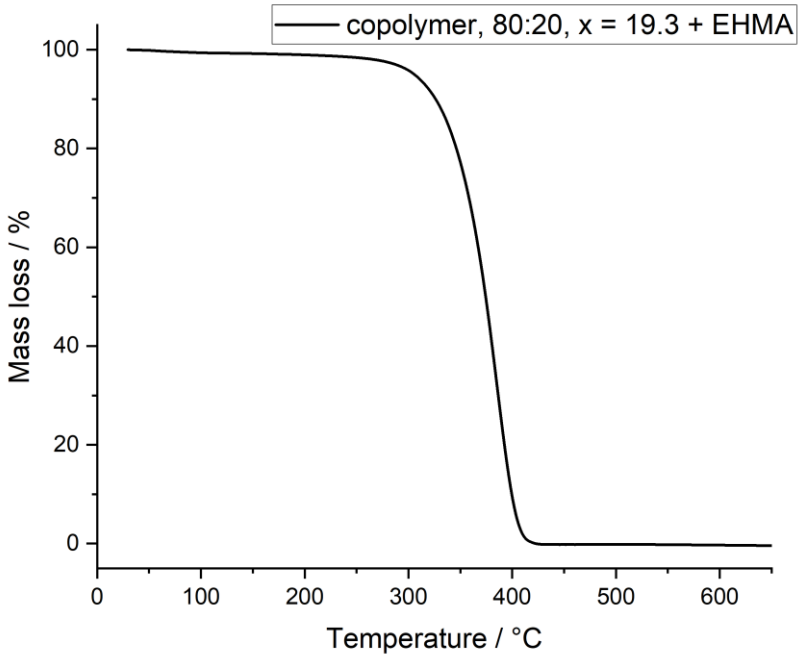

FIGURE 45: *TGA curve of the copolymer from mPEO19.3MA and EHMA in a ratio of 80:20.*

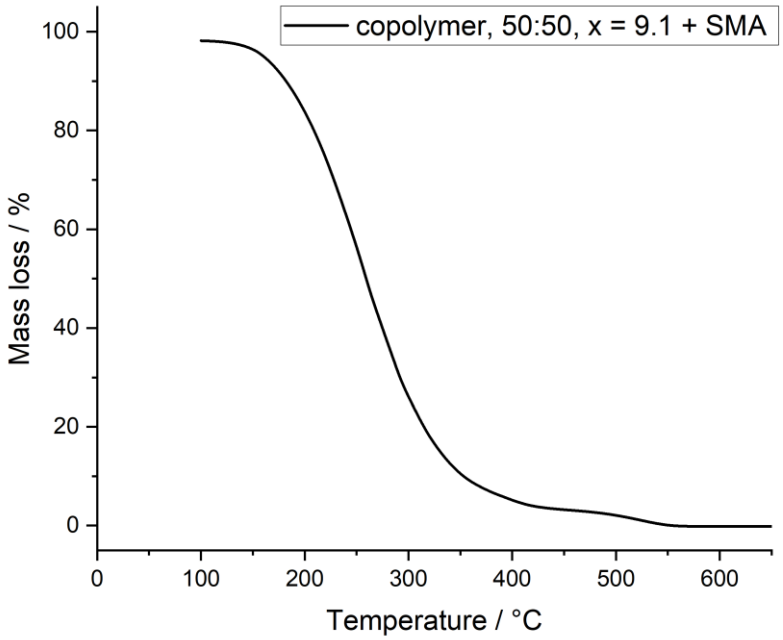

FIGURE 46: *TGA curve of the copolymer from mPEO9.1MA and SMA in a ratio of 50:50.*

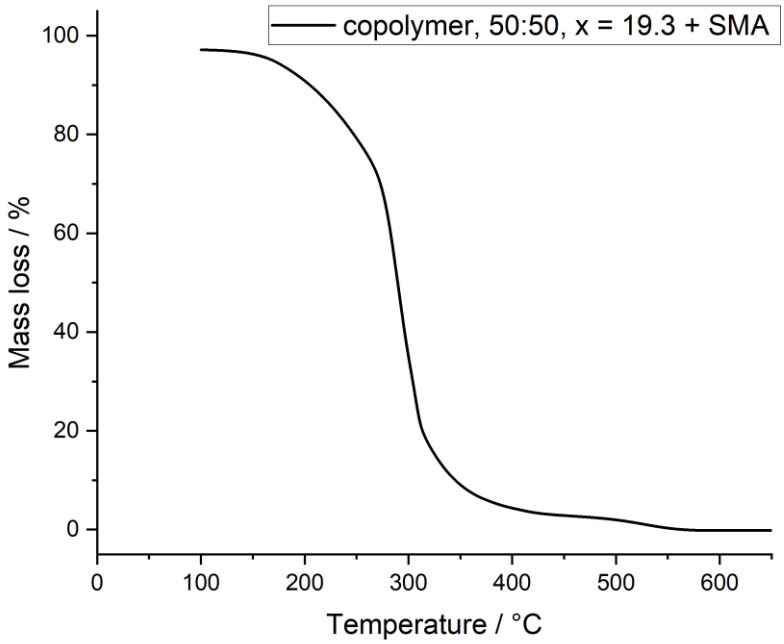

FIGURE 47: *TGA curve of the copolymer from mPEO19.3MA and SMA in a ratio of 50:50.*

8.2. NMR data

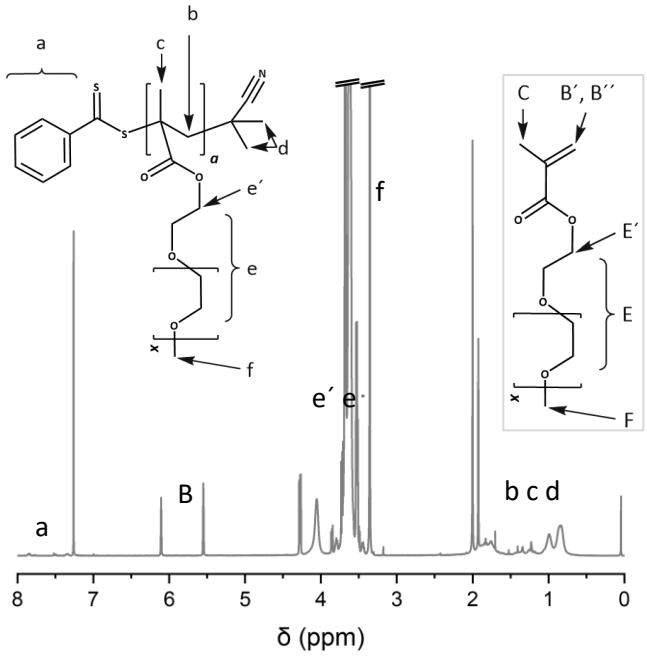

FIGURE 48: *Representative ^{1}H-NMR in deuterated chloroform of poly(mPEOxMA) after 5 h. B denotes the two signals of the doble bond protons of the monomer, all other signals of monomer lie under the respective proton signal of the polymer.*

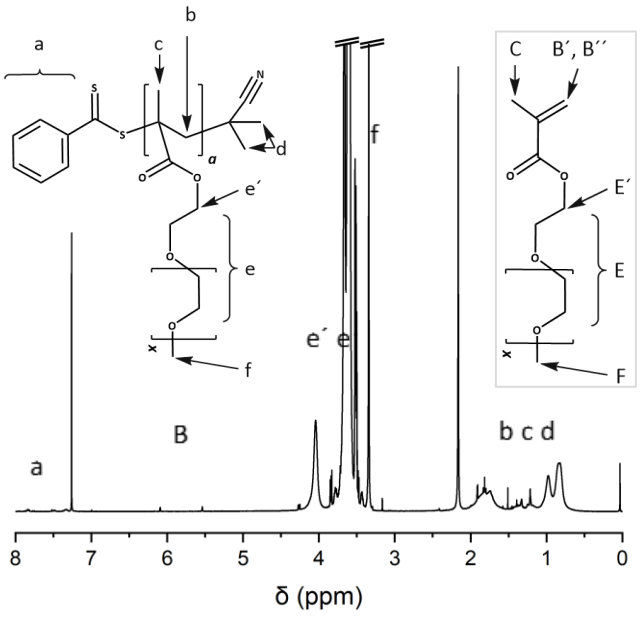

FIGURE 49: *Representative ^{1}H-NMR in deuterated chloroform of poly(mPEOxMA) before dialysis. B denotes the two signals of the doble bond protons of the monomer, all other signals of monomer lie under the respective proton signal of the polymer.*

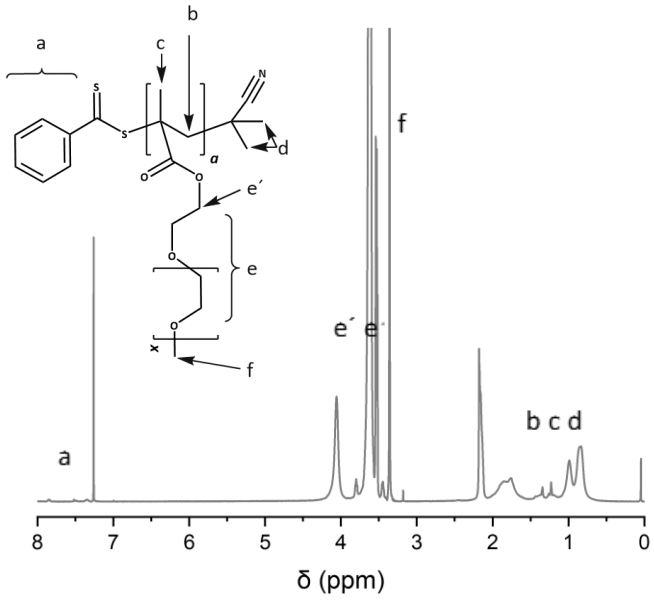

FIGURE 50: *Representative ^{1}H-NMR in deuterated chloroform of poly(mPEOxMA) after dialysis.*

TABLE 5 *Assignment of the names of the synthesized homopolymers to the M_n of the monomers and polymers (value determined by size exclusion chromatography (SEC)) together with yield and conversion determined by NMR.*

polymer	M_n(mPEOxMA) [g mol^{-1}]	$M_{n,SEC}$(polymer) [g mol^{-1}]	yield [%]	conversion [%]
Poly(mPEO4.5MA)$_{25}$	300	7 500	87	100
Poly(mPEO4.5MA)$_{50}$	300	13 000	88	99
Poly(mPEO4.5MA)$_{100}$	300	20 500	72	97
Poly(mPEO9.1MA)$_{15}$	500	10 500	98	98
Poly(mPEO9.1MA)$_{25}$	500	13 200	98	97
Poly(mPEO9.1MA)$_{50}$	500	20 300	86	81
Poly(mPEO9.1MA)$_{100}$	500	42 800	66	86
Poly(mPEO9.1MA)$_{200}$	500	85 500	52	86
Poly(mPEO19.3MA)$_{12}$	950	15 200	98	95
Poly(mPEO19.3MA)$_{25}$	950	22 100	86	83
Poly(mPEO19.3MA)$_{50}$	950	32 700	65	64
Poly(mPEO19.3MA)$_{100}$	950	-	67	77

TABLE 6 *Assignment of the names of the synthesized polymers to the M_n of the monomers and polymers (theoretical value) together with the yield.*

polymer	M1	M2			
	M_n(mPEOxMA) /g mol^{-1}	M_n(mPEOyMA) /g mol^{-1}	initial ratios [M1] : [M2] : [RAFT] : [I]	$M_{n,theo}$(P) /g mol^{-1}	yield [%]
Poly(mPEO4.5MA-*co*-mPEO9.1MA)	300	500	80:20:1.00:0.10	34 000	92
Poly(mPEO4.5MA-*co*-mPEO9.1MA)			50:50:1.00:0.10	40 000	96
Poly(mPEO4.5MA-*co*-mPEO9.1MA)			20:80:1.00:0.10	46 000	84
Poly(mPEO4.5MA-*co*-mPEO19.3MA)	300	950	80:20:1.00:0.10	43 000	95
Poly(mPEO4.5MA-*co*-mPEO19.3MA)			50:50:1.00:0.10	62 500	95
Poly(mPEO4.5MA-*co*-mPEO19.3MA)			20:80:1.00:0.10	82 000	94
Poly(mPEO9.1MA-*co*-mPEO19.3MA)	500	950	80:20:1.00:0.10	59 000	90
Poly(mPEO9.1MA-*co*-mPEO19.3MA)			50:50:1.00:0.10	72 500	56
Poly(mPEO9.1MA-*co*-mPEO19.3MA)			20:80:1.00:0.10	86 000	92

TABLE 7 *Assignment of the names of the synthesized copolymers containing EHMA to the M_n of the mPEOxMA monomer and polymers (theoretical value) together with the yield*

polymer	M1			
	M_n(mPEOxMA) /g mol^{-1}	initial ratios [M1] : [EHMA] : [RAFT] : [I]	$M_{n,theo}$(polymer) /g mol^{-1}	yield [%]
Poly[mPEO4.5MA-*ran*-EHMA]	300	10:90:1.00:0.10	20 800	41
Poly[mPEO4.5MA-*ran*-EHMA]		20:80:1.00:0.10	21 900	64
Poly[mPEO4.5MA-*ran*-EHMA]		50:50:1.00:0.10	24 900	52
Poly[mPEO9.1MA-*ran*-EHMA]	500	20:80:1.00:0.10	25 900	69
Poly[mPEO9.1MA-*ran*-EHMA]		30:70:1.00:0.10	28 900	84
Poly[mPEO19.13MA-*ran*-EHMA]	950	20:80:1.00:0.10	34 900	53
Poly[mPEO19.13MA-*block*-EHMA]		20:80:1.00:0.10	34 900	55
Poly[mPEO19.13MA-*ran*-EHMA]		50:50:1.00:0.10	57 400	81
Poly[mPEO19.13MA-*block*-EHMA]		50:50:1.00:0.10	57 400	78
Poly[mPEO19.13MA-*ran*-EHMA]		80:20:1.00:0.10	80 000	96

8.3. DSC data

TABLE 8: *Overview over glass transition temperatures and melting points for the synthesized homopolymers according to DSC heating curves.*

			polymer		polymer + LiTFSI in ratio [Li^+]:[EO] of				
	M_n(mPEOxMA)				1:10	1:15		1:20	
homopolymers	/g mol^{-1}	ru	T_g	T_m	T_g	T_g	T_m	T_g	T_m
Poly(mPEO4.5MA)	300	100	-62	n.e.	-22	-32	n.e.	-40	ne
		50	-58	-18	-22	-	-	-	
		25	-59	n.e.	-22	-31	n.e.	-38	ne
Poly(mPEO9.1MA)	500	200	-	-	-43	-50	n.e.	-54	ne
		100	-	-	-43	-49	n.e.	-53	ne
		50	-	-	-	-49	n.e.	-	-
		25	-	-	-41	-49	n.e.	-53	ne
		15	-	-	-42	-49	n.e.	-53	ne
Poly(mPEO19.3MA)	950	100	-	-	-	-51	n.v.	-57	26
		50	-	-	-46	-52	22	-56	27
		25	-	-	-46	-52	22	-55	27
		12	-	-	-46	-52	22	-55	27

n.e. = not existent, n.v. = not visible, - = not determined.

TABLE 9: *Overview over glass transition temperatures and melting points for the synthesized copolymers from mPEOxMA and mPEOyMA according to DSC heating curves.*

				Polymer + LiTFSI in ratio [Li⁺]:[EO] of			
copolymers	M_n(mPEOxMA) /g mol^{-1}	M_n(mPEOyMA) /g mol^{-1}	ratio [M1]:[M2]	1:10 T_g	1:15 T_g	1:20 T_g	T_m
Poly[mPEO4.5MA-*ran*-mPEO9.1MA]	300	500	80:20	-40	-45	-49	*n.e*
			20:80	-42	-49	-52	*n.e*
Poly[mPEO9.1MA-*ran*-mPEO19.3MA]	500	950	80:20	-	-51	-54	*n.e*
			20:80	-46	-53	-56	25
Poly[mPEO4.5MA-*ran*-mPEO19.3MA]	300	950	80:20	-45	-47	-52	*n.e*
			50:50	-42	-46	-49	*n.e*
			20:80	-44	-52	-56	26

n.e. = not existent, - = not determined.

TABLE 10: *Overview over glass transition temperatures and melting points for the synthesized copolymers from mPEOxMA and EHMA according to DSC heating curves.*

			Polymer + LiTFSI in ratio [Li⁺]:[EO] of 1:10	
	/g mol^{-1}	[M1]:[M2]	T_g	T_m
Poly[mPEO4.5MA-*ran*-EHMA]	300	50:50	-22	n.v.
Poly[mPEO4.5MA-*ran*-EHMA]		20:80	-32	n.v.
Poly[mPEO9.1MA-*ran*-EHMA]	500	20:80	-62	n.v.
Poly[mPEO19.3MA-*ran*-EHMA]	950	50:50	-45	n.v.
Poly[mPEO19.3MA-*b*-EHMA]		50:50	-44	n.v.
Poly[mPEO19.3MA-*ran*-EHMA]		20:80	-52	n.v.
Poly[mPEO19.3MA-*b*-EHMA]		20:80	-49	n.v.

n.v. = not visible.

8.4. SEC data

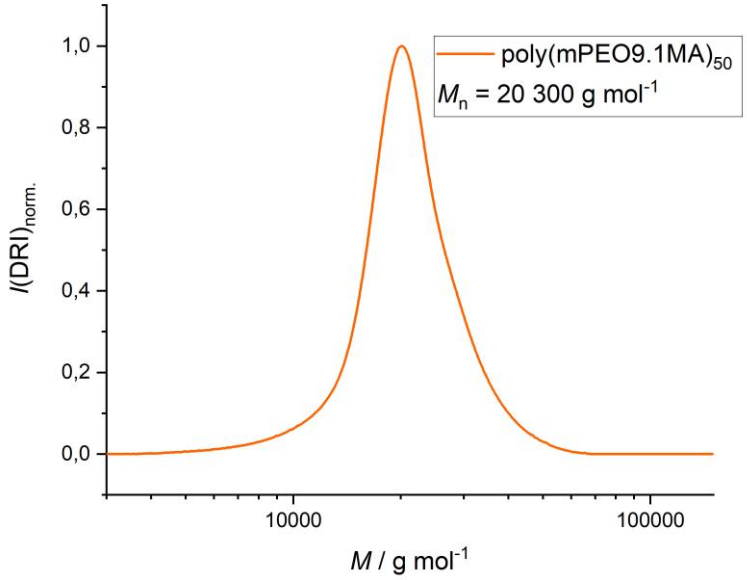

FIGURE 51: *weight distribution of poly(mPEO9.1MA) with a backbone length of 40 ru measured by SEC in THF at 40 °C. Only representative for short side chain polymers.*